



# Fire Resistance Of Non-Loadbearing LSF Walls

**Luiz Antônio de Souza Fernandes Silva**

Thesis Presented to the School of Technology and Management of Polytechnic Institute of Bragança to the Fulfilment of the Requirements for the Master of Science Degree in Industrial Engineering (Mechanical Engineering branch) .

Supervised by:

Prof. Doutor Paulo Alexandre Gonçalves Piloto

Prof. Doutor Henrique Cotait Razuk

Bragança

February 2018





# Fire Resistance Of Non-Loadbearing LSF Walls

**Luiz Antônio de Souza Fernandes Silva**

Thesis Presented to the School of Technology and Management of Polytechnic Institute of Bragança to the Fulfilment of the Requirements for the Master of Science Degree in Industrial Engineering (Mechanical Engineering branch) .

Supervised by:

Prof. Doutor Paulo Alexandre Gonçalves Piloto

Prof. Doutor Henrique Cotait Razuk

Bragança

February 2018



# Acknowledgement

First of all, to God, that provides me the opportunity to come so far to follow a dream and be a better man and professional.

Special thanks to the Federal Technological University of Paraná (UTFPR) that guides me in this construction of knowledge in a humanistic and technical way, and to the Polytechnic Institute of Bragança (IPB), that accept me to expand my horizons and receiving me so well . Here I want to thank to Prof. Adriano Borges, Prof. Romeu Rony Cavalvante da Costa, Prof. Fernando Câmara and Prof. Edson Hideki Koroishi for the trust in send me to the double diploma.

Thanks to Prof. Paulo Piloto and Prof. Henrique Razuk, that supervised me in this work in a such competent way. Thanks to Eng. Luisa Barreira from the Laboratory of Structures and Resistances of Materials for the companionship and dedication, to Mr. João and Mr. Otávio from Construction Materials Laboratory, to Mr. André from Maintenance Office and for Eng. Jorge Paulo and Eng. Abílio from the Mechanical Technology Laboratory. Their participation was invaluable. Thanks to Ms. Eng. Seddik Khetata and Eng. Cesar Marinho, partners in the research that turned in friends. We are all together in this.

For the partnership and support in this research, thanks to Amorin Composites, F. Pereira Materias de Construção, FALPER/Fibroplac and Normago, that provides all the materials to the experimental tests.



# Abstract

The present work presents a study across the effects of fire in nonloadbearing Light-Steel Frame (LSF) walls. Eight experimental tests and twenty-two parametric analyses were performed to evaluate the influence the thickness of the cavity, the thickness of the structural steel, the effect of the protection layer and the influence of insulation material in the cavity. The thickness of the protection layer presents the bigger influence in fire resistance, followed by the effect of the insulation material in the cavity. Four configurations of protection layers and three different LSF structures were evaluated, and a test with insulation in the cavities.

**Keywords:** LSF Walls, Fire Resistance, Ansys Fluent, Ansys Multiphysics, Experimental Tests.





# Resumo

Este trabalho apresenta um estudo acerca dos efeitos de incêndios em estruturas de Light-Steel Frame (LSF) com paredes não portantes. Foram realizados oito ensaios experimentais e vinte e duas análises paramétricas para avaliar a influência da espessura da cavidade, espessura do aço da estrutura, efeito da camada protetora e influência do material isolante na cavidade. Dentre os fatores analisados, conclui-se que a espessura da camada protetora tem a maior influência na resistência ao fogo, seguido pelo efeito do material isolante nas cavidades. Quatro camadas protetoras e três estruturas foram analisadas, além de um teste com isolante na cavidade.

**Palavras-chave:** Paredes de LSF; Resistência ao Fogo, Ansys Fluent, Ansys Multiphysics, Ensaios Experimentais.



# Contents

<b>Acknowledgement</b>	<b>v</b>
<b>Abstract</b>	<b>vii</b>
<b>Resumo</b>	<b>ix</b>
<b>1 Introduction</b>	<b>1</b>
1.1 Objectives . . . . .	1
1.2 LSF Constructions . . . . .	2
1.3 Plan of Thesis . . . . .	3
<b>2 State of the Art</b>	<b>5</b>
2.1 Preliminary Studies . . . . .	5
2.2 Light Steel Frame Studies . . . . .	7
2.3 Cavities and Composites: the new concept . . . . .	8
<b>3 Fire</b>	<b>11</b>
3.1 Heat Transfer Theory . . . . .	11
3.2 Natural Fire Curve . . . . .	12
3.3 Standard Fire Curves . . . . .	14
<b>4 Wall Specimens</b>	<b>15</b>
4.1 Standards to be used . . . . .	15
4.1.1 EN 1363-1 . . . . .	15

4.1.2	EN 1364-1 . . . . .	17
4.1.3	EN 1993-1-2 . . . . .	17
4.2	Laboratory Facilities . . . . .	18
4.3	Sensors Specifications . . . . .	19
4.4	Specimens . . . . .	21
4.4.1	Specimen 0 and Specimen 1 . . . . .	23
4.4.2	Specimen 2 . . . . .	24
4.4.3	Specimen 3 . . . . .	25
4.4.4	Specimen 4 . . . . .	26
4.4.5	Specimen 5 . . . . .	27
4.4.6	Specimen 6 . . . . .	28
4.4.7	Specimen 7 . . . . .	29
<b>5</b>	<b>Experimental Tests</b>	<b>31</b>
5.1	Specimen 0 . . . . .	32
5.2	Specimen 1 . . . . .	33
5.3	Specimen 2 . . . . .	34
5.4	Specimen 3 . . . . .	36
5.5	Specimen 4 . . . . .	37
5.6	Specimen 5 . . . . .	38
5.7	Specimen 6 . . . . .	39
5.8	Specimen 7 . . . . .	40
<b>6</b>	<b>Numerical Simulation</b>	<b>43</b>
6.1	Material Properties . . . . .	43
6.2	Solution Methods . . . . .	44
6.2.1	Solution Method 1 . . . . .	45
6.2.2	Solution Method 2 . . . . .	47
6.2.3	Solution Method 3 . . . . .	48
6.3	Numerical Validation . . . . .	48

6.3.1	Numerical Validation of Specimens with Geometry A . . . . .	49
6.3.2	Numerical Validation of Specimens with Geometry B . . . . .	55
<b>7</b>	<b>Parametric Analysis</b>	<b>59</b>
7.1	Parametric Analysis based on geometry A . . . . .	59
7.2	Parametric Analysis based on geometry B . . . . .	64
<b>8</b>	<b>Discussion of the Results</b>	<b>73</b>
8.1	Influence of the Protection Layer . . . . .	73
8.1.1	Influence of the material . . . . .	73
8.1.2	Influence of the thickness of gypsum plasterboard . . . . .	75
8.2	Insulation versus Protection Layer . . . . .	76
8.2.1	Insulation of Protection Layer versus Cavity insulation . . . . .	76
8.2.2	Influence of insulation density and cavity thickness . . . . .	78
8.3	Influence of LSF Structure . . . . .	79
8.3.1	Influence of studs . . . . .	80
8.3.2	Influence of Steel thickness . . . . .	81
<b>9</b>	<b>Conclusions</b>	<b>83</b>
<b>A</b>	<b>Experimental Results</b>	<b>89</b>
A.1	Specimen 0 . . . . .	89
A.2	Specimen 1 . . . . .	92
A.3	Specimen 2 . . . . .	94
A.4	Specimen 3 . . . . .	97
A.5	Specimen 4 . . . . .	100
A.6	Specimen 5 . . . . .	102
A.7	Specimen 6 . . . . .	104
A.8	Specimen 7 . . . . .	107
<b>B</b>	<b>Material Properties</b>	<b>111</b>

<b>C Numerical Validation</b>	<b>116</b>
C.1 Specimens Geometry A . . . . .	116
C.2 Specimens Geometry B . . . . .	120
<b>D Specimens DataSheet</b>	<b>124</b>

# List of Tables

- 4.1 Specimens to be tested. . . . . 21
- 5.1 Results of the Tests. . . . . 32
- 6.1 Results of the Tests. . . . . 49
- 6.2 Characteristics and fire resistance of the wall assemblies used for validation. 55
- 7.1 Characteristics and fire resistance of the wall assemblies used for parametric analysis, geometry A. . . . . 60
- 7.2 Characteristics and fire resistance of the wall assemblies used for parametric analysis, geometry B. . . . . 65
- 8.1 Influence of the variation of the material of the protection layer . . . . . 75
- 8.2 Influence of the increase of the plasterboard thickness versus RockWool insulant. . . . . 77
- 8.3 Influence of studs. . . . . 80
- 8.4 Influence of Steel Thickness. . . . . 81





# List of Figures

1.1	Principle of design of light-weight steel construction [3]. . . . .	3
3.1	Natural Fire Curve [24]. . . . .	13
3.2	ISO 834 Standard Curve. . . . .	14
4.1	Furnace . . . . .	18
4.2	Bed Thermocouple and Welded Thermocouple. . . . .	20
4.3	Plate Thermocouple and Disk Thermocouple. . . . .	20
4.4	Position of the screws in the plasterboards with 5 studs. . . . .	22
4.5	Thermocouples Position on Specimen 0 and 1. . . . .	23
4.6	Specimens 0 and 1. . . . .	24
4.7	Thermocouples Position on Specimen 2. . . . .	25
4.8	Specimen 2. . . . .	25
4.9	Thermocouples Position on Specimen 3. . . . .	26
4.10	Specimen 3. . . . .	26
4.11	Thermocouples Position on Specimen 4. . . . .	27
4.12	Specimen 4. . . . .	27
4.13	Thermocouples Position on Specimen 5. . . . .	28
4.14	Specimen 5. . . . .	28
4.15	Thermocouples Position on Specimen 6. . . . .	29
4.16	Specimen 6. . . . .	29
4.17	Thermocouples Position on Specimen 7. . . . .	30
4.18	Specimen 7. . . . .	30

5.1	Specimen 0 - Average Temperature Results. . . . .	33
5.2	Specimen 1 - Average Temperature Results. . . . .	34
5.3	Specimen 2 - Average Temperature Results. . . . .	35
5.4	Specimen 3 - Average Temperature Results. . . . .	36
5.5	Specimen 4 - Average Temperature Results. . . . .	37
5.6	Specimen 5 - Average Temperature Results. . . . .	38
5.7	Specimen 6 - Average Temperature Results. . . . .	39
5.8	Specimen 7 - Average Temperature Results. . . . .	40
6.1	Boundary Conditions. . . . .	44
6.2	Finite cells used for specimens in solution method 1. . . . .	45
6.3	Finite cells used for specimens in solution method 1 (detailed views). . . . .	45
6.4	Finite element mesh used for specimens in solution method 2 (specimen 3). . . . .	47
6.5	Finite element mesh used for specimens in solution method 3 (specimen 4). . . . .	48
6.6	Specimen 1 - Numerical Results (time=56min, temperature [K]). . . . .	50
6.7	Specimen 1 - Error. . . . .	50
6.8	Specimen 2 - Numerical Results (time=118min, temperature [K]). . . . .	51
6.9	Specimen 2 - Error. . . . .	51
6.10	Specimen 3 - Numerical Results (time=87.43min, temperature [K]). . . . .	51
6.11	Specimen 3 - Error. . . . .	52
6.12	Specimen 4 - Numerical Results (time=55.61min, temperature [K]). . . . .	52
6.13	Specimen 4 - Error. . . . .	52
6.14	Specimen 5 - Numerical Results (time=60.28min, temperature [K]). . . . .	53
6.15	Specimen 5 - Error. . . . .	53
6.16	Specimen 6 - Numerical Results (time=68.47min, temperature [K]). . . . .	53
6.17	Specimen 6 - Error. . . . .	54
6.18	Specimen 7 - Numerical Results (time=95min, temperature [K]). . . . .	54
6.19	Specimen 7 - Error. . . . .	54
6.20	Selected specimens 1, 3, 4 and 5 under validation.[34] . . . . .	56

7.1	Finite element models used for specimens based on geometry B. . . . .	59
7.2	Case 2. . . . .	60
7.3	Case 3. . . . .	61
7.4	Case 4. . . . .	61
7.5	Case 5. . . . .	62
7.6	Case 6. . . . .	62
7.7	Case 7. . . . .	63
7.8	Case 8. . . . .	63
7.9	Case 9. . . . .	64
7.10	Model with one gypsum plate - Solution Method 2. . . . .	64
7.11	Model with two gypsum plate - Solution Method 2. . . . .	65
7.12	Case 05. . . . .	66
7.13	Case 06. . . . .	66
7.14	Case 07. . . . .	67
7.15	Case 08. . . . .	67
7.16	Case 09. . . . .	68
7.17	Case 10. . . . .	68
7.18	Case 11. . . . .	69
7.19	Case 12. . . . .	69
7.20	Case 13. . . . .	70
7.21	Case 14. . . . .	70
7.22	Case 15. . . . .	71
7.23	Case 16. . . . .	71
8.1	Unexposed Side Temperatures from Specimens 1, 2, 4 and 7. . . . .	74
8.2	Comparison of the different gypsum plasterboard thickness to LSF configurations. . . . .	76
8.3	Unexposed Side Temperatures from Specimens 1, 2 and 3. . . . .	77
8.4	Unexposed Side Temperatures from Cases 1 to 9. . . . .	78

8.5	Fire Resistance in function of the density of the Rockwool. . . . .	79
8.6	Unexposed Side Temperatures from Specimens 4, 5 and 6. . . . .	80
A.1	Test 0 - IR Thermal Camera Results. . . . .	89
A.2	Test 0 - IR Thermal Camera Results. . . . .	90
A.3	Specimen 0 after the end of the test. . . . .	91
A.4	Test 1 - IR Thermal Camera Results. . . . .	92
A.5	Test 0 - IR Thermal Camera Results. . . . .	93
A.6	Specimen 1 after the end of the test. . . . .	93
A.7	Specimen 1 after the end of the test. . . . .	94
A.8	Test 2 - IR Thermal Camera Results. . . . .	94
A.9	Test 2 - IR Thermal Camera Results. . . . .	95
A.10	Test 2 - IR Thermal Camera Results. . . . .	96
A.11	Specimen 2 during and after the end of the test. . . . .	96
A.12	Specimen 2 during and after the end of the test. . . . .	97
A.13	Test 3 - IR Thermal Camera Results. . . . .	98
A.14	Test 3 - IR Thermal Camera Results. . . . .	99
A.15	Specimen 3 during and after the end of the test. . . . .	99
A.16	Specimen 3 during and after the end of the test. . . . .	100
A.17	Test 4 - IR Thermal Camera Results. . . . .	100
A.18	Test 4 - IR Thermal Camera Results. . . . .	101
A.19	Specimen 4 during and after the end of the test. . . . .	101
A.20	Specimen 4 during and after the end of the test. . . . .	102
A.21	Test 5 - IR Thermal Camera Results. . . . .	103
A.22	Test 5 - IR Thermal Camera Results. . . . .	104
A.23	Specimen 5 during and after the end of the test. . . . .	104
A.24	Test 6 - IR Thermal Camera Results. . . . .	105
A.25	Test 6 - IR Thermal Camera Results. . . . .	106
A.26	Specimen 6 during and after the end of the test. . . . .	106

A.27 Specimen 6 during and after the end of the test. . . . .	107
A.28 Test 7 - IR Thermal Camera Results. . . . .	107
A.29 Test 7 - IR Thermal Camera Results. . . . .	108
A.30 Test 7 - IR Thermal Camera Results. . . . .	109
A.31 Specimen 7 during and after the end of the test. . . . .	109
B.1 Thermal properties of steel. . . . .	111
B.2 Thermal properties of gypsum. . . . .	112
B.3 Thermal properties of wood. . . . .	112
B.4 Thermal properties of cork. . . . .	113
B.5 Thermal properties of rockwool, density 75kg/m <sup>3</sup> . . . . .	113
B.6 Thermal properties of rockwool, density 120kg/m <sup>3</sup> . . . . .	114
B.7 Thermal properties of rockwool, density 300kg/m <sup>3</sup> . . . . .	114
B.8 Thermal properties of glass fiber. . . . .	115
B.9 Thermal properties of air. . . . .	115
C.1 Specimen 01 – Numerical results. . . . .	116
C.2 Specimen 02 – Numerical results. . . . .	117
C.3 Specimen 03 – Numerical results. . . . .	117
C.4 Specimen 04 – Numerical results. . . . .	118
C.5 Specimen 05 – Numerical results. . . . .	118
C.6 Specimen 06 – Numerical results. . . . .	119
C.7 Specimen 07 – Numerical results. . . . .	119
C.8 Case 01 – Experimental results [34]. . . . .	120
C.9 Case 01 – Numerical results. . . . .	120
C.10 Case 02 – Experimental results [34]. . . . .	121
C.11 Case 02 – Numerical results. . . . .	121
C.12 Case 03 – Experimental results [34]. . . . .	122
C.13 Case 03 – Numerical results. . . . .	122
C.14 Case 04 – Experimental results [34]. . . . .	123

C.15 Case 04 – Numerical results. . . . . 123

# Notation

## Latin Lower Case Letters

$g_y$  Gravity acceleration in direction y

$\dot{h}$  Heat flux [ $W/m^2$ ]

$\dot{h}_{net}$  Net heat flux [ $W/m^2$ ]

$p$  Pressure [MPa]

$t$  Time [s]

## Latin Upper Case Letters

$C_p$  Specific heat at constant pressure [kJ/(kg K)]

$E_{fi,d}$  Design effect of actions for the fire design situation [adimensional]

$K_{xx,yy,zz}$  Thermal conductivity in x,y,z directions [W/mK]

**PDE** Partial Differential Equation

$R_{fi,d,t}$  Fire design resistance of the steel member at time t

$T_y$  Viscous Loss Terms

$T_\infty$  Ambient temperature [ $^{\circ}C$ ]

$\vec{V}$  Velocity vector [m/s]

## Greek Letters

$\alpha_c$  Coefficient of heat transfer by convection [W/kgK]

$\varepsilon_m$  Surface Emissivity of Member [adimensional]

$\varepsilon_f$  Emissivity of the fire [adimensional]

$\sigma$  Stephan Boltzmann constant =  $5,67 \times 10^{-8}$ [W/m<sup>2</sup>K<sup>4</sup>]

$\lambda$  Thermal conductivity [kW/(m<sup>o</sup>C)]

$\rho$  Density [kg/m<sup>3</sup>]

$\rho_0$  Specific Mass [kg/m<sup>3</sup>]

$T_g$  Gas Temperature in the Vicinity of the Fire Exposed Member [ $^{\circ}C$ ]

$T_m$  Surface Temperature of the Member [ $^{\circ}C$ ]

$\vec{\nabla}$  Delta Operator

$\mu_e$  Effective Viscosity of the fluid



# Chapter 1

## Introduction

Since the prehistory, the men are improving his ability to construct buildings. This constructions started with the stone buildings, like the famous Stonehenge, and this constructions techniques are evolving until nowadays. The initial art of construction, which was aimed as main objective to provide some protection against animals and changes in climate has been improved over the centuries, and new goals have been added to these buildings like artistic expressions, religious representations, and now the current constructions have as principle to be aesthetically pleasant.

Even with these new goals, the search about safer constructions never stopped. Gas, electricity and hidrosanitaryes installations, in buildings everytime taller and more complex increases the risks of fire, collapse, and so on.

### 1.1 Objectives

This work presents a study across the fire effects on a non-loadbering walls Light Steel Frame (LSF) structure, to improve the knowledge when using different configurations and materials.

Specific tasks are included to be investigated: different types of insulation materials (rock wool, glass fibre, and cork), position of insulation materials, different types of panels; different types of steel sections, spacing between studs.

Special numerical tasks aim to develop an accurate model to predict fire resistance, using ANSYS Fluent and ANSYS Multiphysics. The validation of the 2D finite element model with and without fluid interaction is presented.

Special experimental tests aim to validate the numerical model. Experimental tests should be developed to define the fire resistance of non-loadbearing wall, according to EN1363-1 [1] and EN1364-1 [2].

## 1.2 LSF Constructions

The LSF constructions appeared in the end of the XX century, and have as principal advantages: the weight of the structure, high-loadbearing capacity and a wide range of possibilities and configurations [3]. The definition of LSF, given by [3], is a composite of a steel mesh supporting all loads, with plate-like walls covering the spans and shaping the construction. They are made of sandwich type and the metal structure has a plate on each side as protection layer. Walls can or do not withstand loads, and the material commonly used for the design of the protection layer is gypsum.

The construction of a frame in lightweight sections is made with each upright stud inserted at the top and base of a horizontal U-section tracks, that is responsible to distribute the load on upright studs. The difference between the lightweight steel structure construction and the traditional frame is that the load can be distributed over the building shell. In LSF constructions, the load is borne by the panels that can also divide the structure, as showed in the Figure 1.1, in this case a partition wall.

This structure is embraced by rigid panels, in a sandwich construction, that bear perpendicular pressures and horizontal loads and forces. These panels need to be rigid enough and correctly fixed to ensure that the sections will not sag or buckle. Between the panels exist a cavity, defined by the space between the internal plates, and these spaces are usually used to put ducts, sheaths and cables. These spaces can be fulfilled with some protection material, to increase the fire resistance, or acoustic performance and thermal resistance.

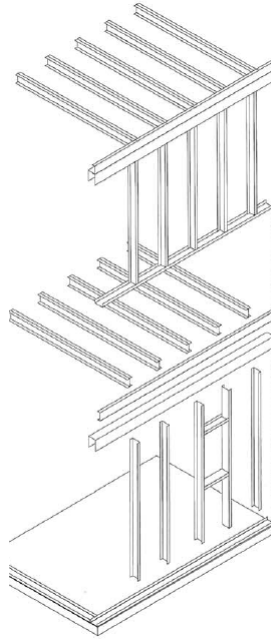


Figure 1.1: Principle of design of light-weight steel construction [3].

The non-loadbearing LSF wall is normally used as a partition and is one of the most frequently used method. In these cases, according the Association for Specialist Fire Protection [4], when a partition is installed into a new building, it may be required to contain a fire within a space (compartment) or to provide a means of escape for personnel into which a fire cannot readily penetrate. The requirements in these cases are a structure that will not collapse and will contain the fire for a certain period of time, with a range from 30 to 240 minutes (or more), depending on the protection layer, studwork, head and base track and the insulation material in the cavity. The presence of items of construction as doors, ducts, cables and pipes have considerable influence in this rating also, and need to be considered.

### 1.3 Plan of Thesis

The second chapter presents the state of the art, that makes a retrospective about the studies related with the fire resistance of LSF structures, and the third chapter brings a explanation about the fire, showing the main characteristics and the most used standard

curves that quantify this event.

The fourth chapter presents the specifications of the walls, and all the parameters of the experimental analysis. The results of this experimental analysis are in the fifth chapter, and the mathematical model, validated by this experiments is given in the sixth chapter.

The seventh chapter presents a parametric analysis, with studies changing the number of layers and trying new insulation materials in the vacuums.

The eighth chapter presents the discussion of the results, and the last chapter gives the conclusions about this work, and some informations about the materials and the tests are given in the annex pages.

# Chapter 2

## State of the Art

The present chapter presents a review of the research of the LSF walls. The research achievements are going to be presented, taking into account the experimental and numerical investigation of LSF walls panels under fire conditions. The state of the art explores the current knowledge of the LSF wall panels on a time line basis, including the behaviour of all the components, failure modes, temperature fields and displacement behaviour.

Local instability may be one of the failure modes in LSF wall panels due to the compressive stress that may arise from a restraint to steel expansion. This compressive stress is normally below the yield stress, due to the factor that the steel elements are defined as class-4. This behaviour depends on the level of restrains imposed to the studs and tracks and also on the temperature level imposed.

### 2.1 Preliminary Studies

The first design principles were introduced by the American Iron and Steel Institute (AISI) in 1946. Prof. G. Winter made an extensive research on cold formed steel elements at Cornell University in 1963, analysing the effects of cold-straining on structural sheet steels and corner properties of cold-formed steel shapes among other things. The American Iron and Steel Institute sponsored a research investigation at Cornell University for the purpose of identifying the effects of cold-forming on the mechanical properties, as well as

on structural behaviour of members.

The British steel standard was modified in 1961 to include the design of cold formed steel members, based on the investigations of Prof. A. H. Chilver [5]. The Australian standard for the design of cold formed steel structural members was first published in 1974. This standard was based on the 1968 edition of the American specifications, but with modifications with respect to beams and columns design curves to keep them aligned with Australian Steel Structures code [5].

The cold working to which sheet steels are subjected when being cold-formed into structural shapes for light-gage steel construction was studied by Chajes and Britvec et al [6] in 1970, showing good results about the mechanical resistance and properties strong enough to handle a structure. The structural members that are used in light-gage steel construction are produced by several cold-forming processes, such as cold-rolling or brakeforming, and it is well known that cold working by stretching, bending, affects the mechanical properties of mild structural steels. This work verified that the cold-forming causes a significant increase in yield strength of corners and to smaller increase in flat parts of thin-walled steel members, validating the LSF construction model.

In 1985, a new study, presented by Schwartz and Lie[7], shows the concern about the resistance of exposed surfaces under fire conditions, in this case guided by the ASTM E119 criteria for the unexposed surface to fire. The information and data increased the knowledge concerning the relationship between the unexposed surface temperature rise criteria of ASTM E119 and the ignition temperature of common combustible materials, assuming three modes of failure: structural collapse of the assembly, openings in the assembly which allow flames and hot gases to pass through, or excessive heat transfer through the assembly, resulting in high temperatures on the unexposed surface sufficient to ignite materials in contact or in close proximity with the barrier. This study concludes that the standards had a large safety factor included, and more economic solutions, without loss of safety, could be performed.

In 1994, the finite difference numerical model was presented by Mehaffey and Cuerrier et al [8] to perform studies across heat transfer in surfaces, and between surfaces and

cavities. The model was validated with experimental tests. Similar numerical methods are used in this work, applied to the calculations of heat transfer, being those calculations performed by the software ANSYS Fluent and ANSYS Multiphysics. This model is a bidimensional heat transfer model with and without fluid interaction, that uses partial differential equations to approach the results, using iterative and incremental procedures.

## 2.2 Light Steel Frame Studies

Facing the increase of use of LSF in constructions, fire resistance studies are performed to improve the reliability of the constructive method. In 1996, Gerlich et al [9] performed a study about fire behaviour on load bearing walls, with focus on the deflections caused by high temperatures on the steel structure, using a finite element model in TASEF software. A parametric study was also performed varying the thickness of the studs and tracks, aiming to minimize of the deflection. This work shows, among other conclusions, the use of the numerical simulations in design of this kind of walls.

Anyway, until the beginning of the XXI century, this research was limited, according Alfawakhiri et al [10], that made a literature survey and realize that the data available was limited to narrow choice from a few listed assemblies, and very little experimental data was available on the performance of loadbearing LSF walls exposed to fire. It was also noted that the numerical heat transfer models for non-insulated gypsum board cavity walls can predict temperatures with reasonable accuracy as long as the gypsum board stays in place. It is generally expected that future developments in numerical techniques will address cavity insulation and the fall-off of gypsum board. This wish expressed by Alfawakhiri et al [10] was partially fulfilled recently, where instigations were developed using a large amount of insulating materials in the cavities, with different thickness of the plasterboards and steel parts, and different configurations of the plasterboards and formats of the steel structures.

In 2003, Sakumoto et al [11] performed experimental studies of the fire resistance of walls and floor ceiling systems using galvanized light-gauge steel shapes with thickness up

to 1.6 mm, with increase in the number and thickness of gypsum boards and the use of reinforced gypsum boards. Effective results on partition walls, external walls and floors were obtained, with fire rating up to 60 minutes.

In 2006, Telue and Mahendran [12] developed numerical studies of gypsum structural influence in LSF walls, with models covered just by one side, that was also analysed by the authors in a previous experimental study, comparing the ultimate loads, load-deflection curves and failure models. The authors developed a design method based on the numerical results, that was proposed as a improvement to the standard method.

In 2007, Manzello et al [13] developed studies about LSF non-loadbearing walls in real fire conditions and standard tests, comparing this experimental results between them and with simulations, bringing huge contributes in the accuracy in the prediction of the wall failure by computational methods, related to failure of the gypsum boards. These failures increase the error in computational models, once that they are difficult to predict.

In 2011, Park et al [14] performed non-standard tests also in real fire conditions, with real walls, instrumented, as a attempt to increase the reliability of the parametric fire curves. The parametric fire temperature curve produced a fair approximation of maximum temperature and the time to reach was overestimated. There was a large difference in the temperature of the cooling phase, but this investigation provided valuable experimental data.

## 2.3 Cavities and Composites: the new concept

The cavities of the wall, filled initially with air, are one of the most promising objects of study, because filling this cavities with some material modifies the heat flux through the wall, the fire resistance and the acoustic performance.

In 2012 Balachandren Baleshan [15] developed an experimental and numerical study related to floor-ceiling using LSF systems, based on the innovative composite panel with insulation material. Author concluded that the structural and thermal behaviour of this innovative solution is superior than traditional LSF floor systems with and without cavity



insulation. A hybrid simulation used the experimental temperature results as inputs and runs were simulated under both steady and transient state conditions. The mechanical properties at elevated temperatures were considered based on the equations proposed by Dolamune, Kankanamge and Mahendran [16]. The results confirmed the superior performance of the innovative solution and a set of parametric simulations were developed. Kolarkar and Mahendran [17] perform an study inserting glass fiber, rock fiber and cellulose fiber, inside the cavities and between two plates of gypsum. This model of composite panels is an innovative way of construction, as an attempt to decrease the heat transfer and increase the fire resistance. Results were used to validate the numerical model for composite panels using time-temperature measurements. Studies as Kontogeorgos et al [18], consider more than just the heat transfer, but the effects of the mass transfer that occurs with the gypsum dehydration in high temperatures, and their effects on the LSF wall, as a way to obtain more accuracy in the simulations, and proposed to include this effect on the future mathematical models to increase the reliability.

Anyway, the research about new configurations continued. Kesawan and Mahendran [19][20] proposed modifications in the steel studs profile, usually a "C" profile, changing to welded profile, creating two enclosures inside the "C", increasing the fire performance of the LSF walls. Rusthi et al[21] performed a numerical study with 3D models using gypsum plasterboards showing good and accurate results for temperature field. Authors also present new material properties measured in gypsum and magnesium plasterboards. Preliminary numerical analysis indicates worse fire resistance when using magnesium plasterboards. Similar results to fire resistance were found when using calcium silicate board, as showed by Ariyanayagam and Mahendran [22], in a similar study using this material. This mixture of different materials with gypsum in a single layer is a new research line, assumed in this work.

Some investigations were developed in floors design with LSF, Jatheeshan and Mahendran[23], that analysed the fire resistance in floors, with and without insulation and considering single and dual plasterboards per floor. They also analysed the fire resistance of a new joint design, using welded hollow flange channel and the effect of web openings.

They concluded that the fire resistance in these cases only depend on the thickness of the steel and the yield strength reduction factors for cold-formed steels used to manufacture these joists.

The current research should contribute to the development of a new formula to avoid experimental tests and to provide exact fire resistance rating, based on the thermal analysis of the cross section. Experimental tests were performed with three different steel LSF structures, four different walls and also with fulfilled cavity, to increase the knowledge about the influence of the thickness of the gypsum plasterboard, the influence of the steel thickness and structure and the influence of the material of the wall in the fire resistance.

Non-loadbearing walls under fire tends to develop compressive load on the steel structure and usually achieve the mode of instability as a failure mode. Studs will bend towards the exposed side of the wall due to thermal gradient of the cavity of the wall is full scale. Local buckling and distortional buckling are going to occur in reduced scale walls. The variation of the stiffness within the cross section leads to a shift in the neutral axis of the cross section, being this effect already included in current version of Eurocode.

# Chapter 3

## Fire

This chapter presents the thermal load during a fire and some considerations that are necessary to perform numerical and experimental studies in this field of investigation.

A fire needs the combination of three simultaneous factors: a heat source, a fuel and an oxidizing, starting when the mix of fuel and oxidizer is hot enough to ignite [24].

### 3.1 Heat Transfer Theory

Heat is one of the two possible interactions of a system and its surroundings that transfer energy. The heat transfer is an extension of the thermodynamic analysis through the relations to calculate heat transfer rates. Bergman and Incropera [25] define heat transfer as thermal energy in transit due to a spatial temperature difference. When this temperature difference exists in solid or fluid stationary medium, the heat flux across the medium is defined as conduction. When this temperature difference exists between a surface and a moving fluid, the heat flux is defined as convection. A third mode of heat transfer between two surfaces that exchanges energy in form of electromagnetic waves is called radiation. This mode of heat transfer does not depend on the medium.

On the fire exposed surface, according to Eurocode 1, part 1-2 [26], the net heat flux should be determined as a summation of convection and radiation, see eq. 3.1 here the  $\dot{h}_{net,c}$  is the heat transfer by convection, see eq. 3.2 and  $\dot{h}_{net,r}$  represents the heat transfer

by radiation, see eq. 3.3.

$$\dot{h}_{net} = \dot{h}_{net,c} + \dot{h}_{net,r}[W/m^2] \quad (3.1)$$

$$\dot{h}_{net,c} = \alpha_c \cdot (T_g - T_m)[W/m^2] \quad (3.2)$$

$$\dot{h}_{net,r} = \Phi \cdot \epsilon_m \cdot \epsilon_f \cdot \sigma \cdot [(T_g + 273)^4 - (T_m + 273)^4][W/m^2] \quad (3.3)$$

On the unexposed side of separating members and partition walls, the net heat flux should be determined with  $\alpha_c = 9[W/m^2]$  when assuming it contains the effects of heat transfer by radiation or  $\alpha_c = 4[W/m^2]$  if the radiation effects is also to be considered. If the surface emissivity of the member ( $\epsilon_m$ ) is not specified by standards, this value can be assumed as  $\epsilon_m = 0.8$ . The view factor ( $\Phi$ ) should be taken as  $\Phi = 1.0$ , or a lower value can be assumed to take into account the so called shadow effects. The emissivity of fire is usually consider as  $\epsilon_f = 1$  [26].

The gas temperature ( $T_g$ ) may be adopted as a nominal temperature-time curve. This work uses the standard temperature-time curve, that is presented in the section 3.3.

## 3.2 Natural Fire Curve

The natural fire curve is composed by four periods: the ignition, the propagation, the development and the extinction, as demonstrated in the Figure 3.1.

The ignition period has low temperatures, and does not have significant influence in the fire resistance of the structures, and, because of this fact, this period isn't included in the standard models of fire. This period, without structural significance, is the period when the toxic gases are produced, and have a critical significance when dealing with human lives.

The propagation period englobes the "flashover" and the continuous combustion. The "flashover" is the period when the fire is expanded to the compartment, that occurs wen

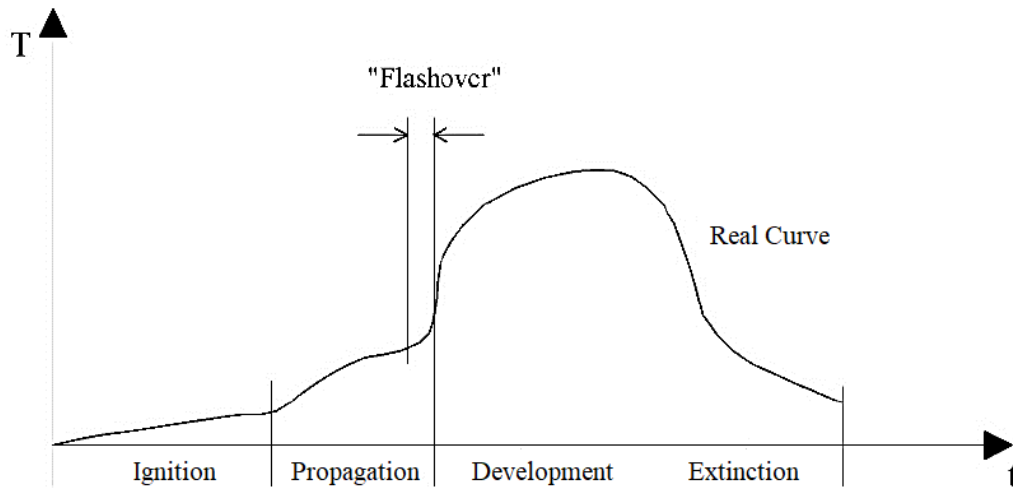


Figure 3.1: Natural Fire Curve [24].

the temperature near the ceiling is between  $450^{\circ}\text{C}$  and  $600^{\circ}\text{C}$  or when the heat flux in the floor reads  $20\text{ W/m}^2$ . The continuous combustion period is the period immediately after the "flashover", and is the period when the maximum temperature is obtained and this value remains approximately constant. High levels of concentration of carbon dioxide ( $\text{CO}_2$ ) and carbon monoxide ( $\text{CO}$ ) are verified in this period caused by the heat release of the most part of the combustible.

After the propagation period, the extinction period, or cooling period, initiates, and is when the rest of the combustible is burned, and the rate of combustion decreases, as the temperature, until the completely end of the fire.

Natural fire is a trend and a must to future design rules (performance based design). This requires a better understanding of the element or structure during cooling. The material behaviour under cooling also requires knowledge, but this behaviour depends essentially of the cooling rate. Research on structural behaviour after the time of maximum temperature are very scarce and focus mainly on residual load bearing capacity. Element failure under natural fire depends also in its security. A new indicator was already suggested by Thomas and Jean Marc-Franssen [27] to determinate the fire resistance.

### 3.3 Standard Fire Curves

The standard models of fire are approaches of the natural fire curve and are independent of space and fire load density. These curves generally approach the "flashover" and the continuous combustion, that is the most critical periods of fire in the structural and thermal studies.

The Eurocode 1 dealing with actions on structures exposed to fire [28] presents three nominal curves of fire: the standard curve, also called ISO834, the external elements curve and the curve of fire caused by hydrocarbons. This work uses the standard curve, see Equation 3.4 and plotted in the Figure 3.2. For this case, the coefficient of heat transfer is  $\alpha_c = 25W/m^2K$ .

$$\theta_g = 20 + 345 \log_{10}(8t + 1) \quad (3.4)$$

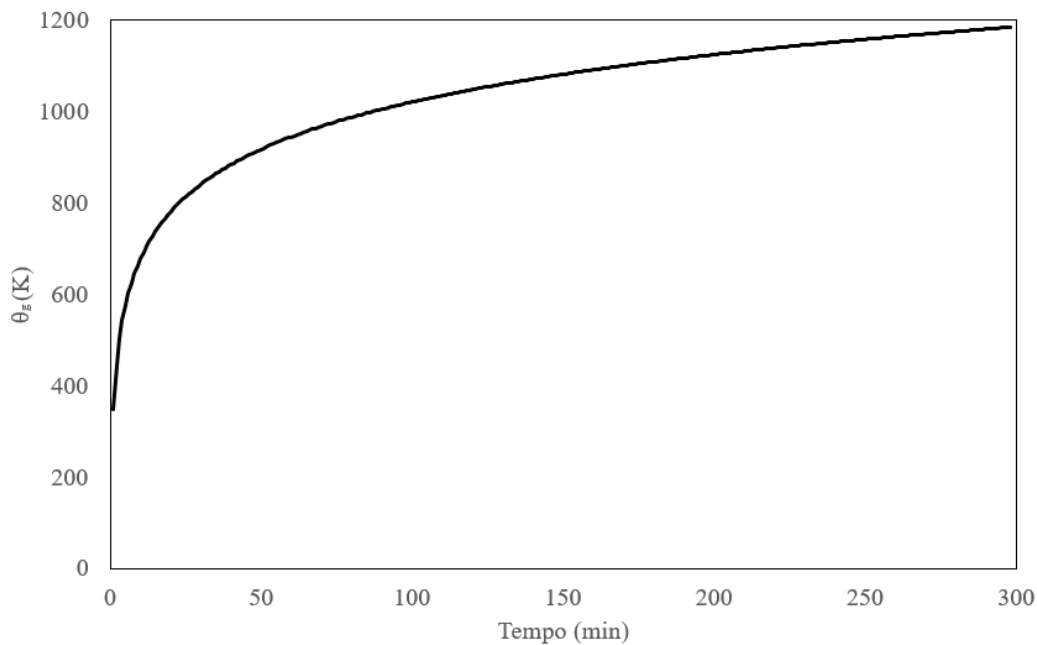


Figure 3.2: ISO 834 Standard Curve.

# Chapter 4

## Wall Specimens

This chapter will present the assembly and design of the wall specimens and characterization of the tests, as recommended by standards.

### 4.1 Standards to be used

The standards used to obtain the fire resistance of non-loading bearing LSF walls are the EN 1363-1 (Fire Resistance Tests - General Requirements), EN 1364-1 (Fire Resistance Tests for Non-loadbearing Elements - Walls) and Eurocode 3 (EN 1993-1-2 - Design of Steel Structures - General Rules: Structural Fire Design).

#### 4.1.1 EN 1363-1

The EN 1363-1 establishes the general principles for determining the fire resistance of different elements of construction, when subjected to standard fire exposure conditions [1]. A specially designed furnace is required to subject the test specimen to the test conditions. The system to control the temperature of the furnace, the equipment to control and monitor the pressure of the hot gases within the furnace, the frame in which the element can be inserted and submitted to appropriate heating, pressure and support conditions. The arrangement for loading and restraint of the test specimen should be appropriate,

including control and monitoring of the load equipment for measuring temperature in the furnace and in the test specimen. For some cases, the system for measuring the deflection of the test specimen is required. Also in some cases, specific devices are required to evaluate the integrity and for establishing compliance with the performance criteria. For very special cases, the equipment for measuring the oxygen concentration of furnace gases is also required. This standard for testing also specifies the design and tolerances about systems, including some sketches about the sensors, such as the disk thermocouples and plate thermocouples.

The performance criteria used to validate the tests of fire resistance of non-load bearing walls are the insulation criteria (I). By definition this is the time, in completed minutes, for which the test specimen continues to maintain its separating function during the test without developing temperatures on its unexposed surface, which increase the average temperature above the initial average temperature by more than 140 K or increase at any location (including the roving thermocouple) above the initial average temperature by more than 180 K [1]. The performance criteria "insulation" shall automatically be assumed not to be satisfied when the "integrity" criterion ceases to be satisfied. The integrity criteria (E), in this case, concern about the time of flame or smoke pass through the unexposed side by some crack.

It's important clarify that the main performance criteria given by this standard is the loadbearing criteria or stability. The load bearing resistance (R) is the ability to support its test load without exceeding specified criteria with respect to the extent of deflection or rate of deflection. The assessment shall be made on the basis of limiting vertical contraction ( $C=h/100$  [mm]), or limiting rate of vertical contraction ( $dC/dt=3.h/1000$  [mm/min]). The measurement of the horizontal deformation is also mandatory. This study concerns about the fire resistance of nonloadbearing walls, reason why this criteria is not analysed.



### 4.1.2 EN 1364-1

The EN 1364-1 contain the procedures to perform the experimental tests to measure the fire resistance of a non-loadbearing wall to resist the fire propagation from one side to another [2].

For this experiments, more information about the requirements are specified. A rigid frame with high stiffness and low thermal expansion is requested to fix the specimen.

The dimension of the specimen should be defined in accordance to the following rule: if the width or the height of the construction element is smaller than 3 m, the specimen should be tested in its actual size. If one of the dimensions of the construction element is bigger than 3m, the dimension should not to be less than 3m in the test. Anyway, the wall dimensions in this investigation were restricted by the furnace aperture, and is highly recommended that the maximum size of the wall coincide with this size, in this case 1m.

This standard also gives information about the instrumentation. The control of the furnace temperature should be made by plate thermocouples in its interior, with the biggest surface turned to the furnace wall. There should be one for each 1,5m<sup>2</sup> of exposed surface to be tested. In case of walls with expected fire insulation bigger than 5 minutes, disk thermocouples shall be attached to the unexposed side in order to obtain the average and maximum temperature developed, see section 4.3. The recommendation is to put 5 thermocouples to measure the average temperature, one in the centre of the specimen, and the another 4 in the centre of each fourth part of the wall. The recommendation to measure the maximum temperature is to use 7 more thermocouples.

### 4.1.3 EN 1993-1-2

The Eurocode 3 (EN 1993-1-2) applies to the design of steel buildings . It complies with the principles and requirements for the safety and serviceability of structures. The basis of their design and edification are given in EN 1990 – Basis of structural design. The EN 1993-1-2 deals specifically with the design of steel structures for the accidental condition in fire [28]. Walls made with LSF have a steel structure. The load-bearing

function of a steel member should be assumed to be maintained after a time  $t$  in a given fire, if the condition in the equation 4.1 is satisfied.  $E_{fi,d}$  is the design effect of actions for the fire design situation, according to EN 1991-1-2 and  $R_{fi,d,t}$  is the corresponding fire design resistance of the steel member at time  $t$ .

$$E_{fi,d} \leq R_{fi,d,t} \quad (4.1)$$

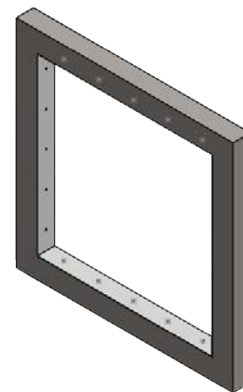
For members with class 4 cross-sections other than tension members it may be assumed that this relation is satisfied, if at time  $t$ , the steel temperature at all cross-sections is not more than a critical temperature, recommended as  $\theta_{crit} = 350^\circ C$ . This criterion may be too conservative and unsafe for specific cases, because this simple method is independent of the load ratio. This criterion is going to be used to assess the stability of the wall, just in case of loadbearing conditions are to be applied.

## 4.2 Laboratory Facilities

The tests were performed in the Laboratory of Structures and Resistance of Materials from the Polytechnic Institute of Bragança. The furnace and the frame are presented in the figure 4.1.



(a) Furnace with the frame attached.



(b) Frame (schematic).

Figure 4.1: Furnace

The furnace has capacity for specimens dimensions of 1x1m and is running with natural gas using four burners lagged in height and depth, with 90kW each of maximum power. The temperature of the gas furnace followed the standard fire ISO curve. The furnace have one door in the front and one opening in the top. The total free volume is 1m<sup>3</sup>. The frame was aligned with the front door.

The data acquisition system is a MGC Plus system manufactured by HBM, with 3 modules with 8 channels each, and was used with frequency of acquisition of 1Hz. A total of 22 channels were available for measurements of temperatures. Additionally to the system of acquisition, an IR thermal camera was used, FLIR BT Series T365, to define the temperature in the unexposed side. The frequency of acquisition of the camera was 1.25Hz, with an amplitude of temperature between 15°C and 250°C and the resolution of the camera is 320x240 pixels.

### 4.3 Sensors Specifications

To measure the temperature in the wall, three types of thermocouples were used. All the thermocouples are type K with wires of 0.7 mm in diameter.

The temperature of the exposed side of the wall was measured with a mineral-insulated thermocouple from RÖSSEL-Messtechnik, specification AL-KB-1,5-1500-0,1,KI.1, with connection cable, made with a nickel-chromium alloy and with 1.5 mm of diameter per 100mm of length, see fig 4.2a. To measure the temperature in the steel, welded thermocouple were in the structure. In some cases, as in the composite walls and in the fulfilled cavity, these cables was twisted and inserted in the material, see fig 4.2b.

To measure the temperature of empty cavities, plate thermocouples were used. They are located at half height of each cavity. The dimensions and construction specifications of these thermocouples are given in the EN 1363-1 [1], see Figure 4.3a. Normal the thermocouple type K are fixed to the plate and the curves of the temperature of the cavities are very smooth, because the plate is in thermodynamic equilibrium with the cavity. The disk thermocouple used to measure the unexposed side, as specified in the

subsection 4.1.2, is presented in the figure 4.3b. These cooper disks are protected with an insulation pad made with a silicate-fibre, that is used to fix these sensors to the surface, once there should be no adhesive between the cooper disk and the surface to be measured.

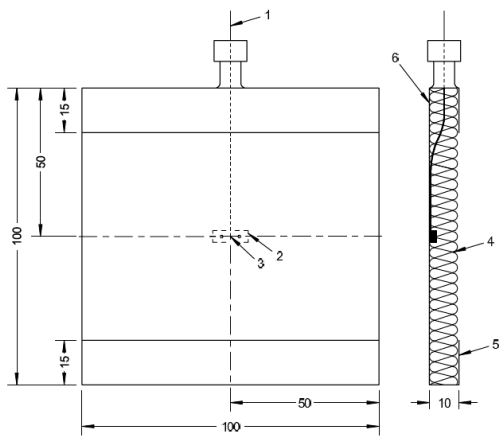


(a) Bed Thermocouple.

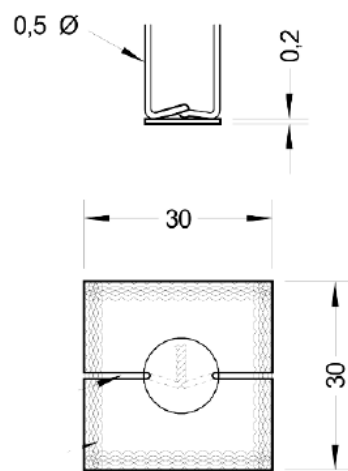


(b) Welded Thermocouple.

Figure 4.2: Bed Thermocouple and Welded Thermocouple.



(a) Plate Thermocouple [1].



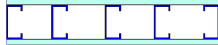
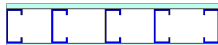

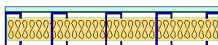


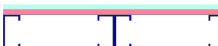

(b) Disk Thermocouple [1].

Figure 4.3: Plate Thermocouple and Disk Thermocouple.

## 4.4 Specimens

The table 4.1 shows the number of specimens to be tested and its configurations.

Table 4.1: Specimens to be tested.

Specimen	Insulation cavity	Plate Layer [mm]	Spacing Studs	Cross section
0 (Test)	No	1x12.5 (Gypsum)	233mm	
1	No	1x12.5 (Gypsum)	233mm	
2	No	2x12.5 (Gypsum)	233mm	
3	Rockwool	1x12.5 (Gypsum)	233mm	
4	No	1x12.5 (Gypsum) 1x 10 (Cork)	233mm	
5	No	1x12.5 (Gypsum) 1x10 (Cork)	466mm	
6	No	1x12.5 (Gypsum) 1x 10 (Cork)	487,5mm	
7	No	1x12.5 (Gypsum) 10 mm (OSB)	233mm	

The tracks used are U93x43x1.5, steel grade S280GD, and the studs are C90x43x15x1,5, steel grade S280GD. A five studs per track was adopted to investigate the effects of the different material for plates in the structure. The material configuration for the walls was: single gypsum plasterboard, double gypsum plasterboard, cork-gypsum plasterboard composite and wood-gypsum plasterboard composite. For the cork, a special study will be conducted, keeping the cork-gypsum plasterboard composite and modifying the steel cross sections. This constructive solution was selected to evaluate the fire performance. A test with rock wool was also conducted, to evaluate the fire performance of the insulation

material inside the cavity.

The plasterboards could be fixed following 4 configurations, see fig 4.4.

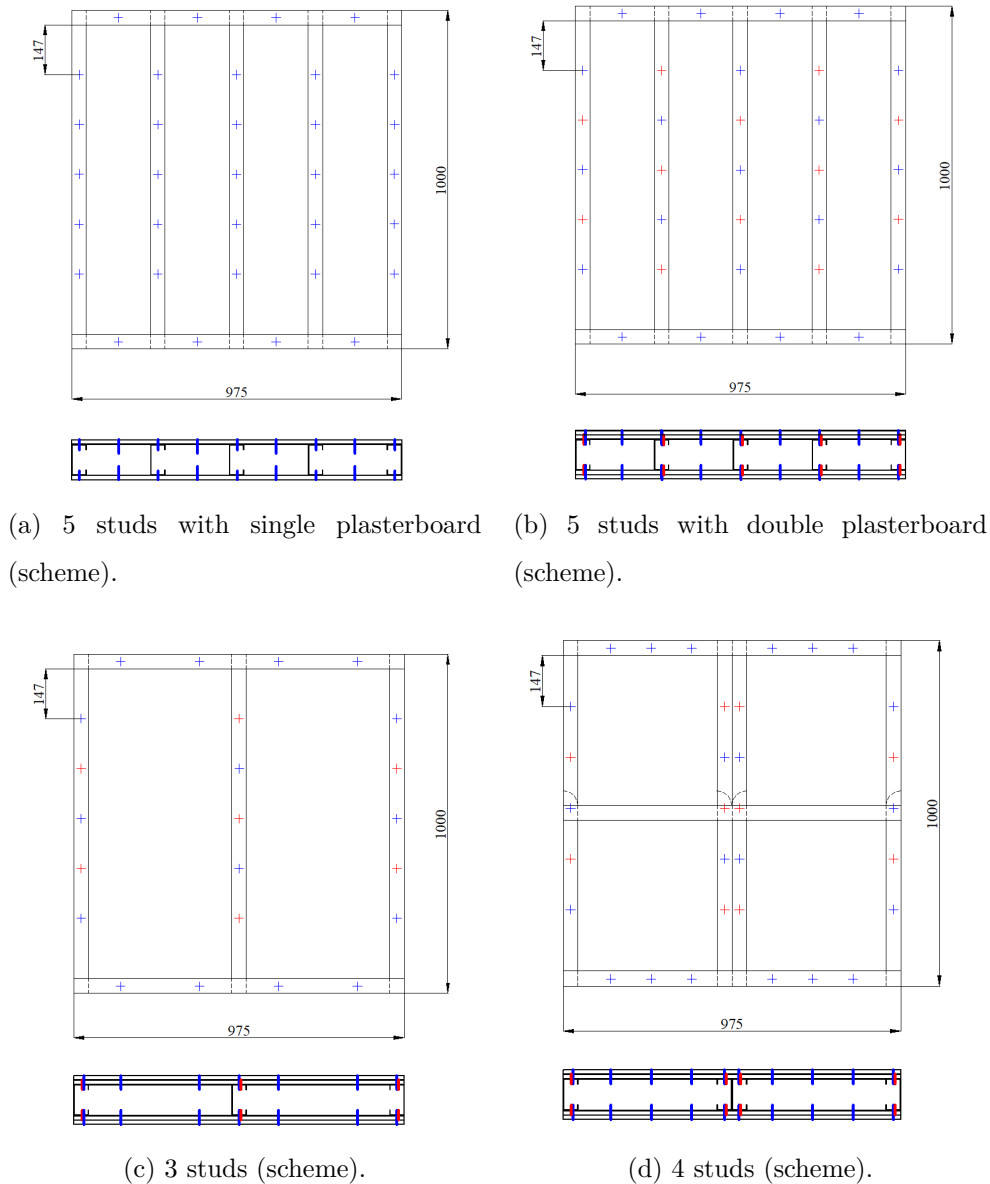


Figure 4.4: Position of the screws in the plasterboards with 5 studs.

The single layer walls were fixed with 30mm self-drilling screws, and the composite walls have the first layer fixed with this same screws and the second layer fixed with 50mm self-drilling screws. To assembly this two layers of plates, the first plate was fixed using

half of the screws, then the second layers of plate was fixed with the second half of the screws. The joints between the studs and tracks were defined with only one self drilling screw positioned at the geometry centre of the joint.

#### 4.4.1 Specimen 0 and Specimen 1

To get some knowledge about the construction method and the procedures to be executed, a test 0 was performed as a preliminary analysis with the same configuration of Specimen 1. The figure 4.5 shows the thermocouples position in this tests, where BT refers to Bed Thermocouples, PT refers to Plate Thermocouples, DT refers to Disk Thermocouples and WT refers to Welded Thermocouples.

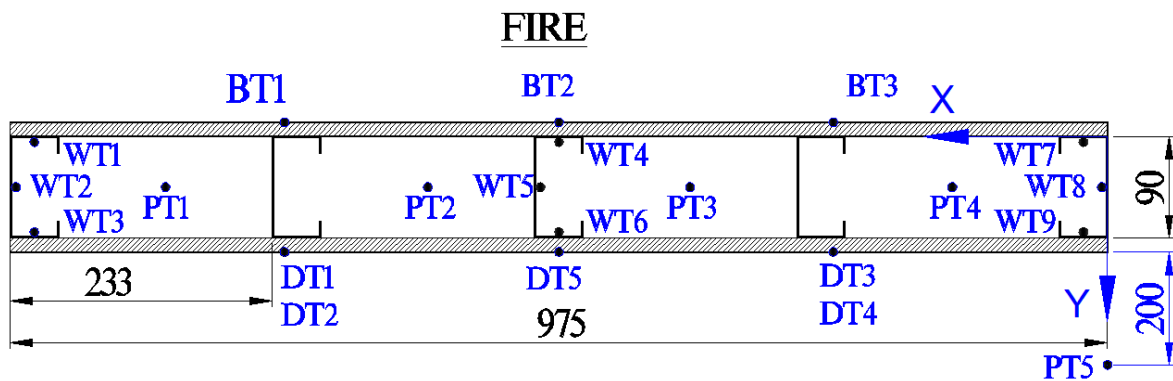


Figure 4.5: Thermocouples Position on Specimen 0 and 1.

First of all, the tracks and studs are drilled. Some drills were done in the structure to fix the steel frame to the partial frame of the furnace and to pass the wire that hold the plate thermocouples in the cavities. A semi circular channel was machined in the bottom of some studs to pass the thermocouples. The thermocouples are positioned and welded in the steel structure, and then the structure is assembled.

After assembling the LSF structure, the plate thermocouples are positioned in the cavities and the specimen is fixed in the frame. Glass fibre is used to fulfill the empty spaces between the wall and the frame, and once all the thermocouples are verified and identify, the specimen is positioned in the furnace. The plasterboards are fixed and a

gypsum coating is applied around the borders of the the plates. The bed thermocouples in the exposed side and the disk thermocouples in the unexposed side are fixed and then the specimen is ready to be tested. The specimen 0 is presented in the figure 4.6a

The test 1 was performed with a pink gypsum plate with a especial treatment, that brings more integrity to the plate with a reinforcement of glass fibre and vermiculite, as is shown in the figure 4.6b.

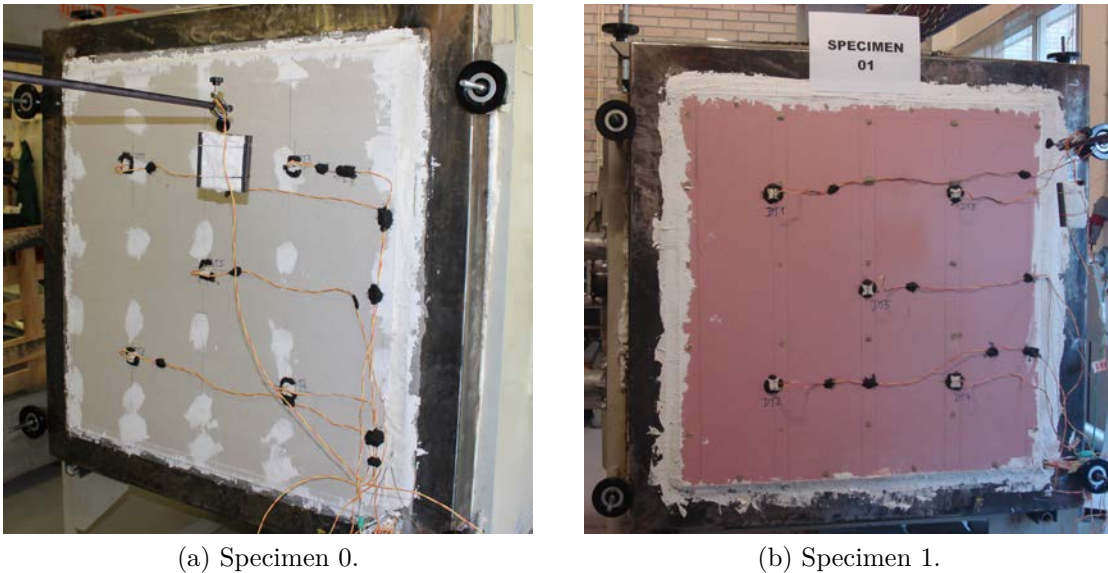


Figure 4.6: Specimens 0 and 1.

#### 4.4.2 Specimen 2

The specimen 2 was made with two plasterboards, with a total thickness of 25mm of plasterboard in each side. The pink plate was used in this case too, and additional thermocouples were inserted between the plasterboards, WT10 and WT11, as presented in figure 4.7. The figure 4.8 shows the specimen 2 already prepared to be tested in the furnace. The wholes made by the screws were also protected with a small amount of gypsum.



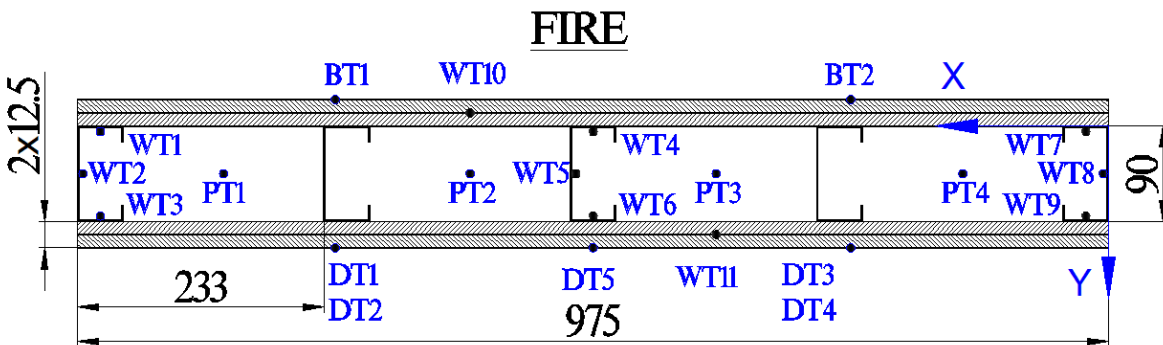


Figure 4.7: Thermocouples Position on Specimen 2.

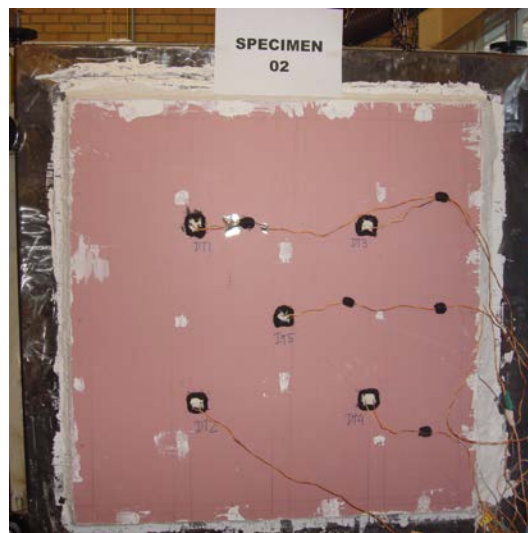


Figure 4.8: Specimen 2.

#### 4.4.3 Specimen 3

The specimen 3 has single layer of plasterboard, but the cavity is filled with Rockwool. The rockwool used in this case has density of  $75\text{kg/m}^3$ . The thermocouples are distributed by the specimen as presented in the figure 4.9.

The figure 4.10a shows the specimen already prepared to be tested in the furnace. The figure 4.10b shows the cavity filled with the rockwool and the thermocouples that are measuring the temperature inside the insulation material (half thickness).

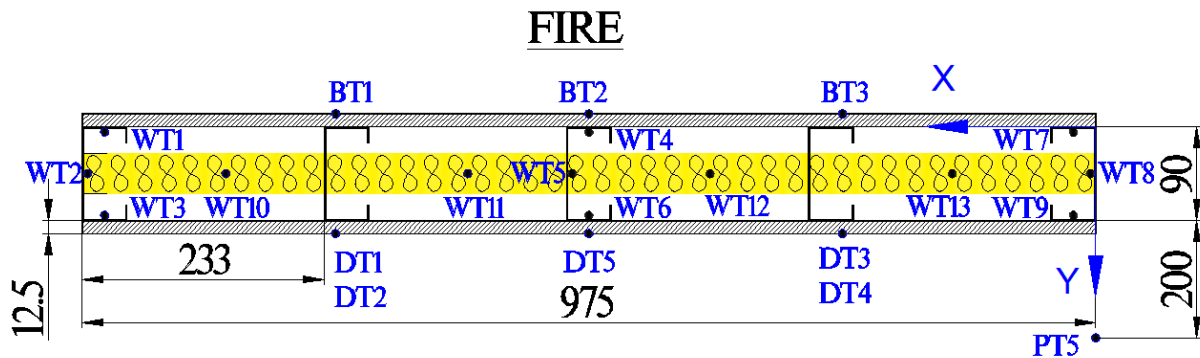
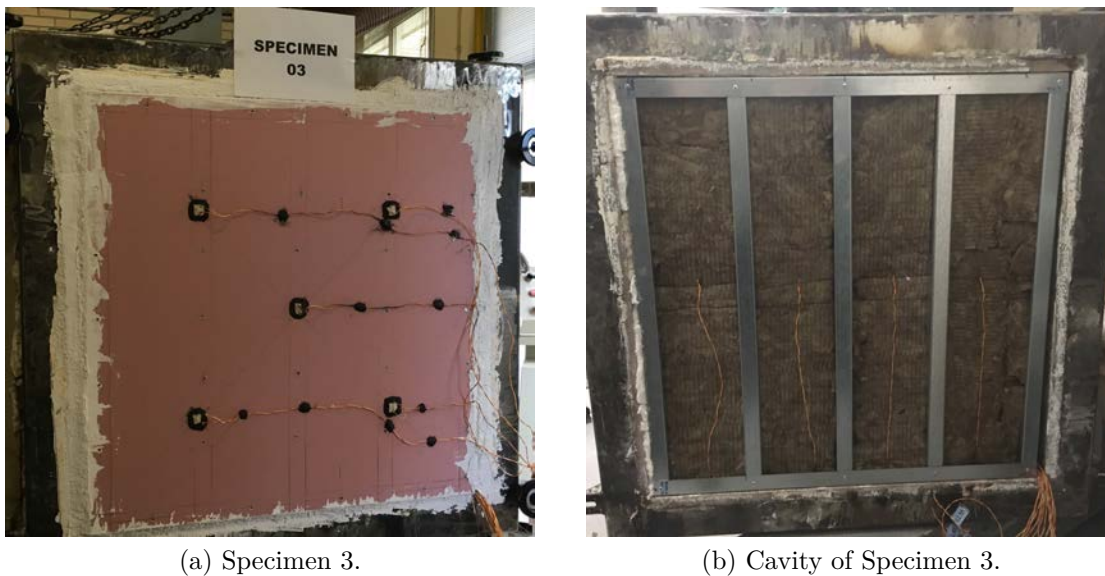


Figure 4.9: Thermocouples Position on Specimen 3.



(a) Specimen 3.

(b) Cavity of Specimen 3.

Figure 4.10: Specimen 3.

#### 4.4.4 Specimen 4

The specimen 4 is the first of three tests using composite layer of cork and gypsum plasterboard. This case has the same LSF structure of the previous tests (5 studs and 2 tracks). The thermocouples distribution is presented in fig 4.11, the figure 4.12a shows the cork layer with the thermocouple position to measure the temperature between the composite plate. Figure 4.12b shows the specimen prepared to be tested.

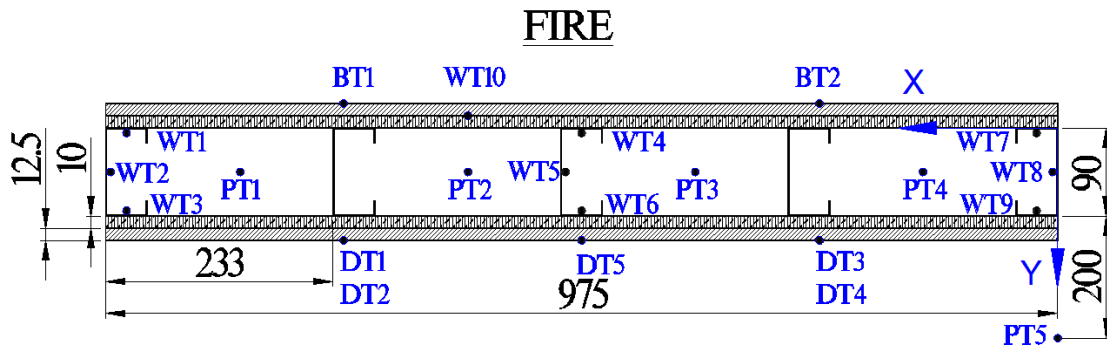
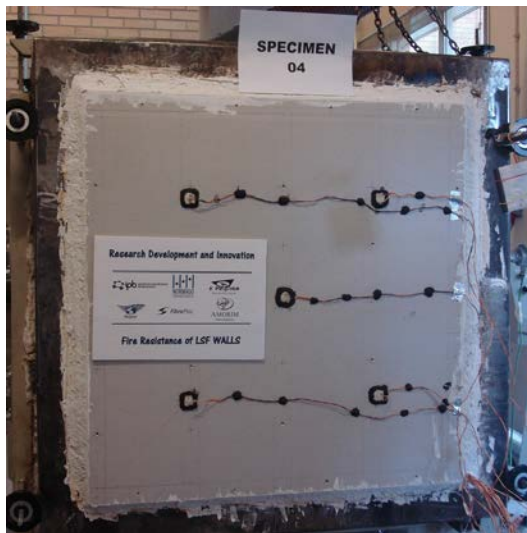


Figure 4.11: Thermocouples Position on Specimen 4.



(a) Cork Layer in Specimen 4.



(b) Specimen 4.

Figure 4.12: Specimen 4.

#### 4.4.5 Specimen 5

The specimen 5 has the same composite layer of the specimen 4, but with different LSF structure (3 studs and 2 tracks). That solution creates in two cavities, bigger than the dimensions of the cavities in LSF structure with 5 studs. The thermocouples used in this test are presented in the figure 4.13 and the figure 4.14b depicts the specimen ready to be tested..

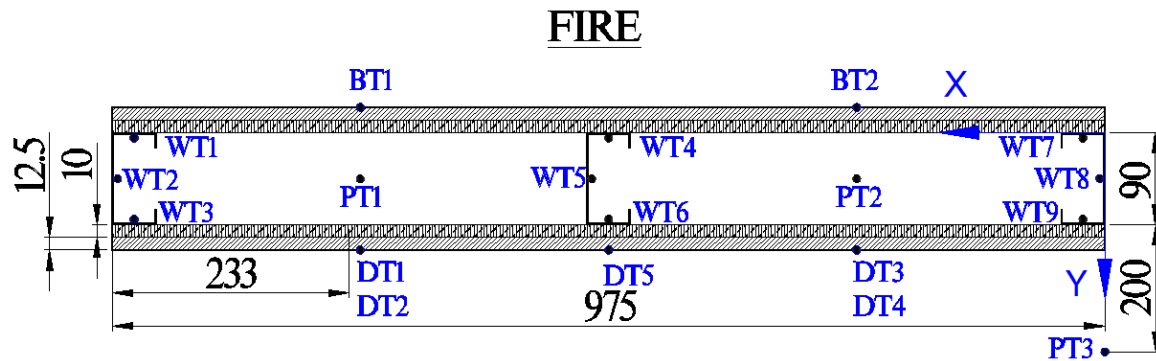


Figure 4.13: Thermocouples Position on Specimen 5.



(a) Cork Layer in Specimen 5.



(b) Specimen 5.

Figure 4.14: Specimen 5.

#### 4.4.6 Specimen 6

The specimen 6 is the third specimen with a composite layer of cork and gypsum. This LSF structure have 4 studs and a reinforcement at mid height, producing 4 cavities. The position of the thermocouples is presented in the figure 4.15 and the figure 4.16 presents the specimen ready to be tested.

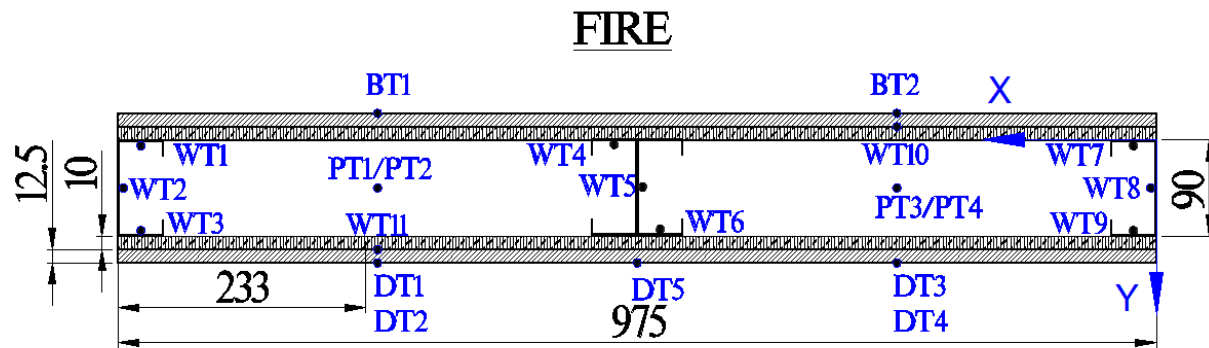
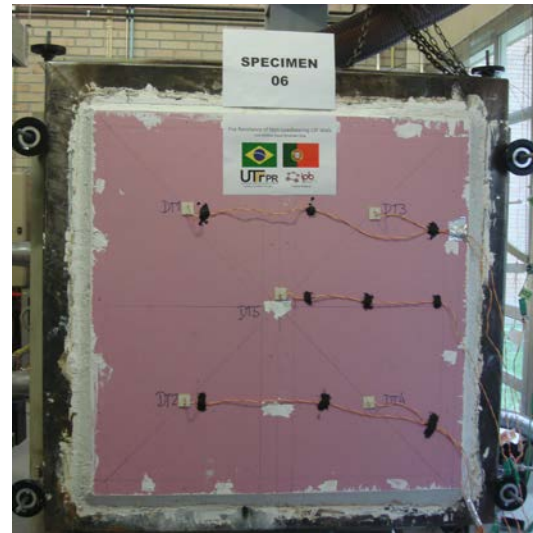


Figure 4.15: Thermocouples Position on Specimen 6.



(a) Structure in Specimen 6.



(b) Specimen 6.

Figure 4.16: Specimen 6.

#### 4.4.7 Specimen 7

The specimen 7 is a single test made with a composite solution of OSB and gypsum plasterboard. This test was included to compare the fire resistance of this composite solution with the previous cork-gypsum composite wall. The LSF structure is made with 5 studs. The thermocouples distribution is presented in fig 4.17 and the figure 4.18 shows the specimen during the assembly and ready to be tested. This composite layer uses the normal gypsum plate (white).

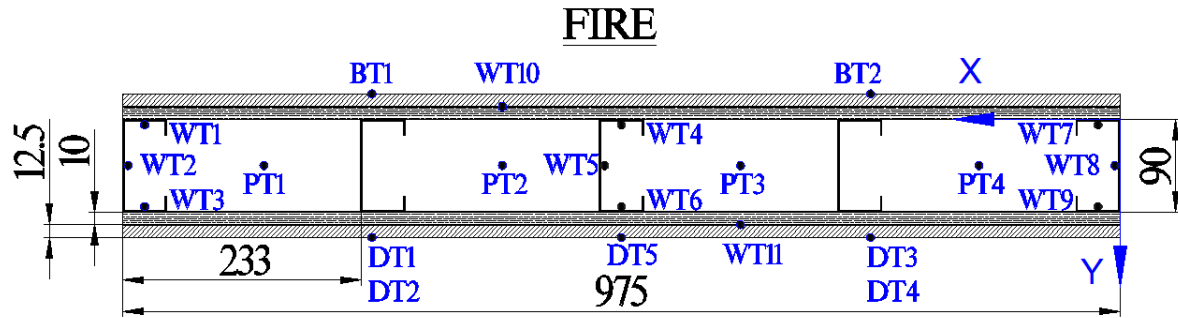


Figure 4.17: Thermocouples Position on Specimen 7.



(a) Cavity in Specimen 7.



(b) Specimen 7.

Figure 4.18: Specimen 7.

# Chapter 5

## Experimental Tests

This chapter presents the results of the experimental tests and some comparisons between them. For better understanding, the average of the measurements was renamed: the Bed Thermocouples have the acronym as "FS", the Disk Thermocouples have the acronym in the graphics as "Unexp", the Welded Thermocouples 1, 4 and 7 have the acronym "HF", the Welded Thermocouples 2, 5 and 8 have the acronym "WEB", the Welded Thermocouples 3, 6 and 9 have the acronym "CF" and the Plate Thermocouples have the acronym "Cav". In some tests, an extra plate thermocouple is positioned outside the furnace to measure the increase of the temperature at 200mm from the unexposed surface. This thermocouple is a single measurement, and is identified as "AMB". The results are presented in the next sections, and more informations about the tests can be observed in the appendix A.

The table 5.1 presents a compilation of the fire resistance results of the experimental tests. The value of fire resistance of the specimen 0 is not calculated by the standard, and this value is inserted in the table just for reference. For this reason, the data of this tests was not considered in the analysis. The last three columns of table 5.1 present the time that each LSF structure took to achieve 350 °C. This criterion can be used to estimate the stability of the structure (R). This fire rating (R) as not considered to the assessment of the non-loadbearing LSF wall, but is an important value to take into consideration for validation purposes.

Table 5.1: Results of the Tests.

Specimen	Insulation cavity	Plate Layer	Spacing Studs [mm]	Fire resistance [min] (I)	HF= 350°C Time [min]	WEB= 350°C Time [min]	CF= 350°C Time [min]
0	No	1x12.5 mm	233	45*	30	39	43
1	No	1x12.5 mm	233	70	31	45	51
2	No	2x12.5 mm	233	118	75	82	85
3	Rock Wool	1x12.5 mm	233	87	35	50	47
4	No	1x12.5 mm 1x 10 mm (Cork)	233	51	32	34	35
5	No	1x12.5 mm 1x 10 mm (Cork)	466	66	39	39	41
6	No	1x12.5 mm 1x 10 mm (Cork)	487,5	69	43	44	42
7	No	1x12.5 mm 10 mm (OSD)	233	75	50	51	55

## 5.1 Specimen 0

The specimen test had some problems with the data acquisition system, and some information was lost in the process. Two failures were identified at time equal to 25 minutes. The fire resistance, for this reason, was not calculated. The IR camera, anyway, capture data during all the test, and a fire resistance of 45 minutes was estimated using the average temperature of the thermal images. This method to determinate the fire resistance using the IR Camera is not specified in the text standard, and this is the reason why the fire resistance in this case is consider as an estimative.



The figure 5.1 shows the average temperature evolution of the thermocouples across the time. With linear regression, some failures were estimated. The estimated points are drawn with dashed line.

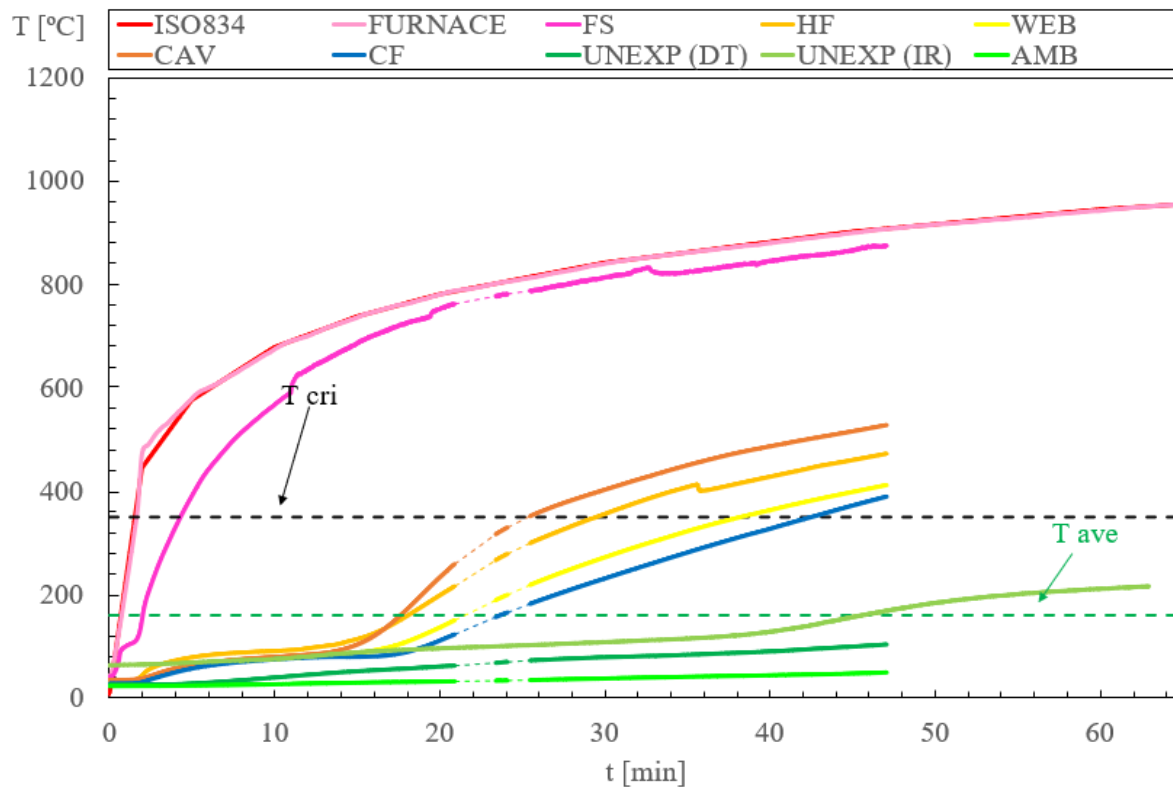


Figure 5.1: Specimen 0 - Average Temperature Results.

More comments and photographs about the this specimen are presented in the appendix A.1.

## 5.2 Specimen 1

The specimen 1 has the same configuration of the specimen 0 (test), and no problem was identified during measurements. The thermal effect of the pink plate was not so evident, because the main function of this pink cover is related to integrity, without significant increases in fire resistance (insulation). The fire resistance was determined for this case in 70 minutes, using the average temperature criterion. The maximum

temperature criterion gives a fire resistance of 71 minutes. The figure 5.2 shows the average temperatures of the thermocouples across the time. The fire resistance, in this case, is quite different of the estimative presented in the previous section to the specimen 0. This increase of fire resistance (I) can be justified by the use of the pink plates, that helps the integrity of the plates, reducing the number of cracks. The cavity 2, with the sensor PT2, was the region where the first crack occurred.

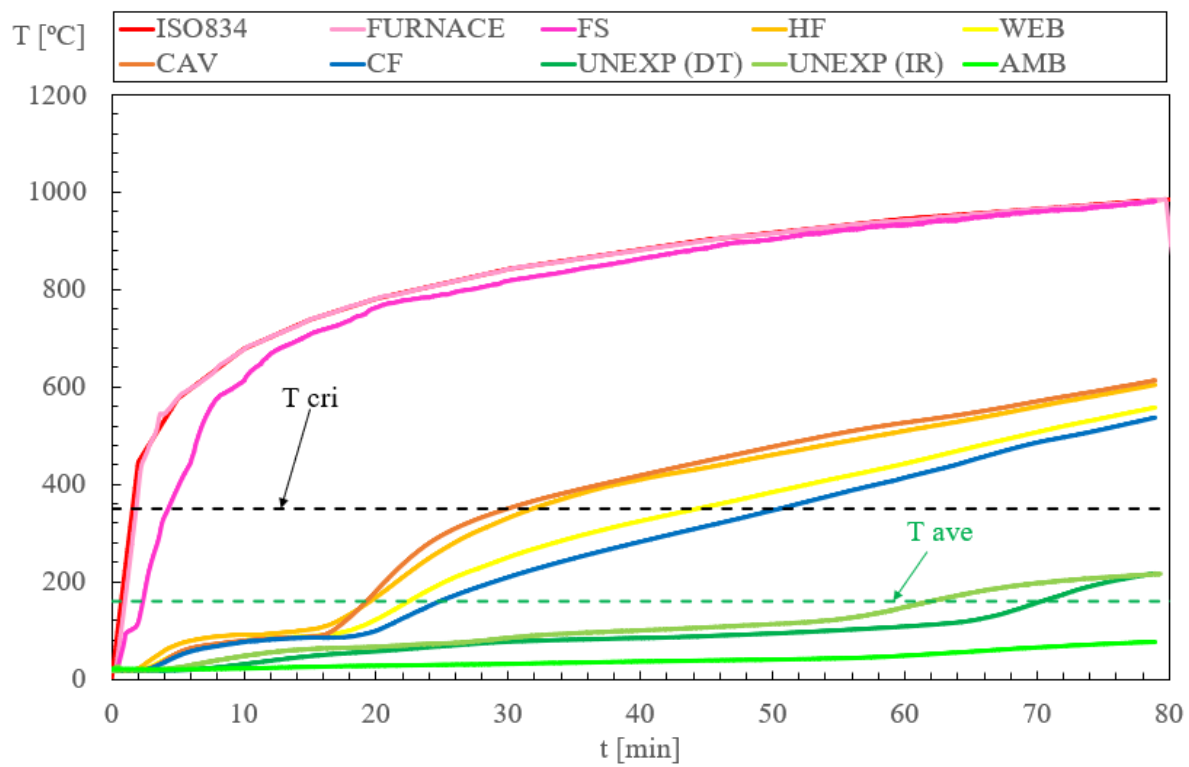


Figure 5.2: Specimen 1 - Average Temperature Results.

More comments and photographs about the this specimen are presented in the appendix A.2.

### 5.3 Specimen 2

The figure 5.3 shows the average temperature measurements of the thermocouples. The specimen 2 has two layers of gypsum plates in each side. Approximately 16 minutes

after the beginning of the test, the BT1 sensor was lost, after 80 minutes of test, the cavity was exposed to fire. This can be verified next figure, with the increase of the temperature evolution. The fire resistance was determined to be 118 minutes, in this case defined by the maximum temperature criterion. The average criterion gives a fire resistance of 119 minutes. After 122 minutes, the unexposed plate broke, and the test was stopped.

In this test, the temperature between the two plates was measured with a thermocouple type K inserted superficially in one of that plasterboards. This thermocouple was identify to be WT11 and WT12. The graphic solution for this results is identified as PB1-PB2 and PB3-PB4, respectively.

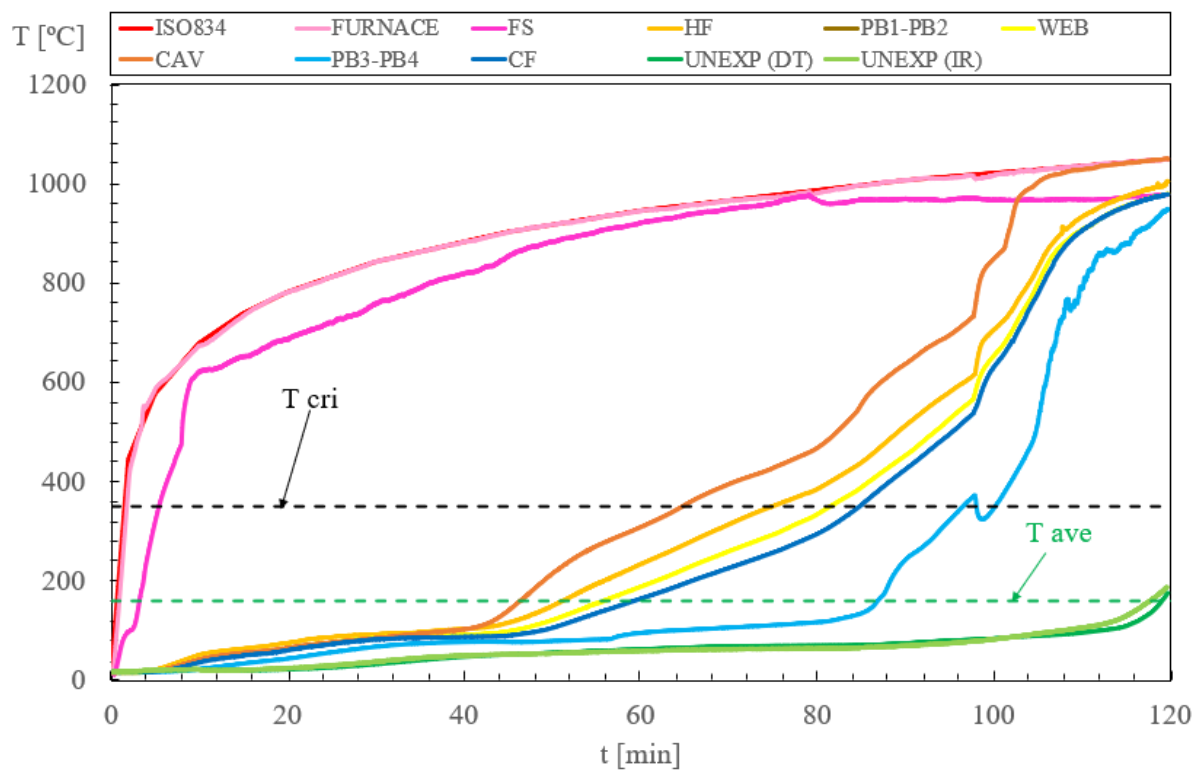


Figure 5.3: Specimen 2 - Average Temperature Results.

More comments and photographs about the this specimen are presented in the appendix A.3.

## 5.4 Specimen 3

The figure 5.4 shows the average temperature measurements. This specimen has one single layer plate and the cavity is filled with rockwool. This construction solution is to be compared with the previous specimens. The sensor WT12, located in the third cavity, presented some problems during the test, so these results were discarded. The second cavity, measured by the sensor WT11, was the first cavity to be exposed to fire, as can be seen in the temperature evolution. The fire resistance was determined by the maximum temperature criterion in 87 minutes. The average criterion gives a fire resistance of 89 minutes. This value is bigger than the fire resistance of the specimen 2, that uses two layers of plasterboard but with no insulation in cavity.

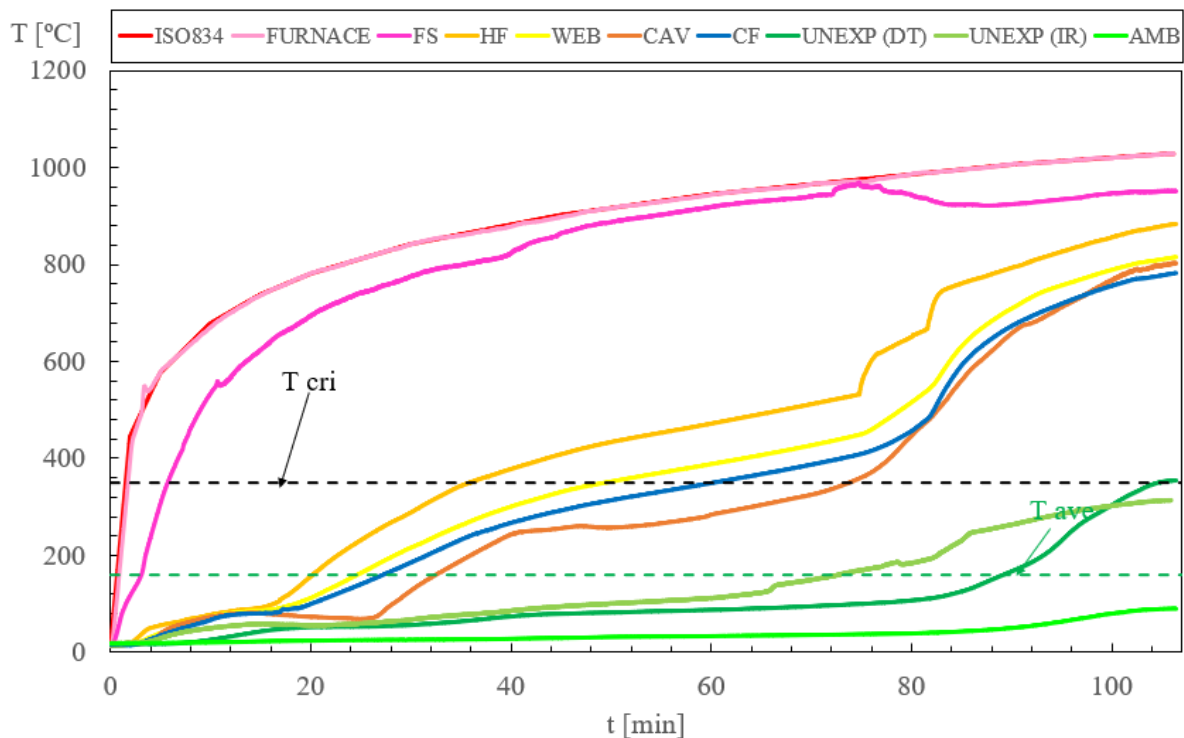


Figure 5.4: Specimen 3 - Average Temperature Results.

More comments and photographs about the this specimen are presented in the appendix A.4.

## 5.5 Specimen 4

The specimen 4 is the first of the three specimens that is protected with a cork-gypsum composite layer. Cork, as a derivative of wood, is combustible, but once the external layer of the material is created (a char layer), this helps to decrease the heat transfer through the plate. The figure 5.5 shows the results of this test, for the average temperature of measurements.

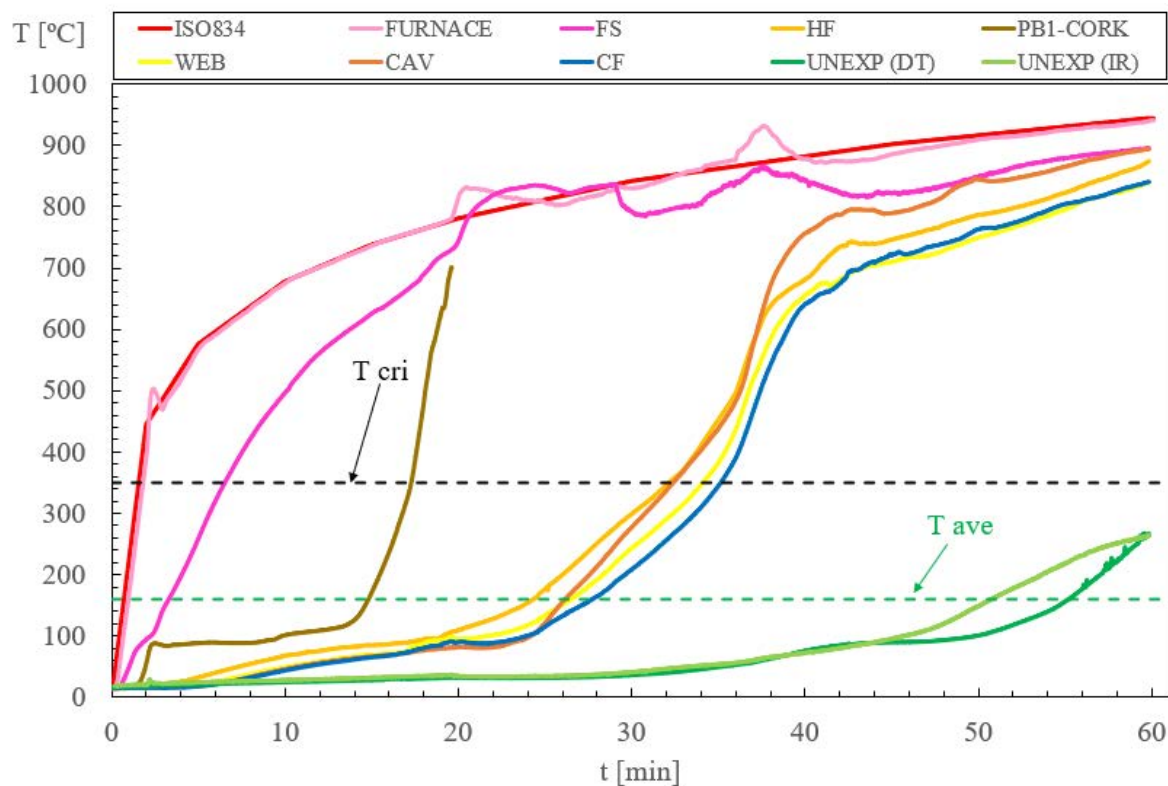


Figure 5.5: Specimen 4 - Average Temperature Results.

It is possible to see that in two periods the furnace temperature presents higher temperatures than the ISO curve, at around 20 minutes and at 36 minutes. This is because it was the moment when the cork layer started to burn, bringing extra heat release rate to the furnace compartment. The first period of extra heat is related to the collapse of the exposed gypsum layer, while the second period of extra heat is related to the burning of the second internal cork layer. It is possible to observe also the increase of the steel

temperature and cavity temperature at 20 mins, and a new increase in 36 mins. The PB1-Cork data sensor was discarded after 19 minutes due to the collapse of the internal layers. The fire resistance was determined by the maximum temperature criterion in 51 minutes. The average criterion gives a fire resistance of 55 minutes.

More comments and photographs about the this specimen are presented in the appendix A.5.

## 5.6 Specimen 5

The specimen 5 is the second specimen with a cork-gypsum composite, and it was assembled with 3 studs, as presented in the schematic draws of the table 4.1. This specimen has just two cavities. The figure 5.6 brings the temperature results of this test.

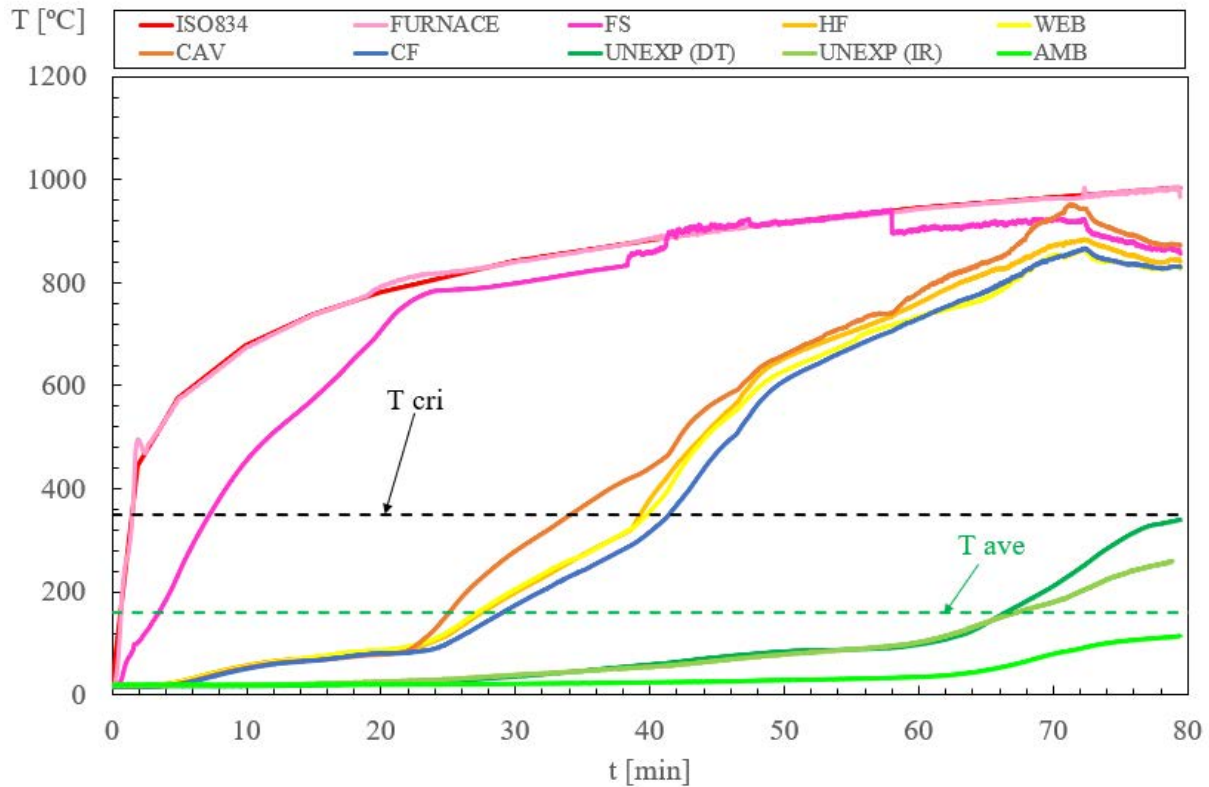


Figure 5.6: Specimen 5 - Average Temperature Results.

As in Specimen 4, the first cork layer started to burn at 18 minutes, and the second cork

layer started to burn at 40 minutes, approximately. The fire resistance was determined by the maximum temperature criterion in 64 minutes. The average temperature criterion gives a fire resistance of 66 minutes.

More comments and photographs about the this specimen are presented in the appendix A.6.

## 5.7 Specimen 6

The specimen 6 is the third specimen with a cork-gypsum composite, built with 4 studs plus the horizontal reinforcement, as presented in the schematic draws of the table 4.1. This specimen has four cavities, as the specimen 4, but with a different geometry. The figure 5.7 brings the results of this test.

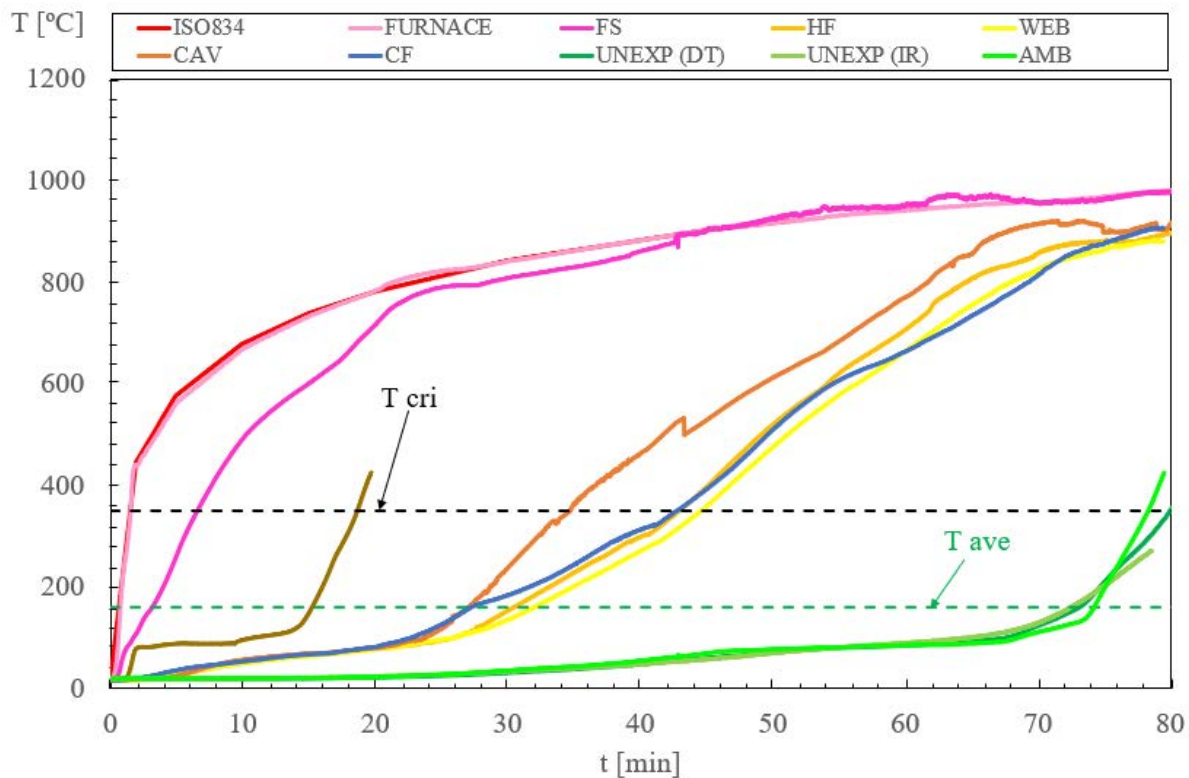


Figure 5.7: Specimen 6 - Average Temperature Results.

The first cork layer started to burn at 16 minutes, and the second cork layer started to burn

at 34 minutes, approximately, as expected. Some measurement problems were observed in the PT2 sensor, but this problem was fixed at 43 minutes, and this data start to be consider at this time, as presented in the respective curve, that was affected. The fire resistance was determined by the maximum temperature criterion in 69 minutes. The average criterion gives a fire resistance of 73 minutes.

More comments and photographs about the this specimen are presented in the appendix A.7.

## 5.8 Specimen 7

This specimen has the LSF structure made with 5 studs and cover with a composite layer of OSB and gypsum. The average temperature results of this tests are presented in figure 5.8.

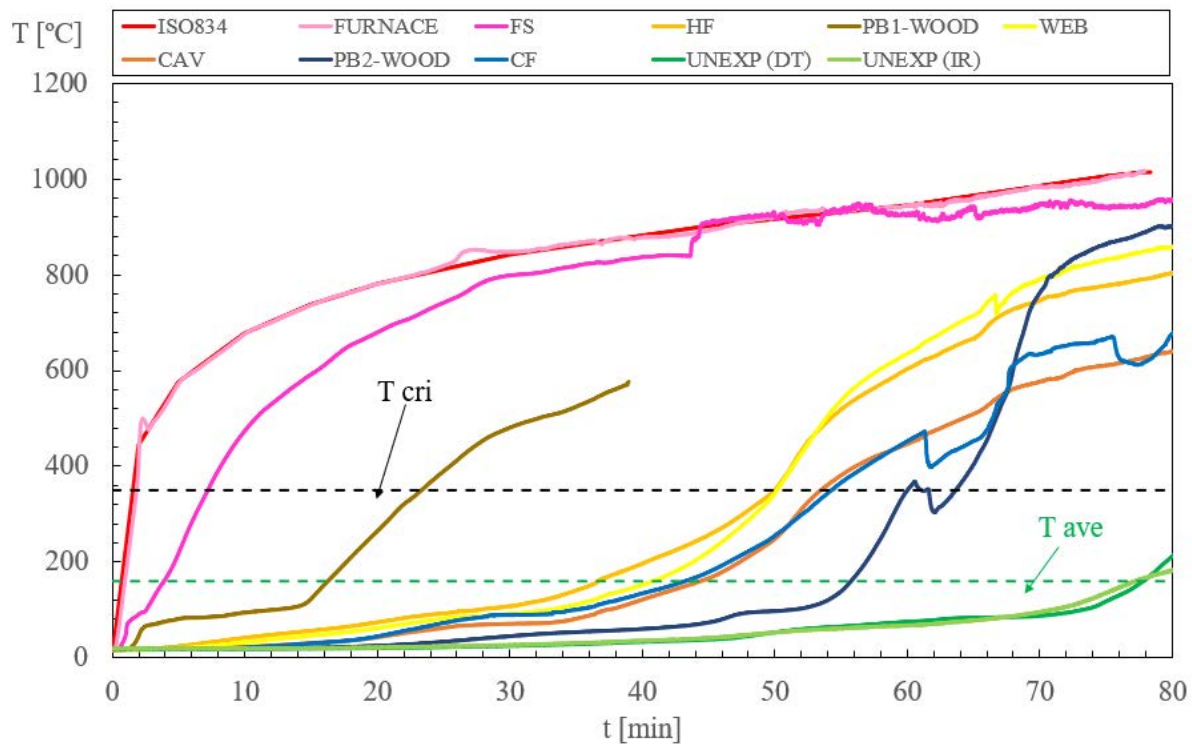


Figure 5.8: Specimen 7 - Average Temperature Results.

The thermocouple WT2 had some problems before the beginning of the test, and was



discarded. The thermocouple WT9 had reading problems after the start of the test and its data was discarded as well. The flames started at 20 minutes, across the crack, and at 27 minutes this flame was still intense, due the combustion of the first layer of wood. At 52 minutes another strong flame was detected. These two intense flames were detected in the graph by an increase in the rate of temperature in some curves. The curve of PB2-Wood, presents some decreasing in its temperature evolution near the 60 minutes, and it occurs probably because the thermocouple that make this measurement felt in a protected place. After a few minutes, the temperature started to increase again. The CF presents the same behaviour in the same time, and it happened because this graph represents the temperature evolution in average, and in this regions the difference of temperature in the middle of the studs increase, affecting the average. This measurement lost the reading of thermocouple WT9, that probably would bring the equilibrium between this differences. The fire resistance was determined by the maximum temperature criterion in 75 minutes. The average criterion gives a fire resistance of 77 minutes.

More comments and photographs about the this specimen are presented in the appendix A.8.



# Chapter 6

## Numerical Simulation

Special numerical tasks aimed to develop an accurate model to predict fire resistance and the validation of the 2D finite element models with and without fluid interaction. This chapter presents the numerical validation of the experimental tests.

### 6.1 Material Properties

The thermal properties are decisive to simulate the performance of the non-loadbearing wall. The thermal properties are temperature dependent for all the materials involved. Steel presents typical evolution for the specific heat with a maximum value that accounts to the allotropic transformation. The thermal conductivity depends on temperature and specific mass is considered constant, [28]. The thermal properties of Gypsum considered in this investigation were proposed by Poologanathan et al. [29] for the specific heat, thermal conductivity and for the specific mass. The thermal properties of the Rockwool depends on the fabrication process. During the production process the fibres are pressed to achieve different densities, being the heaviest ones produced as boards and the lightest as mats. The specific mass of this material was considered equal to 120 kg/m<sup>3</sup>, being the specific heat and thermal conductivity temperature dependent. The fibre itself starts melting around 1000 °C [30]. The material properties of the glass fibre were assumed as proposed by Keerthan et al. in their investigation about the thermal performance of different

insulation materials [31], but considering the density equal to  $15.42 \text{ kg/m}^3$ . The thermal properties of the wood are given by the Eurocode 5 [32]. The thermal properties of the cork was tested by the authors at room temperature, and the behaviour was extrapolated using the shape curves of wood. The properties are presented in appendix B.

## 6.2 Solution Methods

One side of the wall was submitted to fire and the other side is assumed to remain in contact with room temperature. The boundary conditions are defined in accordance to EN1991-1-2 [26], assuming heat transfer by radiation (emissivity of fire  $\xi = 1$ ) and convection (convection coefficient  $\alpha_c = 25 \text{ W/m}^2 \text{ K}$ ) in the exposed side and heat transfer by convection (convection coefficient  $\alpha_c = 9 \text{ W/m}^2 \text{ K}$  to include the radiation component) in the unexposed side. The gas temperature in the exposed side follows the standard ISO834 [33]. The room temperature of the unexposed side was consider equal to the initial temperature ( $T_\infty = 20^\circ \text{ C}$ ), during all the simulation time. See fig. 6.1.

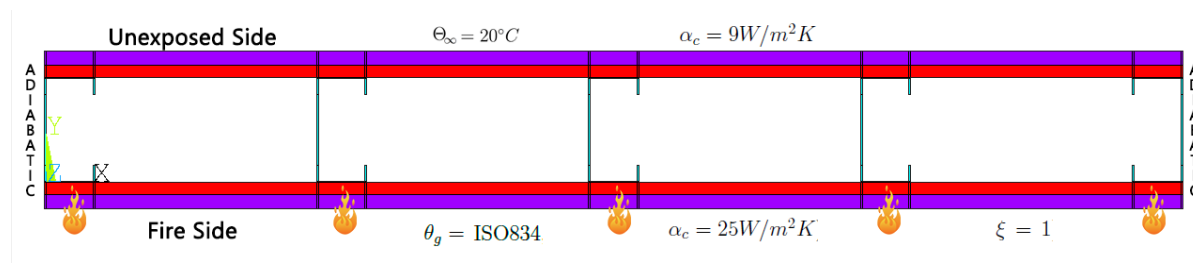


Figure 6.1: Boundary Conditions.

Three different numerical solution methods were used to simulate the fire test of the non-loadbearing LSF wall. The solution method 1 uses thermal and fluid analysis for both solid and fluid parts, while the solution method 2 considers only the thermal analysis for solids, assuming perfect contact between materials. To perform the validation of the experimental tests, some simulations were performed to obtain the field temperature in the walls, being the fire resistance determined by the temperature evolution of the unexposed side. The solution methods and models were validated against experiments developed by

Prakash Kolarkar [34].

### 6.2.1 Solution Method 1

The solution method 1 is performed in ANSYS Fluent, using the Finite Volume Method. The solution domain is subdivided into a finite number of a small control volumes (cells) using a grid. The grid defines the boundaries of the control volumes while the computational nodes lie at the centre of the control volume. The boundary nodes are of linear order. Figures 6.2 and 6.3 represents the grid for all the domains (solid and fluid) for specimen 1, using the minimum size of the cell equal to 0.0005 m.

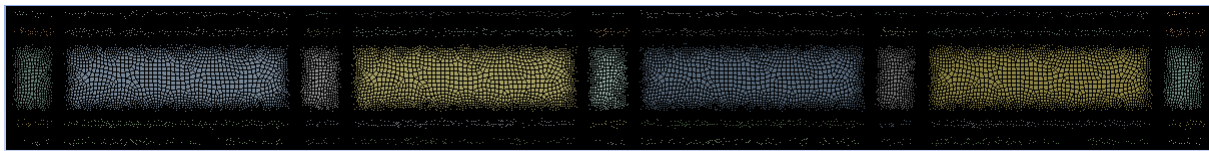


Figure 6.2: Finite cells used for specimens in solution method 1.

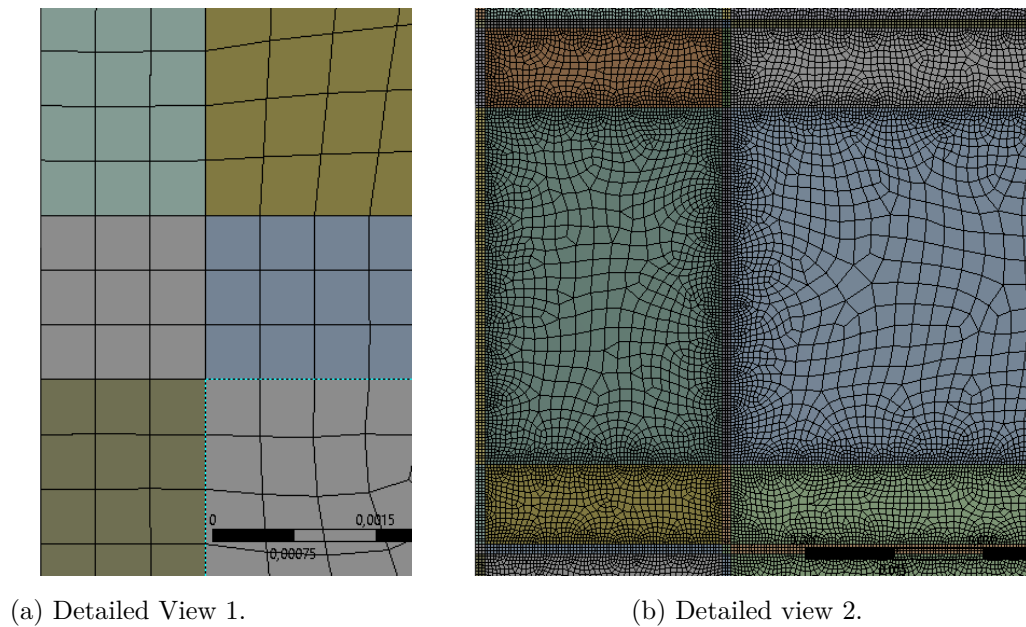


Figure 6.3: Finite cells used for specimens in solution method 1 (detailed views).

The flow analysis for the solution method 1 considers laminar fluid and is based on

density variation. The fluid motion is induced by heat transfer and the solution is transient and nonlinear. The density-based solver solves the governing equations of continuity, momentum and energy simultaneously. Pressure is obtained through the equation of state.

The continuity equation must be solved in a closed system, which means that the conservation of mass must be satisfied. Mass must not be created or destroyed. The equation governing this principle eq.6.1 is known as the continuity equation.

$$\frac{\partial \rho}{\partial t} + \vec{\nabla} \cdot (\rho \vec{V}) = 0 \quad (6.1)$$

The Navier-Stokes equations (momentum equations), see eq. 6.2, are a collection of the 3 dimensional momentum equations for any Newtonian fluid when running a 3D analysis, one for each direction in space. These equations ensure that in any system, the momentum is conserved. This means that the total force generated by the momentum transfer in each direction must be balanced by the rate of change of momentum in each direction. The Navier-Stokes equation written in Y direction. The other directions in space also apply if running a 3D analysis, with exception to the effect of gravity component.

$$\frac{\partial(\rho V_y)}{\partial t} + \frac{\partial(\rho V_x V_y)}{\partial x} + \frac{\partial(\rho V_y V_y)}{\partial y} + \frac{\partial(\rho V_z V_y)}{\partial z} = (\Delta \rho + \rho_0) g_y - \frac{\partial(p)}{\partial y} + \vec{\nabla} \cdot \text{grad}(\mu_e V_y) + T_y \quad (6.2)$$

The first law of thermodynamics requires that the energy of a system be conserved. The two-dimensional energy equation for fluid flow and solid parts must also be solved, following the differential equation presented in eq. 6.3 .

$$\frac{\partial(\rho C_p T)}{\partial t} + \frac{\partial(\rho V_x C_p T)}{\partial x} + \frac{\partial(\rho V_y C_p T)}{\partial y} + \frac{\partial(\rho V_z C_p T)}{\partial z} = \frac{\partial}{\partial x}(\lambda_x \frac{\partial T}{\partial x}) + \frac{\partial}{\partial y}(\lambda_y \frac{\partial T}{\partial y}) + \frac{\partial}{\partial z}(\lambda_z \frac{\partial T}{\partial z}) \quad (6.3)$$

Governing equations for additional scalars are solved afterward and sequentially (radiation). The integration time for each time step was 60 s, with the possibility to be reduced

to 5 s. The convergence criterion was based on the residuals for each equation, that needs to be less than 1E-3 for all the state variables, with exception of the energy equation, used to solve this model, and the radiation model P1, also used in this solution method, that is required to decrease to 1E-6. The numerical model divides the cross section in finite cells. The domain variables (pressure, velocity, temperature) are calculated in each cell, at the same time.

### 6.2.2 Solution Method 2

The solid analysis for the solution method 2 uses transient and nonlinear thermal analysis, with full option solution method, developed in ANSYS Multiphysics. The finite element method requires the solution of equation 6.4 in the domain ( $\Omega$ ) and equation 6.5 in the boundary exposed to fire ( $\partial\Omega$ ). The numerical model uses a 2D finite element (PLANE55) with four nodes and one degree of freedom per node (temperature). The interpolating functions are linear.

$$\nabla(\lambda_{(\theta)} \cdot \nabla\theta) = \rho_{(\theta)} \cdot C_p \cdot \frac{\partial\theta}{\partial t}(\Omega) \quad (6.4)$$

$$\lambda_{(\theta)} \cdot \nabla \cdot \vec{n} = \alpha_c(\theta_g - \theta) + \phi \cdot \epsilon_m \cdot \epsilon_f \cdot \sigma \cdot (\theta_g^4 - \theta^4)(\partial\Omega) \quad (6.5)$$

The same time step was used with similar convergence criterion for the heat flow. The criterion is based on the heat flow, with a tolerance of 0.001 and a minimum reference value of 1E-6. Fig. 6.4 represents the mesh of specimen 3.

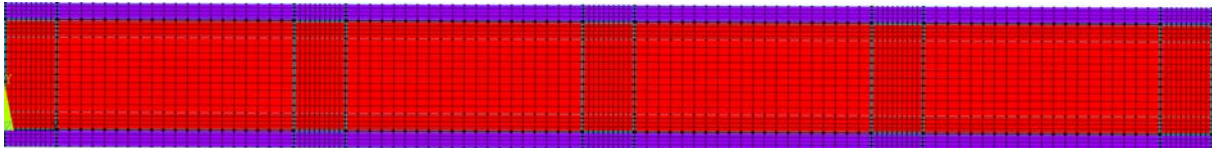


Figure 6.4: Finite element mesh used for specimens in solution method 2 (specimen 3).

The density of the mesh used for ANSYS MULTIPHYSICS is smaller in comparison with the cells used in ANSYS FLUENT, nevertheless the thickness of the studs was

divided into three finite elements as well. The mesh was defined based on a convergence test.

### 6.2.3 Solution Method 3

Some specimens of this work have combustible material in the protection layer and free void cavities. For solution method 1, with ANSYS Fluent, due limitations in the software, can not interpret a variation of the density in solid materials. The solution method 2, with ANSYS Multiphysics, accepts the variation of density to solid materials, but the formulation of this software does not consider CFD approach. The solution to validate this cases was a hybrid method.

This method was developed in the ANSYS Multiphysics, and use the average temperature of the cavities obtained from the experiment. A mixed boundary condition of radiation and convection was applied on lines inside the cavities, being the convective coefficient assumed as an average of the convective coefficients of the fire side and unexposed side. The emissivity in the cavity was assumed as  $\epsilon = 1$ . This method uses the same mesh size of the solution method 2, but the cavities have no mesh. The Fig. 6.5 represents the mesh of specimen 4.

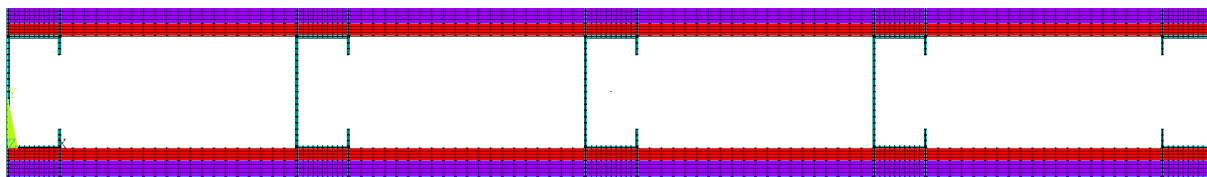


Figure 6.5: Finite element mesh used for specimens in solution method 3 (specimen 4).

## 6.3 Numerical Validation

All the specimens tested by the author were used to validate the numerical models. Four different specimens from the tests developed by Kokalar [34] were also used in for validation. The geometry of the specimens tested by the author are defined by geometry A, and the specimens tested by Kokalar are identify by geometry B.



The relative error is the method adopted to validate the mathematical model, and it is presented in the equation 6.6.

$$RE = \frac{T_{experimental} - T_{simulated}}{T_{experimental}} [\%] \quad (6.6)$$

### 6.3.1 Numerical Validation of Specimens with Geometry A

The compilation of the results can be observed in the table 6.1. The graphical results of the simulations are presented in appendix C.

Table 6.1: Results of the Tests.

Spec.	Insulation cavity	Plate	Spacing Studs [mm]	Fire Resistance Experimental [min] (I)	Fire resistance Numerical [min] (I)	Relative Error [%]	Sol. Method
1	No	1x12.5 mm	233	70	56	20	1
2	No	2x12.5 mm	233	118	165	28	1
3	Rock Wool	1x12.5 mm	233	87	84	3	2
4	No	1x12.5 mm 1x 10 mm (Cork)	233	51	55	7	3
5	No	1x12.5 mm 1x 10 mm (Cork)	466	66	60	9	3
6	No	1x12.5 mm 1x 10 mm (Cork)	487,5	69	68	1	3
7	No	1x12.5 mm 10 mm (OSB)	233	75	94	20	3

The solution method 1 using thermal and fluid analysis for both solid and fluid parts

was adopted to validate the cases 1 and 2, that was composed by non combustible materials, and with cavity filled with air. The case 3 uses the solution method 2, that considers only the thermal analysis for solids, assuming perfect contact between materials. To validate the cases 4, 5, 6 and 7 the third solution method was adopted.

In the table 6.1, the errors correspond to an average of the relative average errors calculated minute after minute to each group of sensors defined in chapter 5. The graphics of these errors during the simulations are presented in the figures 6.6 to 6.19, as the simulated contour of temperature at fire resistance time to each specimen.

The error in the specimen with fulfilled cavity was the smallest, and this is why this kind of wall, without fluid in the cavity, use the conduction theory to preview the temperature field. The errors was also measured in the tests using the average temperatures, and, in the case of the thermocouples between the composite walls, sensor by sensor.

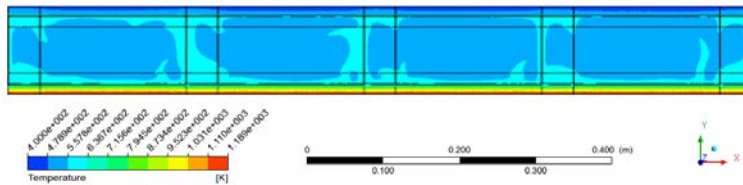


Figure 6.6: Specimen 1 - Numerical Results (time=56min, temperature [K]).

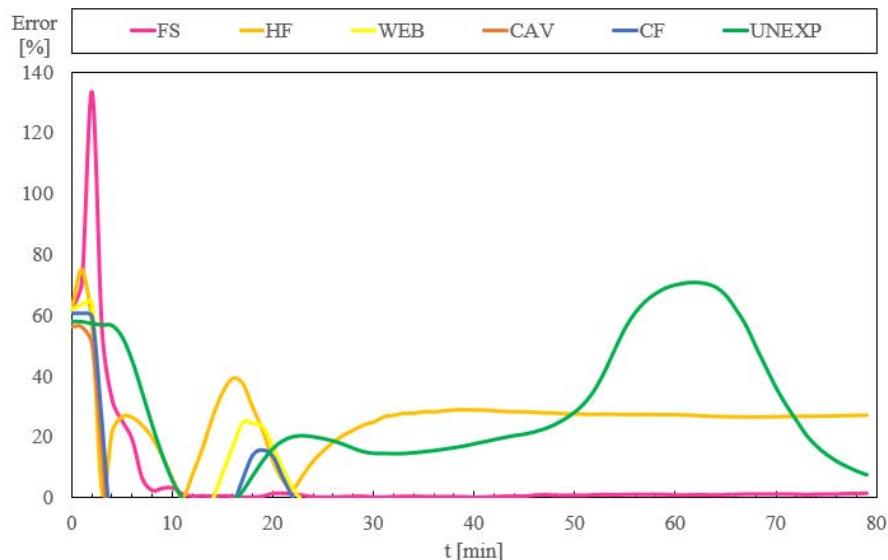


Figure 6.7: Specimen 1 - Error.

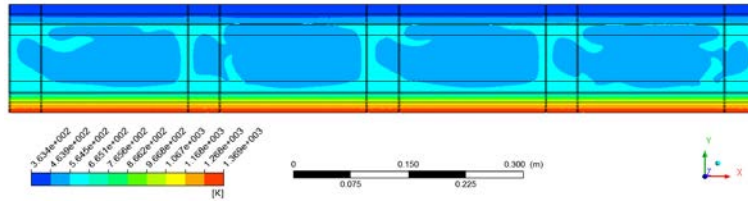


Figure 6.8: Specimen 2 - Numerical Results (time=118min, temperature [K]).

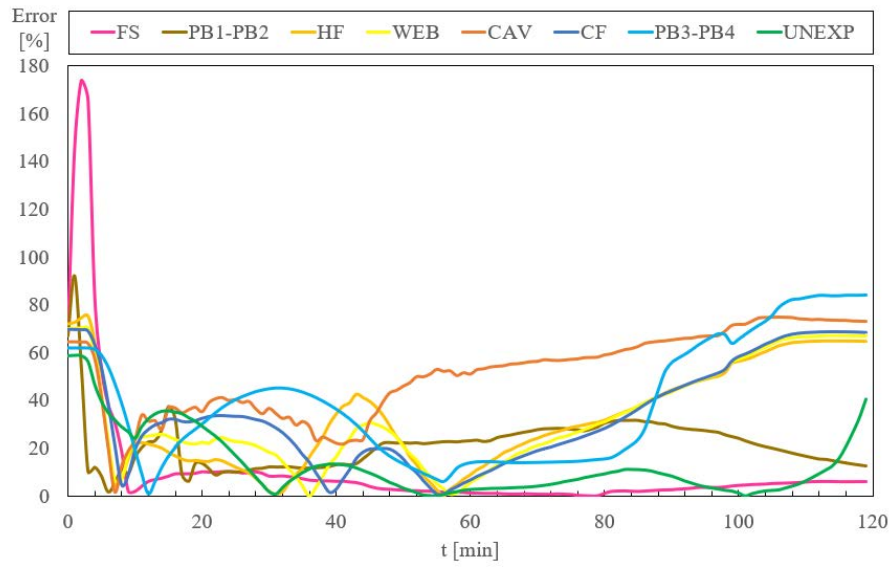


Figure 6.9: Specimen 2 - Error.

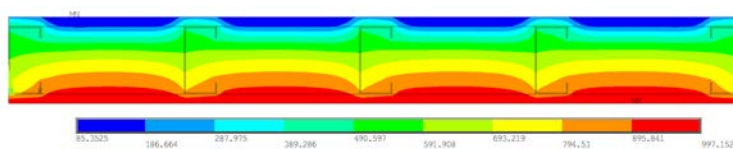


Figure 6.10: Specimen 3 - Numerical Results (time=87.43min, temperature [K]).

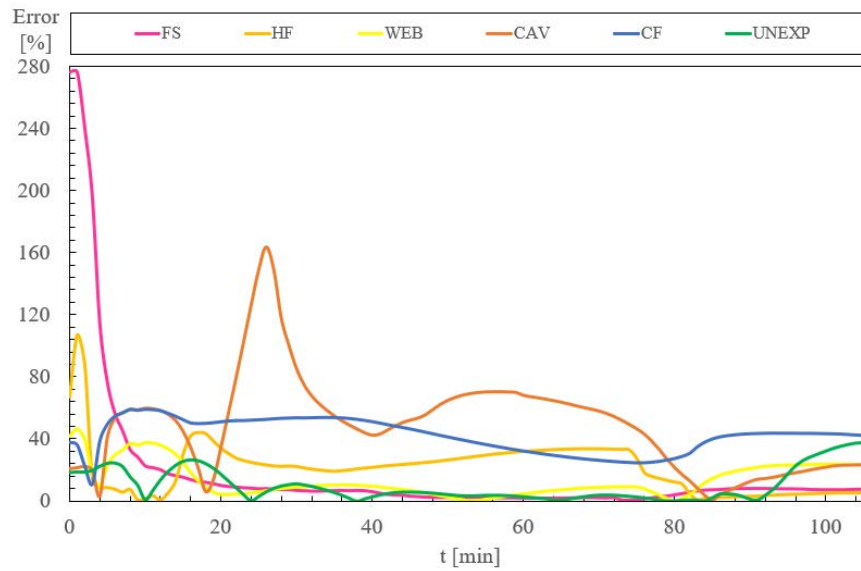


Figure 6.11: Specimen 3 - Error.

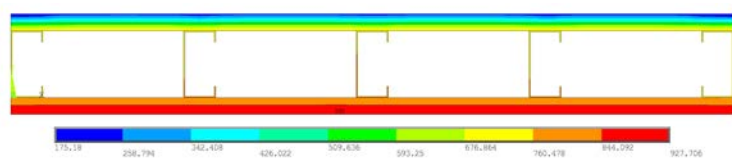


Figure 6.12: Specimen 4 - Numerical Results (time=55.61min, temperature [K]).

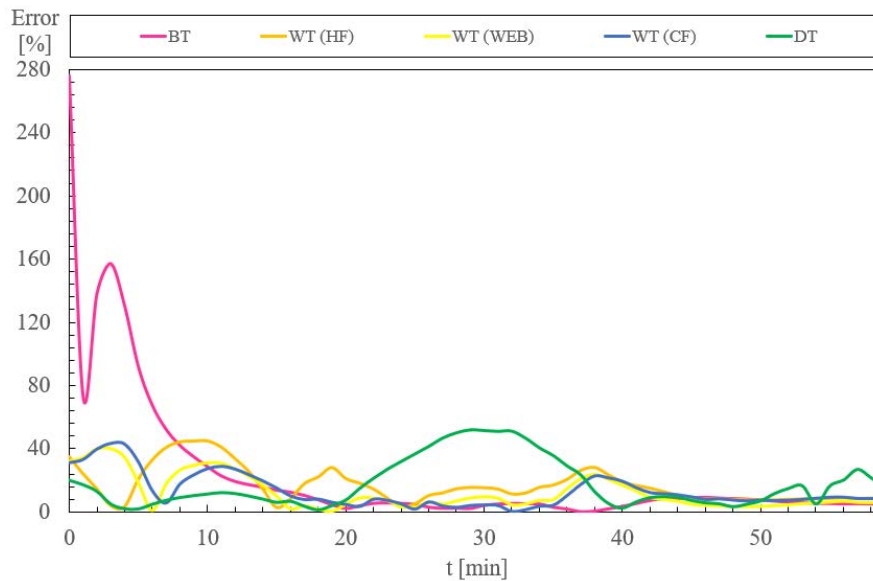


Figure 6.13: Specimen 4 - Error.

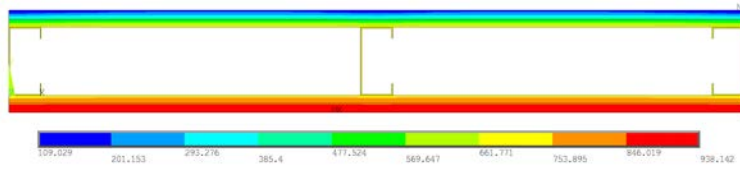


Figure 6.14: Specimen 5 - Numerical Results (time=60.28min, temperature [K]).

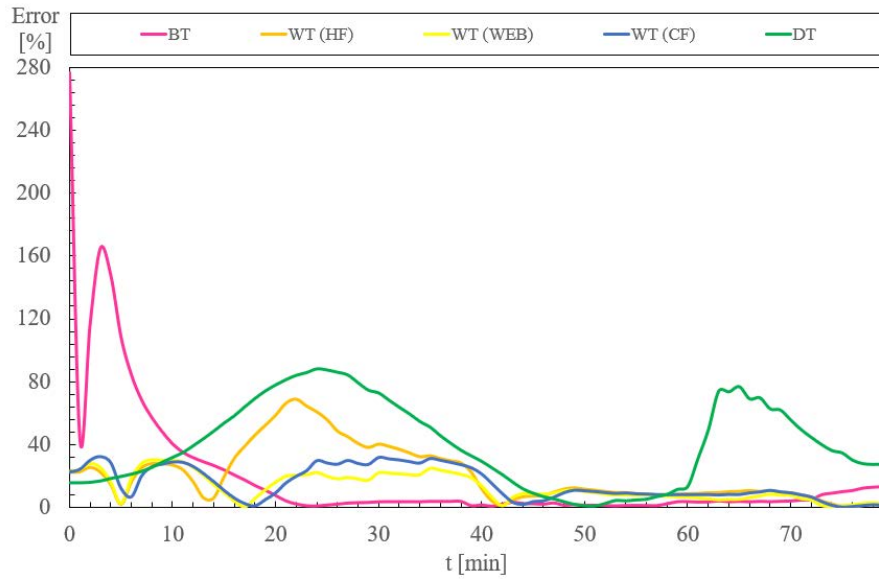


Figure 6.15: Specimen 5 - Error.

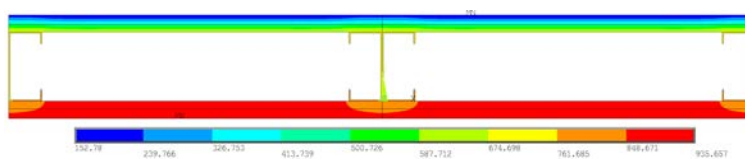


Figure 6.16: Specimen 6 - Numerical Results (time=68.47min, temperature [K]).

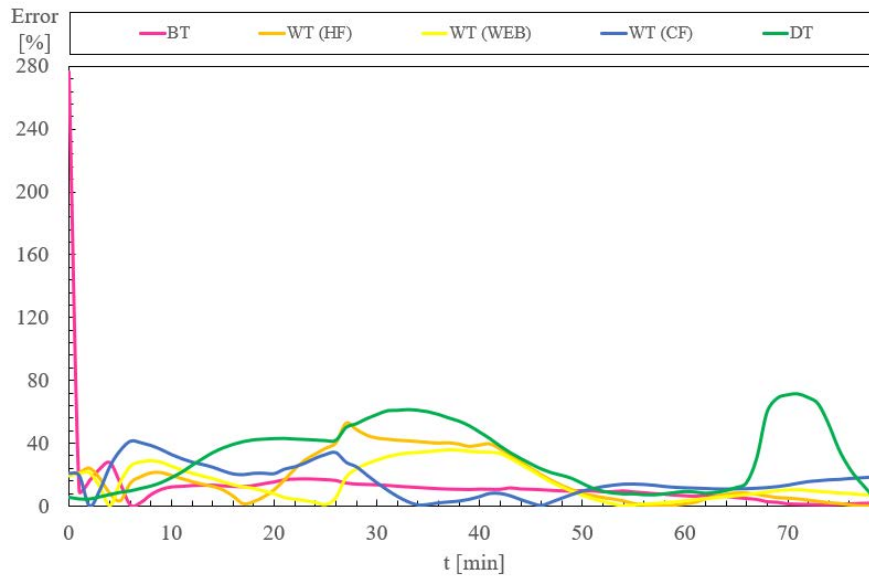


Figure 6.17: Specimen 6 - Error.

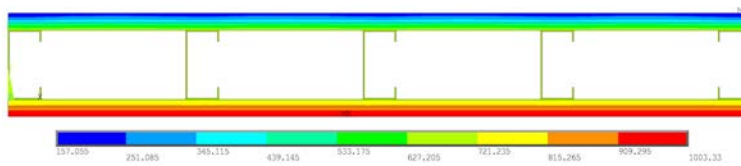


Figure 6.18: Specimen 7 - Numerical Results (time=95min, temperature [K]).

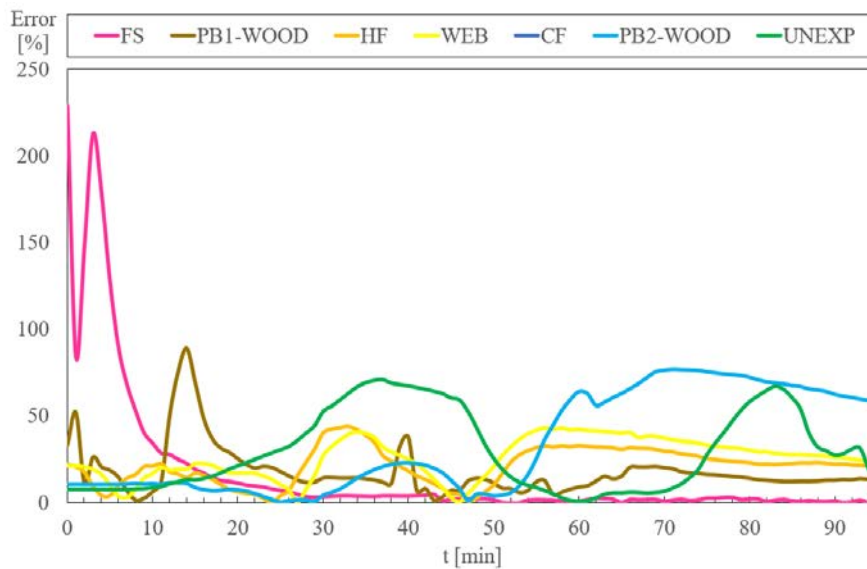


Figure 6.19: Specimen 7 - Error.

### 6.3.2 Numerical Validation of Specimens with Geometry B

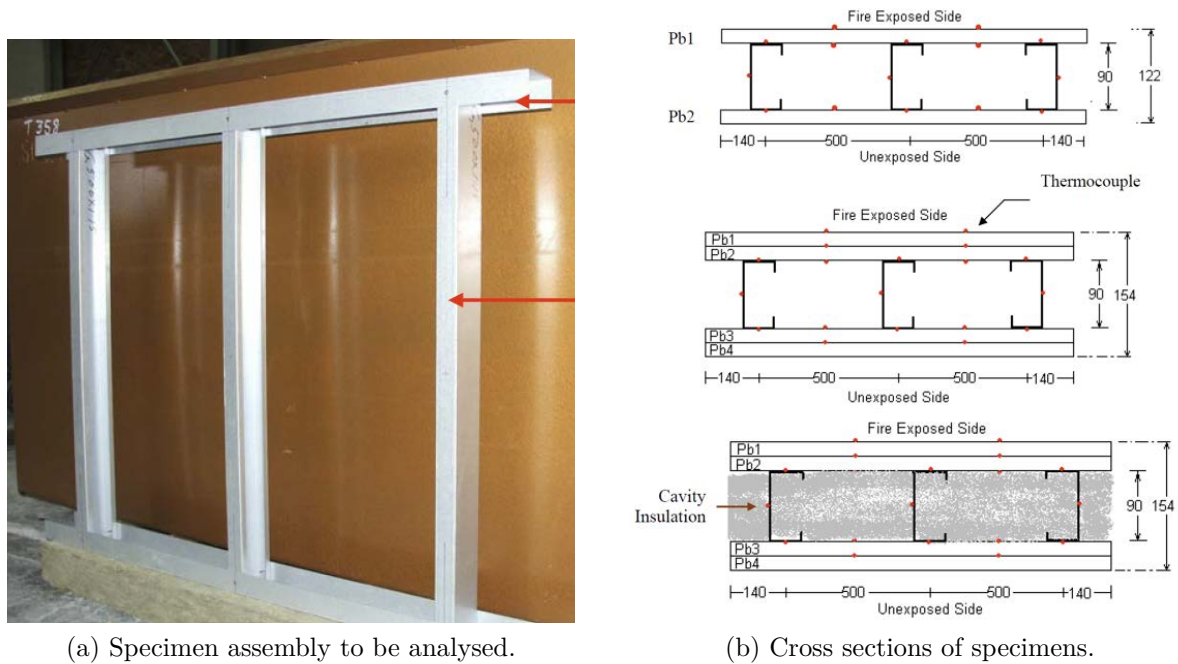
The steel frame is made of three studs G500 lipped channel 90x40x15 with 1.15 mm thickness and two tracks G500 unlipped channel 92x50 with 1.15 mm thickness, see table 6.2. Case 01 uses only one gypsum plate without any insulation material in the cavity, while case 02 uses two gypsum plates. Both cases 03 and 04, use two gypsum plates with different insulation material in the cavity (rockwool and glass fibre). See Fig 6.20.

Table 6.2: Characteristics and fire resistance of the wall assemblies used for validation.

Case	Specimen Kokalar	Thickness steel [mm]	Thick. cavity [mm]	Gypsum plates [number x thickness]	Fire resistance Experi- mental [min]	Fire resistance Numeri- cal [min]	Relative error [%]
1	Specimen 1	1.15	90 -air	1x16=16	82.5	74.4	9.8
2	Specimen 3	1.15	90 - air	2x16=32	>180	>180	-
3	Specimen 5	1.15	90 - rockwool	2x16=32	>180	>180	-
4	Specimen 4	1.15	90 - glass fibre	2x16=32	>180	152.3	-

The gypsum plates are attached to the LSF structure, using self-drilling bugle head screws, spaced every 300 mm along the vertical direction, and at the extremities of the gypsum plates directed into the tracks.

For the case 01, three type K thermocouples were attached to each stud to measure the temperature of the hot flange (HF), the temperature of the web (WEB) and the temperature of the cold flange (CF). These thermocouples were later used to calculate the average temperature of the steel at mid height and the gradient along the thickness. Several additional thermocouples were placed in contact to the gypsum plates to measure their temperatures (PB1-CAV and PB2-CAV or PB2-INS) and also five disc thermocouples were applied to the unexposed side of the wall to follow the average temperature of each assembly (UNEXP). Real temperature of the furnace (FURNACE), the temperature of exposed surface (FS) and the standard ISO834 [33] used for the numerical simulation are also plotted.



(a) Specimen assembly to be analysed.

(b) Cross sections of specimens.

Figure 6.20: Selected specimens 1, 3, 4 and 5 under validation.[34]

More thermocouples were used for cases 02-04 to measure the temperature in between the gypsum plates. PB1-PB2 represents the average temperature between plate 1 and plate 2, while PB2-CAV represents the average temperature of the cavity facing the gypsum plate PB2. PB3-PB4 represents the average temperature between plate 3 and plate 4 and PB3-CAV has the same meaning of PB2. The acronym INS is used instead of CAV, when insulation material is included in the cavity region. The experimental results depicted for the steel section are representing the average value of the measurements. Cracks and drop of gypsum plates are normally responsible for the sudden temperature increase, being this kind of events not simulated. The material properties of the insulation material are also very important during the comparison between experimental results and numerical simulations.

The results of the numerical simulation for case 1 and case 2 agree very well with the experimental results. The major difference between them is related with the conditions of the unexposed side, conditions of the exposed side and with the brittle behavior of the plates. The numerical simulation of the furnace temperature is not following the real



experimental curve and the boundary conditions of the unexposed side applied to the numerical model require the specification of the room temperature. This room temperature is bigger than the initial temperature and should be tracked during experiments (not the case herein). The dehydration process of the gypsum takes more time in the experiment in comparison to the simulation, being this fact related with the shape of the specific heat for this material (numerical) and migration of moisture (experiments). The results of cases 03- 04 include the effect of the thermal properties of the insulation material, being this effect very important to the validation process. More simulations should be developed with other insulation materials. More informations about the numerical validation and the graphs of the simulations are presented in appendix C.



# Chapter 7

## Parametric Analysis

This chapter presents some parametric analysis, following the same designations adopted in the chapter 6.

### 7.1 Parametric Analysis based on geometry A

The parametric analysis based on geometry A considers the variation of the density of the insulation and the thickness of the cavity. This parametric analysis kept a few distances fixed in the model. The fire resistance was determined for most of the cases, taking into consideration the insulation criterion (I). The figure 7.1 presents the data acquisition points setted to perform this analysis.

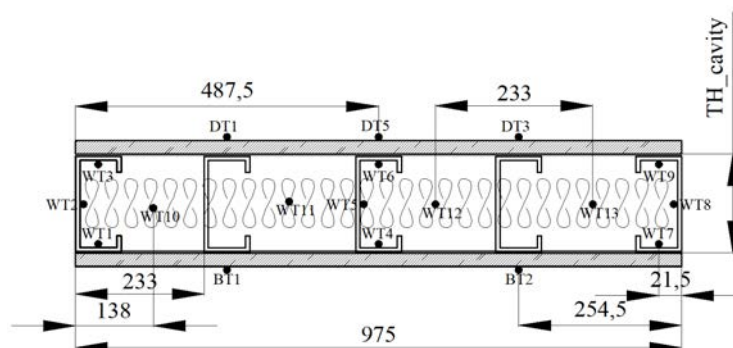


Figure 7.1: Finite element models used for specimens based on geometry B.

The table 7.1 presents the results of this parametric analysis. The fire resistance (R) can be evaluated through the simple calculation method applied to this type of elements (class 4 cross sections). The fire resistance could be satisfied, for a specific time, when the temperature of the cross section is not more than 350 °C [28]. The solution method 2 was used for this parametric analysis. The graphical results of this parametric analysis is presented in fig 7.2 to 7.9.

Table 7.1: Characteristics and fire resistance of the wall assemblies used for parametric analysis, geometry A.

Case	TH_ cavity [mm]	Density RockWool [kg/m <sup>3</sup> ]	Fire resistance [min] (I)	HF= 350°C Time [min]	WEB= 350°C Time [min]	CF= 350°C Time [min]
1 (specimen 3)	90	75	84	35	67	72
2	90	120	77	28	49	78
3	90	300	93	29	58	98
4	45	75	51	25	34	47
5	45	120	53	25	36	49
6	45	300	61	28	42	59
7	150	75	99	24	56	105
8	150	120	113	26	64	120
9	150	300	163	36	87	177

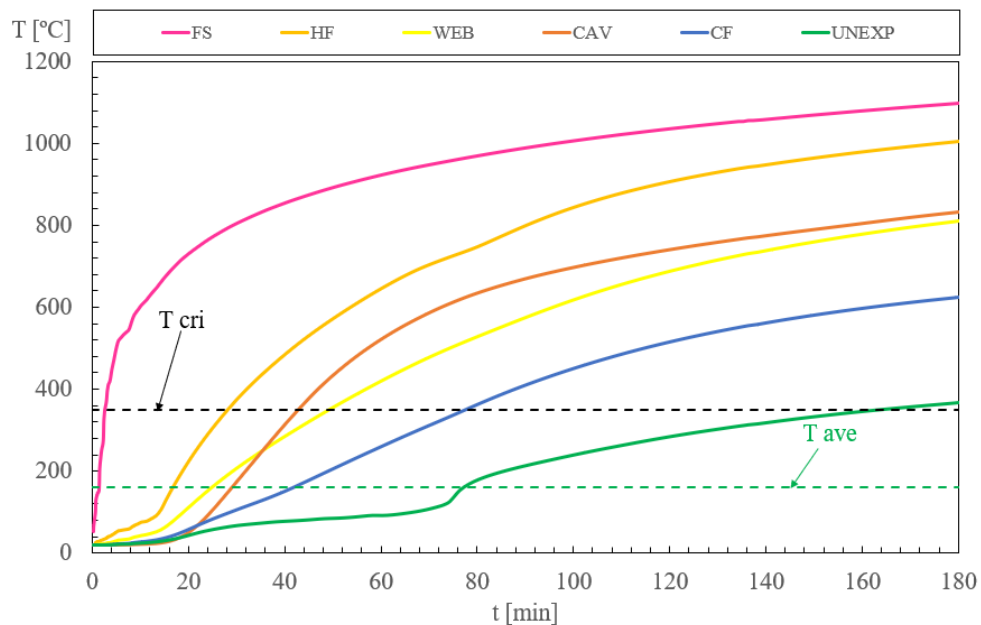


Figure 7.2: Case 2.

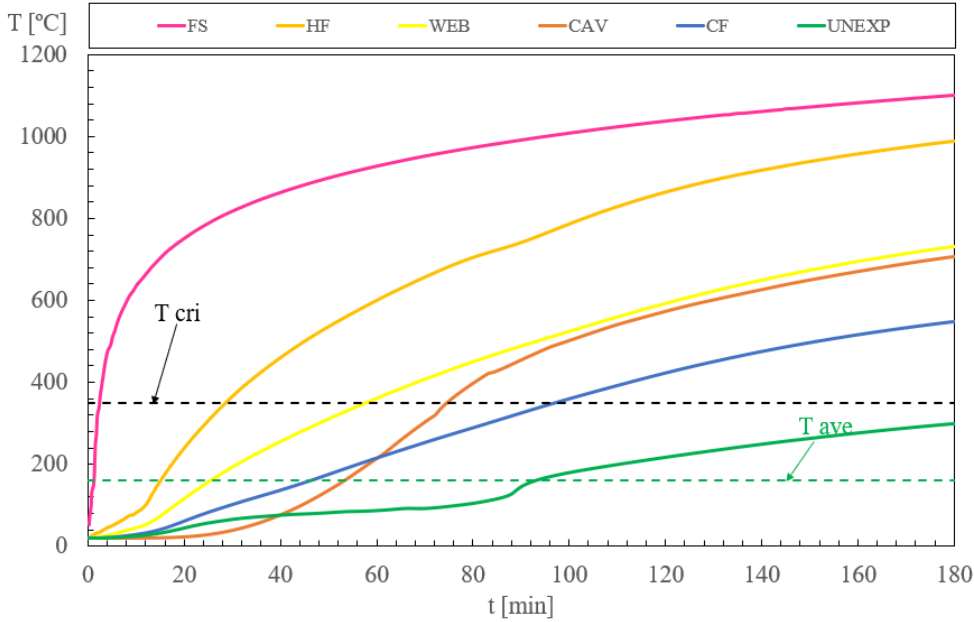


Figure 7.3: Case 3.

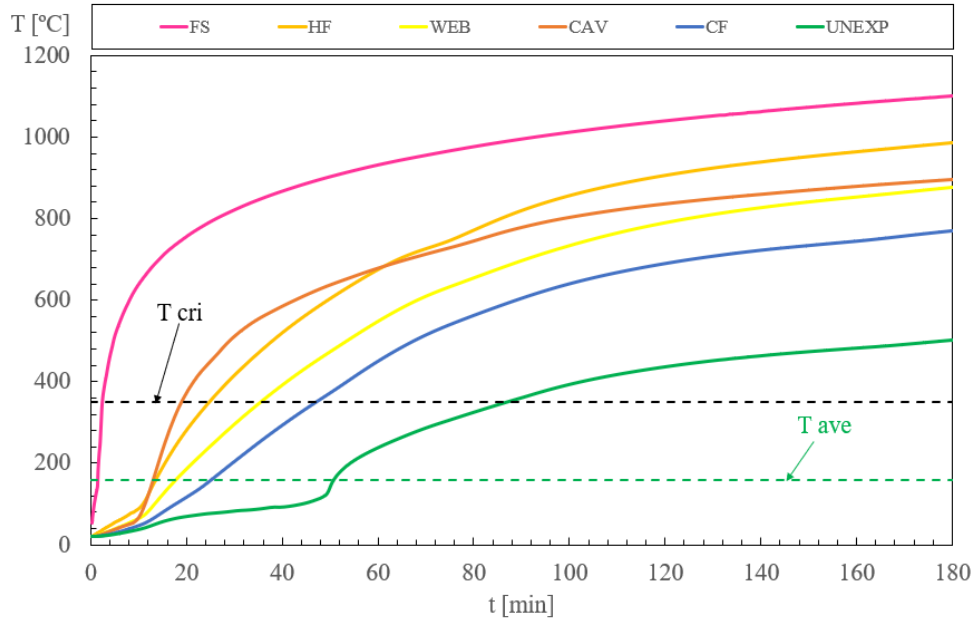


Figure 7.4: Case 4.

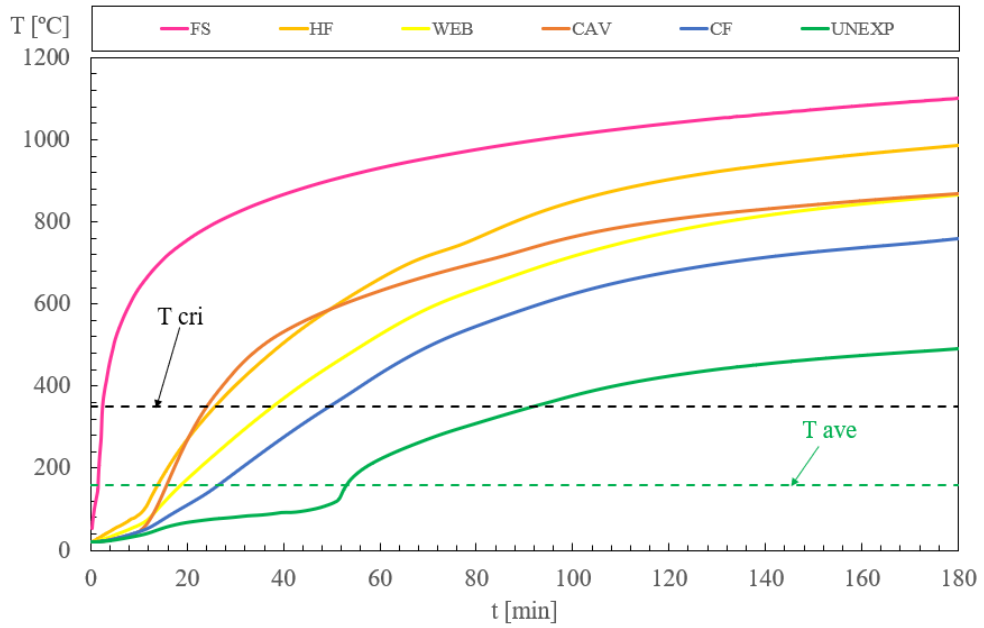


Figure 7.5: Case 5.

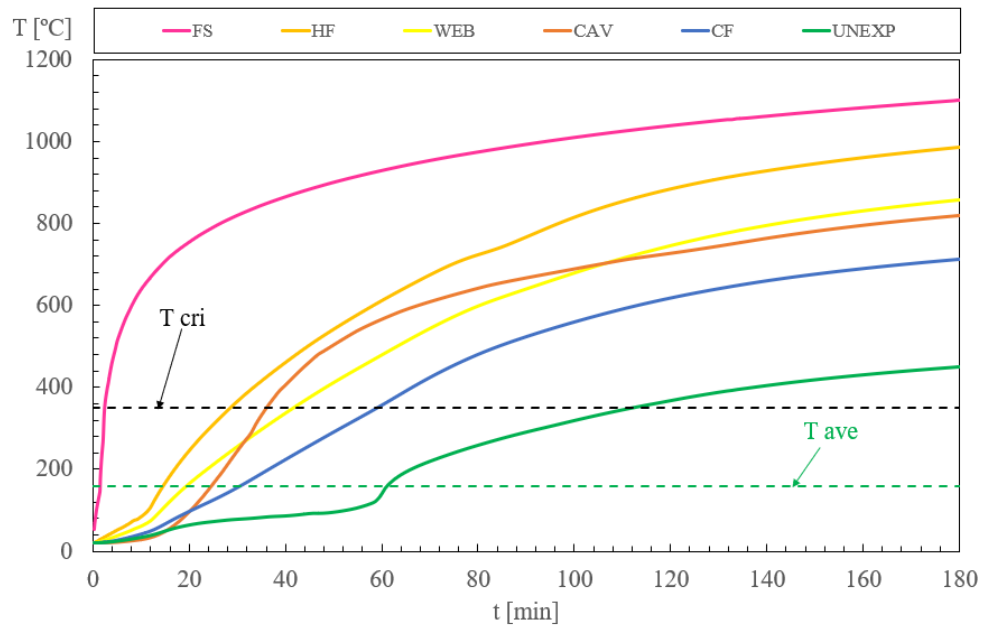


Figure 7.6: Case 6.

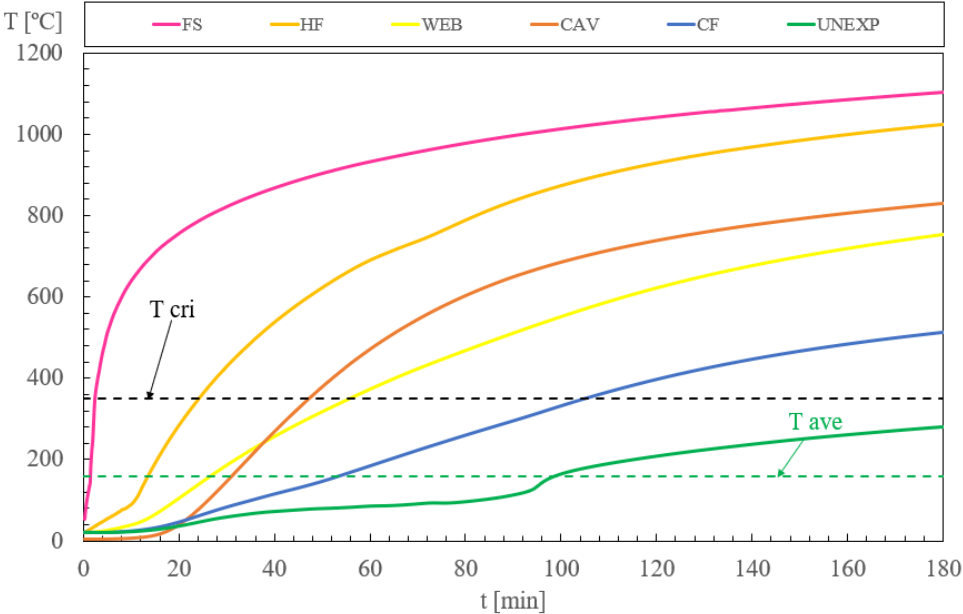


Figure 7.7: Case 7.

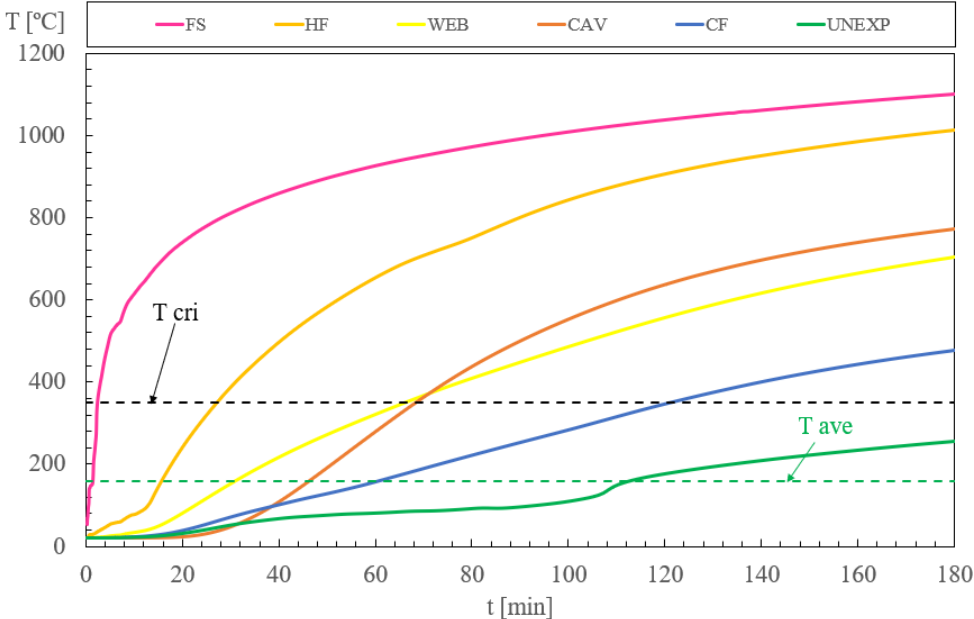


Figure 7.8: Case 8.

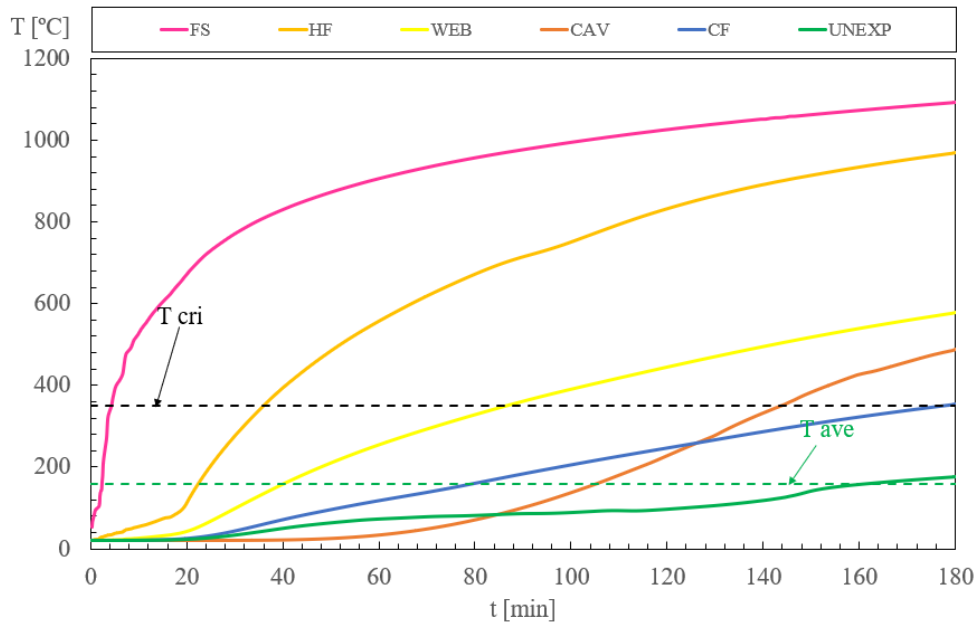


Figure 7.9: Case 9.

## 7.2 Parametric Analysis based on geometry B

Once the models are predicting reasonable well the experimental results, both models were used to analyse the effect of the thickness of the steel, the thickness of the cavity and the thickness of the gypsum plates, see table 7.2 and Fig. 7.10 and 7.11. This parametric analysis kept a few distances fixed in the model. The fire resistance was determined for most all cases, taking into consideration the insulation criterion (I).

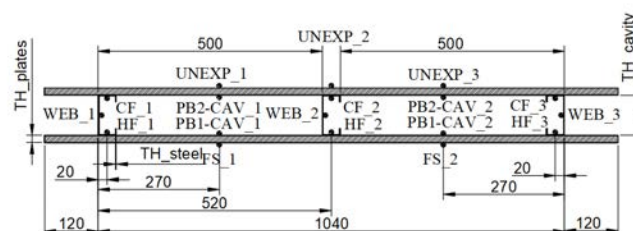


Figure 7.10: Model with one gypsum plate - Solution Method 2.



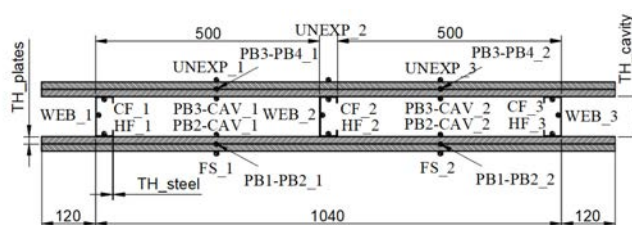


Figure 7.11: Model with two gypsum plate - Solution Method 2.

Table 7.2 also presents the critical time for steel members, when considering the case of load-bearing walls, assuming that the temperature of the cross section is not more than 350 °C. The graphical results of this parametric analysis is presented in fig 7.12 to 7.23.

Table 7.2: Characteristics and fire resistance of the wall assemblies used for parametric analysis, geometry B.

Case	TH_ steel [mm]	TH_ cavity [mm]	TH_ plates [number x thickness plates]	Fire resistance [min] (I)	HF= 350°C Time [min]	WEB= 350°C Time [min]	CF= 350°C Time [min]
5	1.15	45	1x16=16	74.3	57	67	72
6	1.15	45	2x16=32	197	119	128	133
7	1.5	45	1x9.5=9.5	36	33	41	45
8	1.5	45	2x9.5=19	99.4	74	86	92
9	1.5	150	1x16=16	83.2	67	82	86
10	1.5	150	2x16=32	218	133	147	156
11	1.5	90	1x16=16	76.6	61	72	76
12	1.5	90	2x16=32	212	128	140	146
13	2.5	90	1x12.5=12.5	58.4	54	65	68
14	2.5	90	2x12.5=25	153	93	121	129
15	1.5	150	1x12.5=12.5	58.3	50	62	65
16	1.5	150	2x12.5=25	155	106	120	125

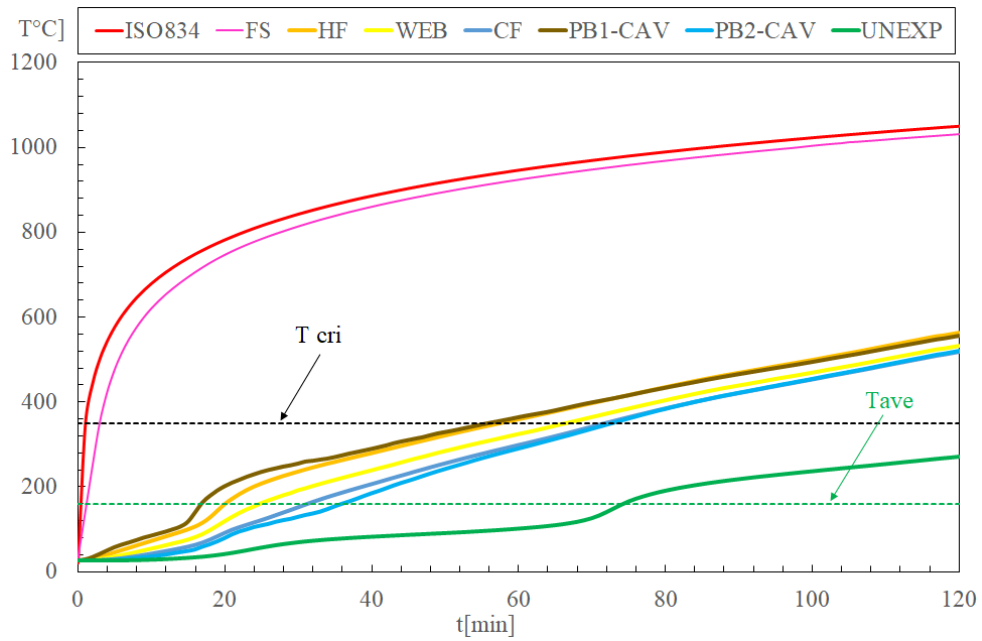


Figure 7.12: Case 05.

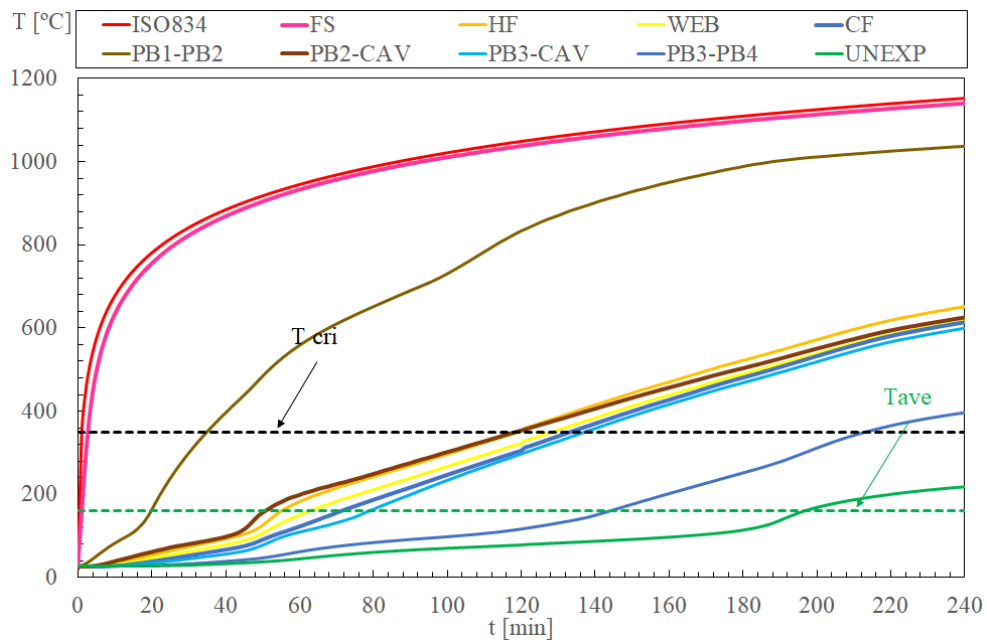


Figure 7.13: Case 06.

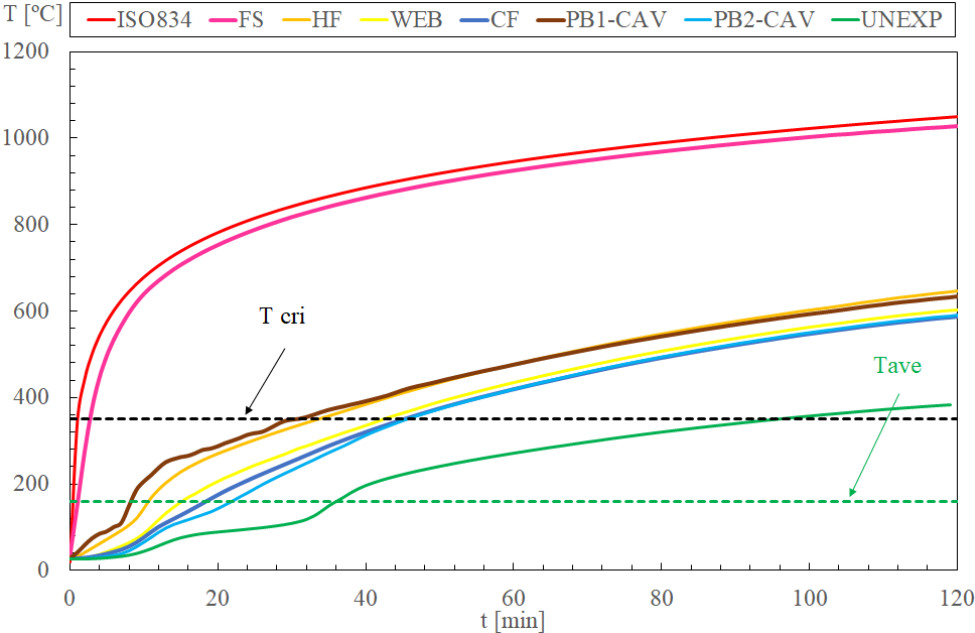


Figure 7.14: Case 07.

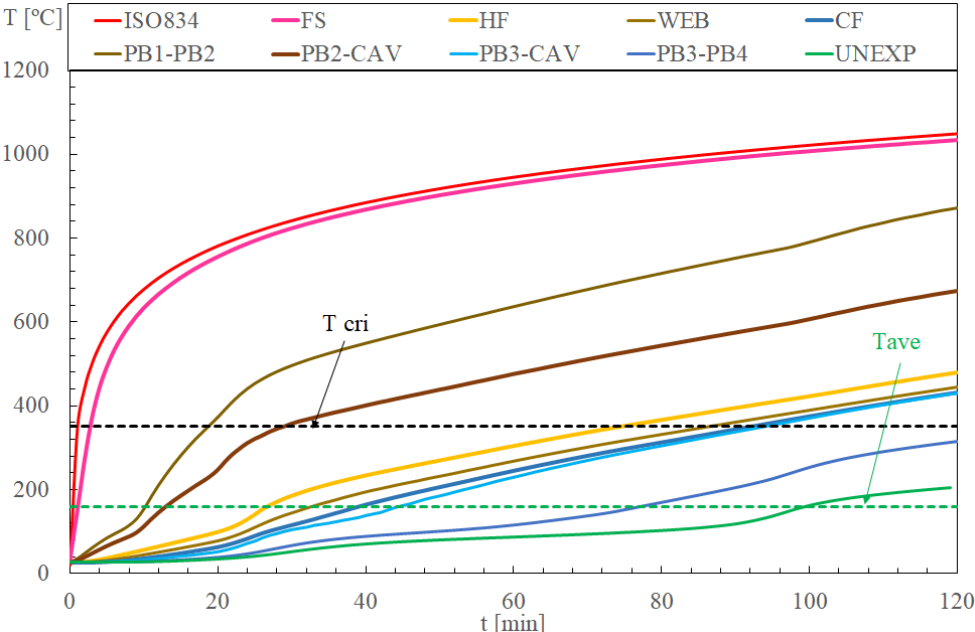


Figure 7.15: Case 08.

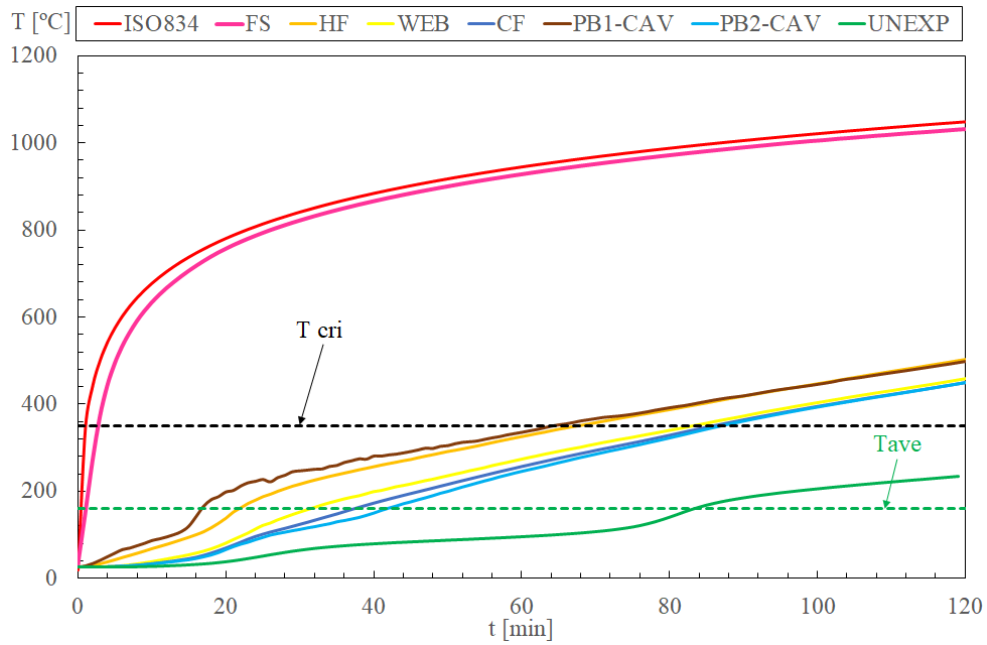


Figure 7.16: Case 09.

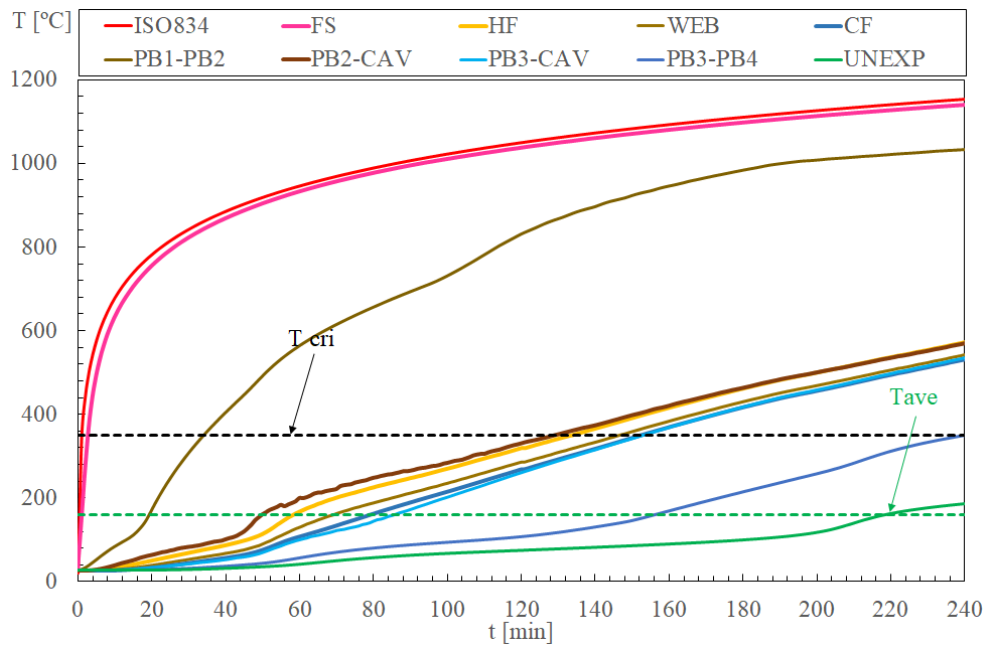


Figure 7.17: Case 10.

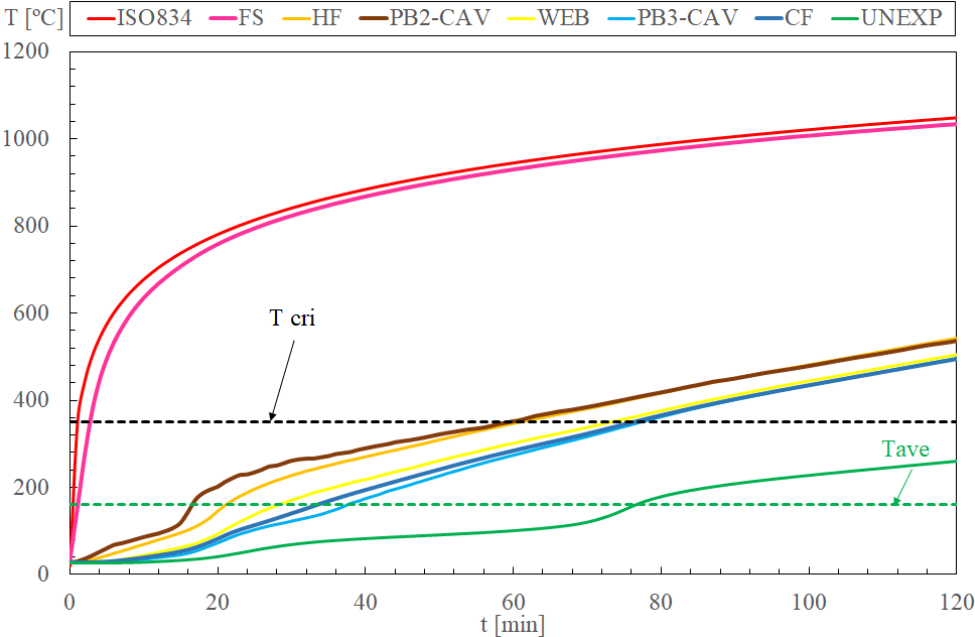


Figure 7.18: Case 11.

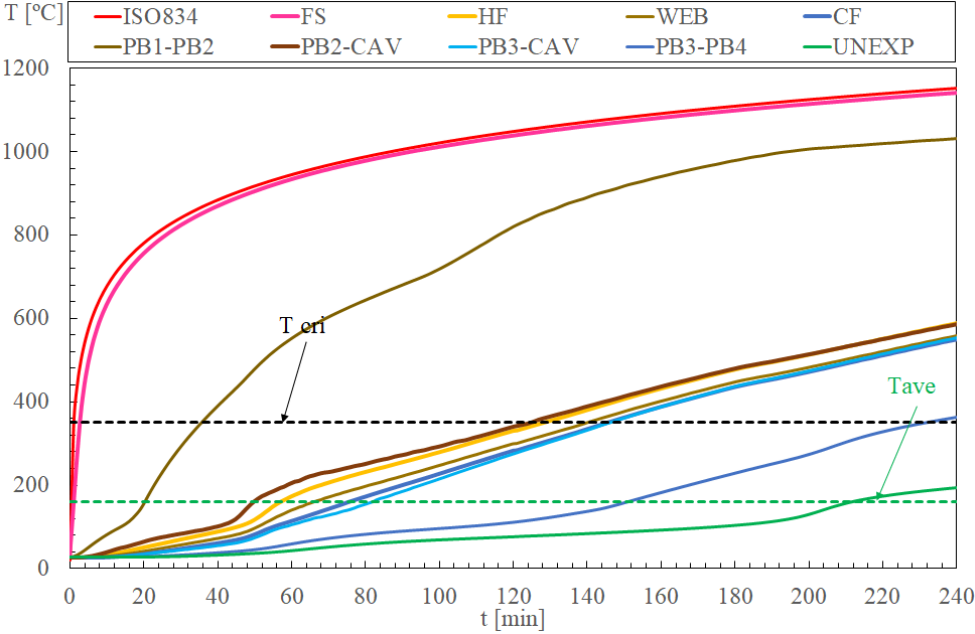


Figure 7.19: Case 12.

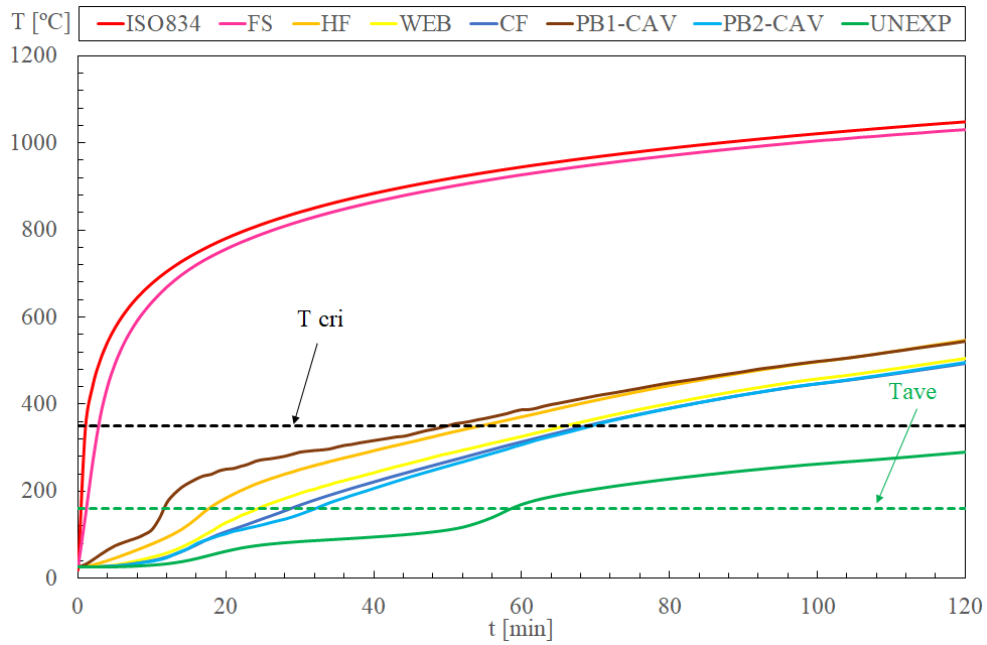


Figure 7.20: Case 13.

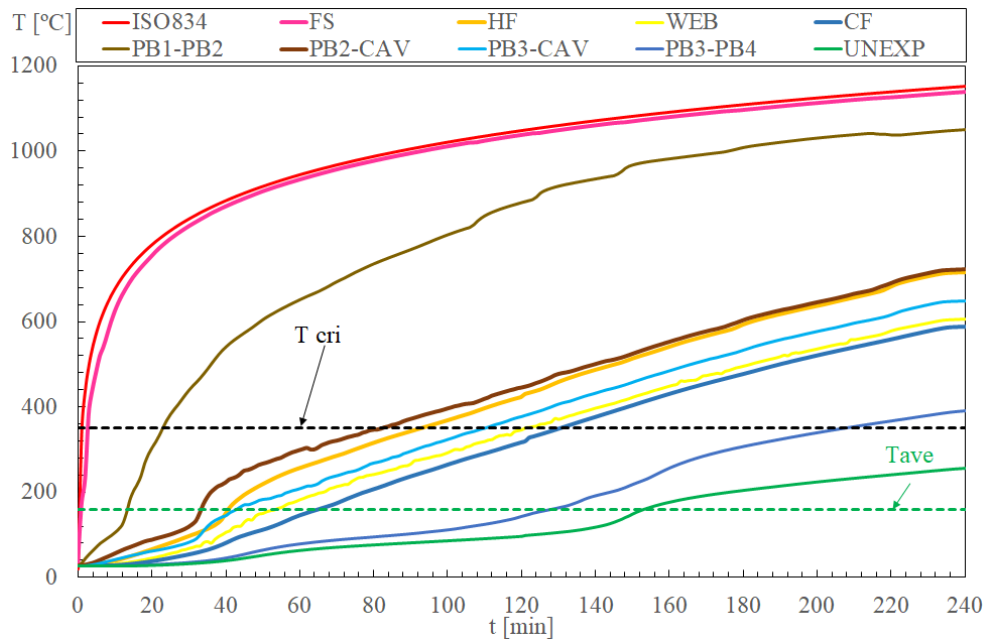


Figure 7.21: Case 14.

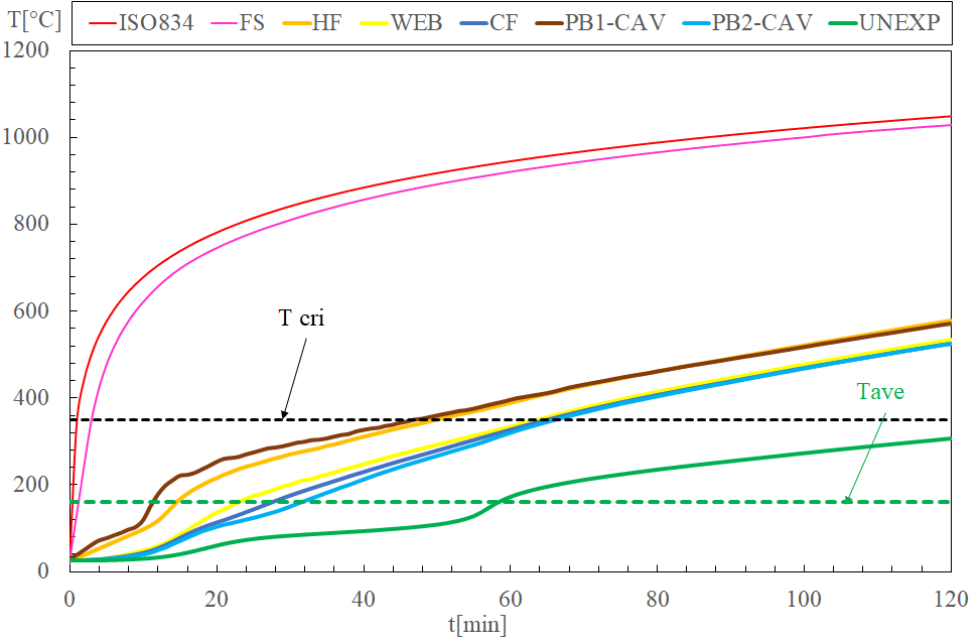


Figure 7.22: Case 15.

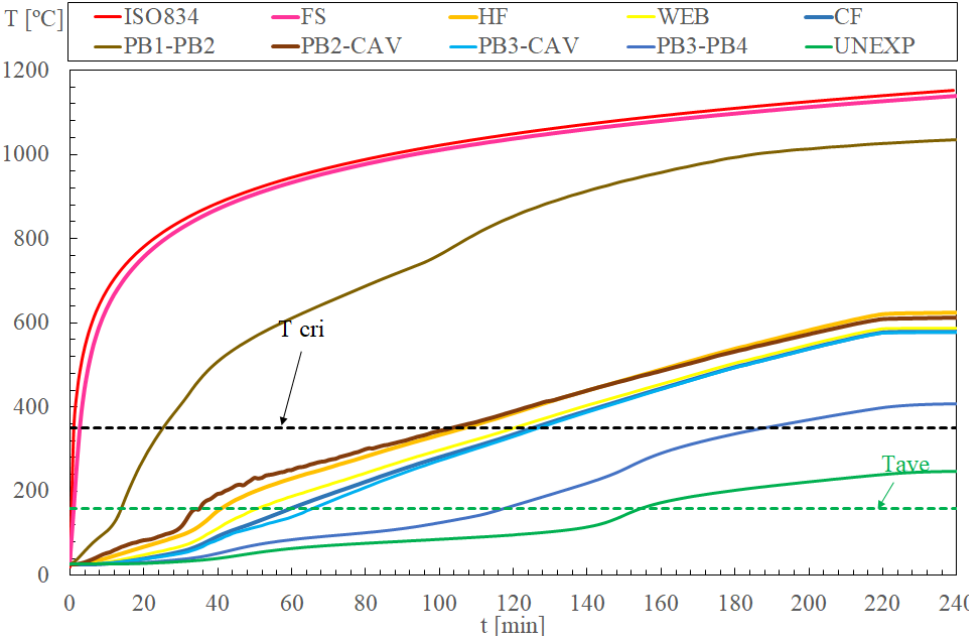


Figure 7.23: Case 16.





# Chapter 8

## Discussion of the Results

Four analyses will be performed: one about the variation of the protection layer of the structure, another about the performance of composite protection layer against the insulation of the cavity, a third one comparing the effect of variation of the LSF structure using the same composite solution with cork and gypsum for protection and one related with the variation of the insulate material. The parametric analysis and the tests were proposed to bring a knowledge about effect of the variation of some parameters to increase the fire resistance in LSF walls.

### 8.1 Influence of the Protection Layer

Two analysis were performed in this section: one about the variation of different protection layers with the same structure, and one with the variation of the thickness of the gypsum.

#### 8.1.1 Influence of the material

The specimens 1, 2, 4 and 7 have the same LSF configuration: 5 studs and empty cavities, but with different protection layers: single gypsum plasterboard, double gypsum plasterboard, composite of cork and gypsum plasterboard and composite of OSB and

gypsum plasterboard, respectively. Taking into consideration the average of temperature and nominal temperatures of the unexposed surface of these cases it is possible take some conclusions.

The figure 8.1 presents the temperature variation of the unexposed surface with time. It is possible to see that the specimen 2 has the best fire resistance. The fire resistance is represented by the intersection of the dashed line and the respective curve. The composite wall of cork and plasterboard (specimen 4) had worst results when compared to the single plasterboard, but the cork kept lower temperatures than the simple wall, with sharper increase. The composite wall with OSB (specimen 7) has the second best performance, even with existence of the combustion material in the layer. The rate of consumption of the cork is bigger than the rate of consumption of the OSB. The cork burns faster than OSB. The cork is a good insulator in ambient temperatures, but seems to be inadequate to fire conditions.

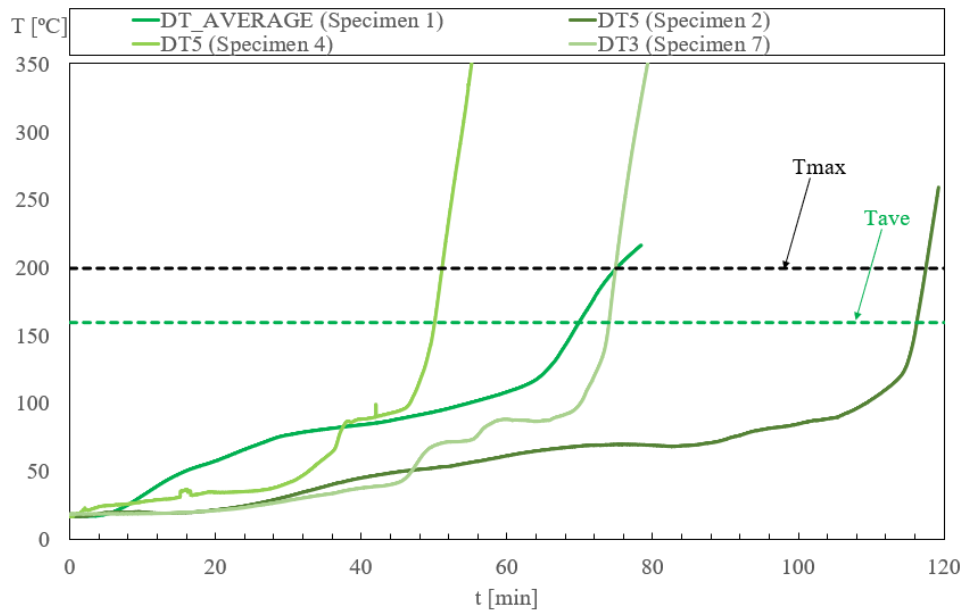


Figure 8.1: Unexposed Side Temperatures from Specimens 1, 2, 4 and 7.

The fire design of steel structures (Eurocode 3, part 1.2 [28]) suggests a criterion to class-4 member, using the average temperature to all the steel cross section, to estimate failure, as explained in the section 4.1.3. In all the cases in this study, the last part to

reach this temperature is the cold-flange (CF), and this time can be used to estimate the fire resistance of this structural element, in the load domain (R). The table 8.1 presents the results of this criterion in comparison with the insulation criterion. Once again it is worth noting that this approximation is over conservative, because this simple method is independent of the load ratio, being truly effective just for some cases.

Table 8.1: Influence of the variation of the material of the protection layer

Spec.	Plate Layer	FR [min] (I)	FR [min] (R)
1	1x12.5mm	70	51
2	2x12.5mm	119	85
4	1x12.5mm 1x10mm (Cork)	55	35
7	1x12.5mm 1x10mm (OSB)	77	55

### 8.1.2 Influence of the thickness of gypsum plasterboard

For the same thickness of the steel and thickness of the cavity, the increase of the plate thickness will produce an increase of the fire resistance, taking into consideration the insulation criterion. The parametric analysis based on geometry B modifies this parameter to three thickness of steel and three thickness of the cavity. The figure 8.2 brings a comparison of the fire resistance of this cases in function of the thickness of the plates.

Linear trend between the fire resistance and the thickness of the cavities, for each five configurations, brings an estimative of increase of 7.9 min in fire resistance for each 1mm of thickness of plasterboards.

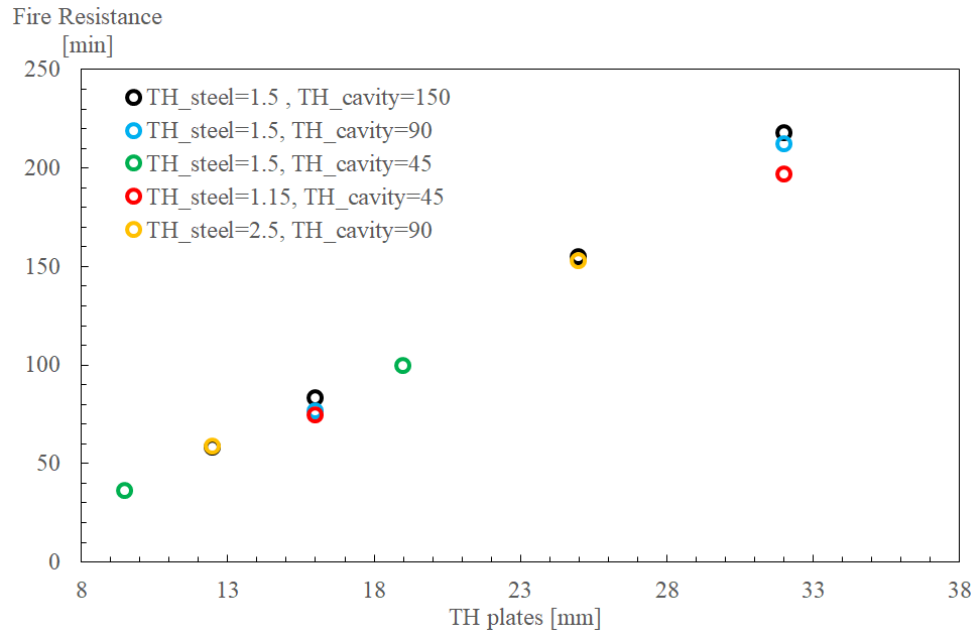


Figure 8.2: Comparison of the different gypsum plasterboard thickness to LSF configurations.

## 8.2 Insulation versus Protection Layer

In this section, the influence of the filled material cavity was analysed in comparison with a non-filled cavity against two different thickness of gypsum plasterboard. The analysis also considers the influence of the insulation materials with different densities and thickness of cavity.

### 8.2.1 Insulation of Protection Layer versus Cavity insulation

Specimens 1, 2 and 3 are going to be compared to analyse the effect of the protection layer versus the insulation of the cavity. The possibility to fill the cavity brings the possibility of increase some properties of the wall, such as acoustic insulation at room temperature, thermal insulation at room temperature and fire resistance. This comparison wants to evaluate the best measure to increase the fire resistance: increase the thickness of the gypsum plate or insert a insulation material in the cavity, in such this case, Rockwool.

The figure 8.3 presents the average and maximum temperatures of the unexposed side

of the specimens 1, 2 and 3, that have single plasterboard, double plasterboard and simple plasterboard with RockWool in the cavity, respectively. The fire resistance of the elements are also analysed, and these results are presented in the table 8.2

Table 8.2: Influence of the increase of the plasterboard thickness versus RockWool insulant.

Spec.	Insulation Cavity	Plate Layer	FR [min] (I)	FR [min] (R)
1	No	1x12.5mm	70	51
2	No	2x12.5mm	119	85
3	Yes	1x12.5mm	89	50

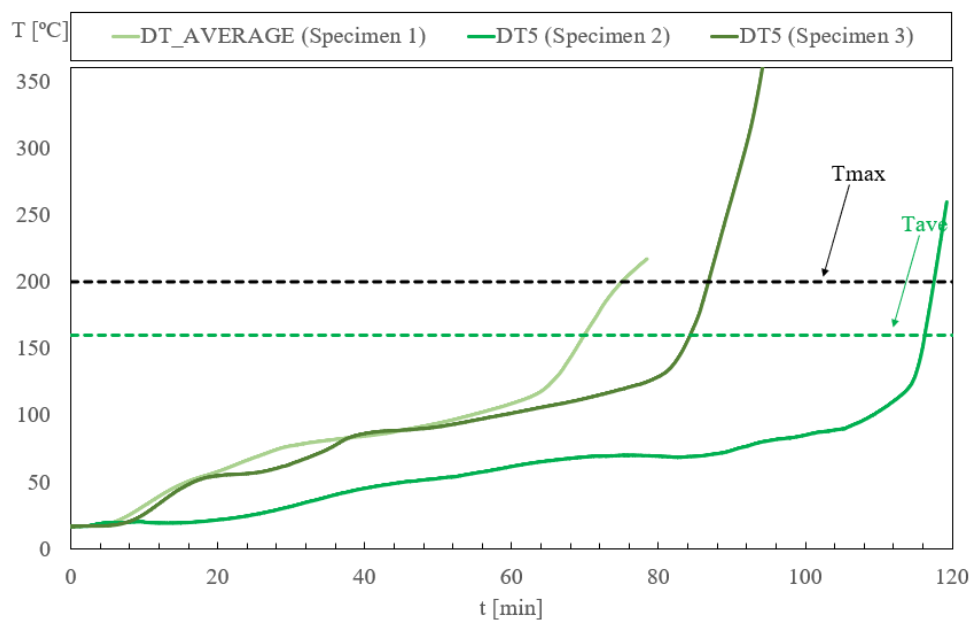


Figure 8.3: Unexposed Side Temperatures from Specimens 1, 2 and 3.

Is possible to observe that the increase the thickness of the plates is more effective to increase fire resistance. However, comparing with the results presented in subsection 8.1, the insulation material inside the cavity was more effective than every composite wall that was tested, that have the same LSF steel structure. The increase the thickness of the gypsum is the best way to improve the fire resistance.

The parametric analysis based on geometry A has some cases with same thickness of the plates, same thickness of the steel and different thickness of the cavity, but without

insulation. In this cases, the increase of the thickness of the cavity seems to produce a small increase of fire resistance, when comparing the cases 9, 10, 11 and 12. A increase of 0.1 minute for each 1mm of cavity was estimated.

## 8.2.2 Influence of insulation density and cavity thickness

The 9 cases of the parametric analysis based on geometry A are going to be compared to analyse the effect of the thickness of the cavity and the density of the insulation material. The figure 8.4 presents the curve corresponding to the fire resistance definition, average or maximum temperatures of the unexposed side, of the cases 1 to 9.

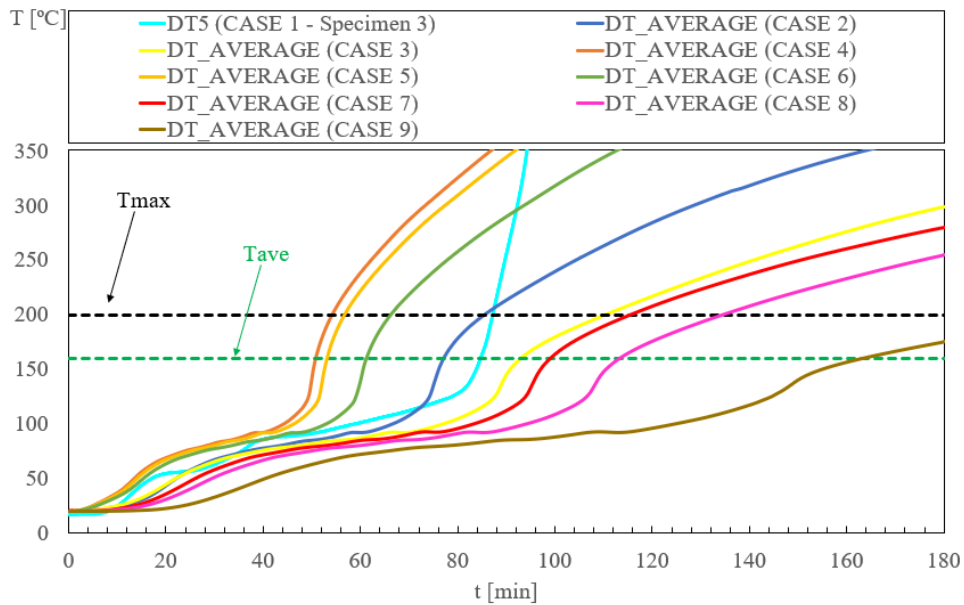


Figure 8.4: Unexposed Side Temperatures from Cases 1 to 9.

The figure 8.5 presents the effect of the increase of the insulation material density in the fire resistance. Is possible to observe that the increase of the density has more influence in bigger thickness of cavities. For the thickness of 45 mm, the increase of the density from 45 kg/m<sup>3</sup> to 300 kg/m<sup>3</sup> brings 10 minutes more of fire resistance. For the thickness of 150 mm, the same increase of density is responsible for the increase of 64 minutes of fire resistance.

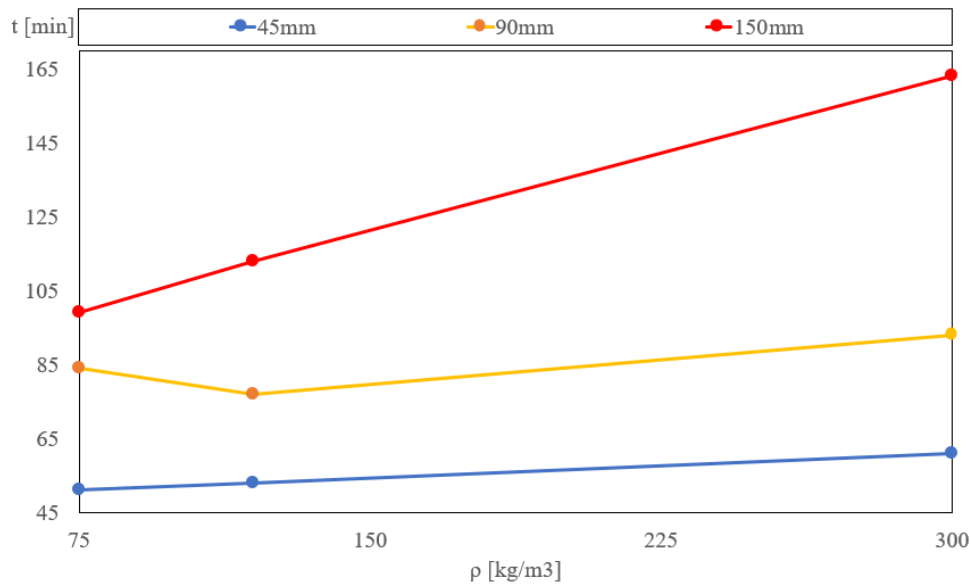


Figure 8.5: Fire Resistance in function of the density of the Rockwool.

The thickness of the cavity has more influence in the fire resistance than the density of the insulation material. For a density of 75 kg/m<sup>3</sup> of rockwool, the increase of the thickness from 45 mm to 150 mm brings 48 min more of fire resistance, and for the density of 300 kg/m<sup>3</sup>, the same increase brings 102 minutes more of fire resistance. The case 1 (specimen 4) presents a bigger fire resistance than the case 2, with a more dense insulation material, but comparing the variation of the results between the density of 75 kg/m<sup>3</sup> and 120 kg/m<sup>3</sup> to the three thicknesses of cavity, the variation of this result is acceptable.

### 8.3 Influence of LSF Structure

This section brings the analysis about the effect of modification of the LSF structure on the fire resistance: the influence of the variation of the number of studs and the influence of the thickness of the steel.

### 8.3.1 Influence of studs

The composite cork-gypsum protection layer was used in the specimens 4, 5 and 6. These was an attempt to use the insulation capacity of the cork to improve the fire resistance of the walls. The comparison performed in the subsection 8.1 has already showed that this protection layer was not so effective as the other tested solutions. The figure 8.6 presents the temperature of the unexposed side of the specimens 4, 5 and 6, that have 5, 3 and 4 studs, respectively. The table 8.3 presents the fire resistance of these specimens.

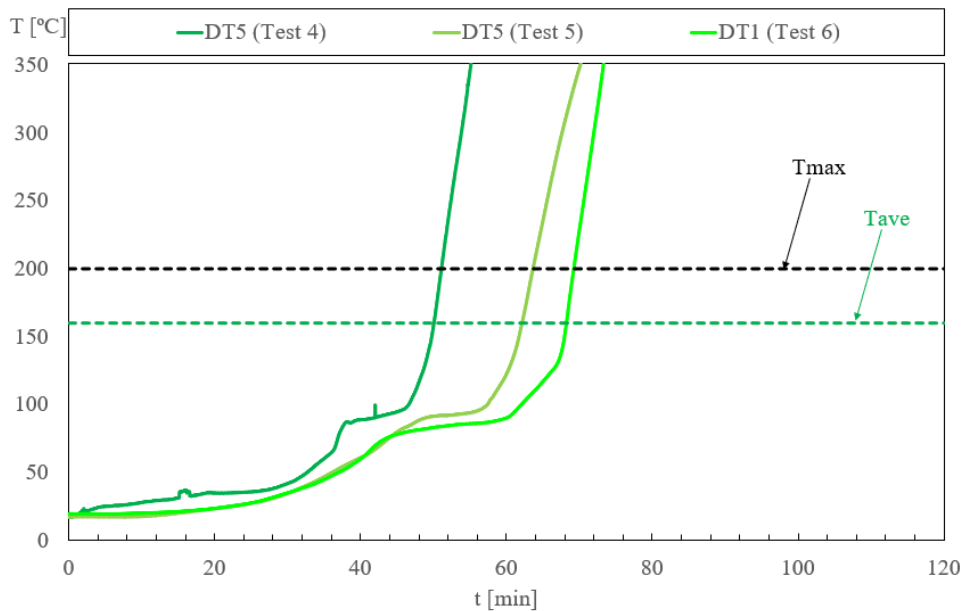


Figure 8.6: Unexposed Side Temperatures from Specimens 4, 5 and 6.

Table 8.3: Influence of studs.

Spec.	N°Studs	Plate Layer	FR [min] (I)	FR [min] (R)
4	5	1x12.5mm 1x10mm (Cork)	51	35
5	3	1x12.5mm 1x10mm (Cork)	66	41
6	4	1x12.5mm 1x10mm (Cork)	69	44

Anyway, to evaluate the influence of the structure in the fire resistance, the specimens



4, 5 and 6 were analysed, keeping the same protection layer of the composite cork-gypsum on the wall and modifying the LSF structure, using 5, 4 and 3 studs. These results shows the LSF structure influence in the fire resistance of the walls. The specimen 6 has approximately the same volume of cavity that the specimen 4 but had 18 min more fire resistance than specimen 4. The extra track provides better thermal insulation because divides the height of the wall into two parts, providing bigger temperatures between the zone of top disk thermocouples and the zone of the bottom disk thermocouples. This fact justifies the increase of fire resistance.

### 8.3.2 Influence of Steel thickness

The parametric analysis based on geometry B brings some analysis with different thickness of steel for the same wall configurations. The table 8.4 presents the fire resistance of the cases for thickness of cavity equal to 90mm.

Table 8.4: Influence of Steel Thickness.

Cases	Thick. Steel	Plate Layer	FR [min] (I)
1	1.15	1x16mm	74.4
2	1.15	2x16mm	211
11	1.5	1x16mm	76.6
12	1.5	2x16mm	212

Comparing the case 1 with case 11 and case 2 with case 12, that have the same protection layer, is possible to observe that the thickness of the steel has not significant influence in the fire resistance. The increase of 100% in the thickness of the gypsum plasterboard increases the fire resistance in almost 300%, but the increase of 30% in the thickness of the steel modifies the fire resistance of 1 and 2 minutes.

This construction method usually do not use steel profiles with more than 2 mm, so it is possible to conclude that this factor can not bring significant increase in the insulation fire resistance. The criterion for class 4 elements from Eurocode 3, part 1.2 [28], was not

evaluated here once that the cases 1 and 2 are the experimental cases from Kokalar [34], and the author did not provide informations about this estimative.

# Chapter 9

## Conclusions

This work presented a study across the fire effects on a non-loadbearing walls made with Light Steel Frame (LSF) structure, to improve the knowledge using different configurations and materials. 12 specimens with 11 different configurations were analysed, and 22 parametric analysis were performed to evaluate the influence of some parameters in the fire resistance.

The insulation of the protection layer, among the LSF structure influence, the thickness of the empty cavity and the insulation of the cavity, were the most relevant parameters in the fire resistance of the LSF nonloadbearing walls. The gypsum plasterboard was the best protection layer, with an increase of approximately 7.9 min per mm of plasterboard.

The insulation of cavities brings relevant improvements to fire resistance also, but the influence of this solution is proportional to the thickness of the cavity. The cavity of 45 mm presents a fire resistance of 51 min to a insulate with 75 kg/m<sup>3</sup> and 10 minutes of improvement when using an four times more dense. The same improvement of the density in a cavity with 150 mm increases 64 minutes. The increase of the cavity in to a density of 75 kg/m<sup>3</sup> brings is the increase 0.21 minutes per mm of cavity. For a density of 120 kg/m<sup>3</sup> one mm of cavity corresponds to 0.25 minutes of fire resistance, and for a density of 300 kg/m<sup>3</sup>, the increase is 0.45 min per mm of cavity. The relation between the fire resistance and thickness of the cavity has a linear trend.

The thickness of the steel did not present a relevant influence on the insulation criterion

of fire resistance, but the geometry of the LSF structure present a considerable influence. The specimen 4 and the specimen 6 presented 4 cavities with approximately the same volume, but the specimen with 3 tracks and 4 studs, with cavities distributed in the four zones of the wall, had 18 min more fire resistance that the specimen with 2 tracks and 5 studs, with cavities as 5 rectangles equally spaced in length.

For future works, some studies are in course to evaluate the fire resistance of loadbearing LSF structure. A mathematical model based on the results of the experimental tests was performed by the authors to define the fire resistance. A validation of this model with loadbearing experimental tests is required, and a proposal for a new criterion should be presented in alternative to the current version of Eurocode 3.

# Bibliography

- [1] E. 1363-1, *Fire resistance tests - part 1: General requirements*. Brussels: European Committee for Standardization, 2012.
- [2] E. 1364-1, *Fire resistance tests for non-loadbearing elements. part 1: Walls*. Brussels: European Committee for Standardization, 1999.
- [3] E. L. S. C. Association, *European lightweight steel-framed construction*. Belgium, 2004.
- [4] T. A. for Specialist Fire Protection (ASFP), *Fire rated non-loadbearing partitions - "the purple book"*, 1st. Surrey: ASFP Publication, 2003, ISBN: 1870409213.
- [5] S. Wanniarachchi, "Flexural behaviour and design of cold-formed steel beams with rectangular hollow flanges", *PHD Thesis*, Queensland University of Technology 2005.
- [6] A. Chajes, S. Britvec, and G. Winter, "Effects of cold-straining on structural sheet steels", *Journal of the Structural Division*, vol. 89, no. 2, pp. 1–32, 1963.
- [7] K. J. Schwartz and T. T. Lie, "Investigating the unexposed surface temperature criteria of standard astm e119", *Fire Technology*, vol. 21, no. 3, pp. 169–180, 1985.
- [8] J. Mehaffey, P. Cuerrier, and G. Carisse, "A model for predicting heat transfer through gypsum-board/wood-stud walls exposed to fire", *Fire and materials*, vol. 18, no. 5, pp. 297–305, 1994.
- [9] J. Gerlich, P. C. R. Collier, and A. H. Buchanan, "Design of light steel-framed walls for fire resistance", *Fire and Materials*, vol. 20, no. 2, pp. 79–96, 1996.

- [10] F. Alfawakhiri, M. A. Sultan, and D. H. MacKinnon, “Fire resistance of loadbearing steel-stud wall protected with gypsum board: A review”, *Fire technology*, vol. 35, no. 4, pp. 308–335, 1999.
- [11] Y. Sakumoto, T. Hirakawa, H. Masuda, and K. Nakamura, “Fire resistance of walls and floors using light-gauge steel shapes”, *Journal of Structural Engineering*, vol. 129, no. 11, pp. 1522–1530, 2003.
- [12] Y. Telue and M. Mahendran, “Design of cold-formed steel wall frames lined with plasterboard on one side under axial compression”, *International Journal of Steel Structures*, vol. 6, no. 1, pp. 1–12, 2006.
- [13] S. L. Manzello, R. G. Gann, S. R. Kukuck, K. Prasad, and W. W. Jones, “Performance of a non-load-bearing steel stud gypsum board wall assembly: Experiments and modelling”, *Fire and Materials*, vol. 31, no. 5, pp. 297–310, 2007.
- [14] S.-H. Park, S. L. Manzello, M. F. Bundy, and T. Mizukami, “Experimental study on the performance of a load-bearing steel stud gypsum board wall assembly exposed to a real fire”, *Fire Safety Journal*, vol. 46, no. 8, pp. 497–505, 2011.
- [15] B. Baleshan, “Numerical and experimental studies of cold-formed steel floor systems under standard fire conditions”, *PhD thesis*, Queensland University of Technology April 2012.
- [16] N. D. Kankanamge and M. Mahendran, “Mechanical properties of cold-formed steels at elevated temperatures”, *Thin-Walled Structures*, vol. 49, no. 1, pp. 26–44, 2011.
- [17] P. Kolarkar and M. Mahendran, “Experimental studies of non-load bearing steel wall systems under fire conditions”, *Fire safety journal*, vol. 53, pp. 85–104, 2012.
- [18] D. Kontogeorgos, K. G. Wakili, E. Hugi, and M. Founti, “Heat and moisture transfer through a steel stud gypsum board assembly exposed to fire”, *Construction and Building Materials*, vol. 26, no. 1, pp. 746–754, 2012.

- [19] S. Kesawan and M. Mahendran, “Fire tests of load-bearing lsf walls made of hollow flange channel sections”, *Journal of Constructional Steel Research*, vol. 115, pp. 191–205, 2015.
- [20] S. Kesawan and M. Mahendran, “Fire design rules for lsf walls made of hollow flange channel sections”, *Thin-Walled Structures*, vol. 107, pp. 300–314, 2016.
- [21] M. Rusthi, P. Keerthan, A. D. Ariyanayagam, and M. Mahendran, “Numerical studies of gypsum plasterboard and mgo board lined lsf walls exposed to fire”, in *Proceedings of the Second International Conference on Performance-based and Life-cycle Structural Engineering (PLSE 2015)*, The University of Queensland, 2015, pp. 1077–1084.
- [22] A. D. Ariyanayagam and M. Mahendran, “Fire tests of non-load bearing light gauge steel frame walls lined with calcium silicate boards and gypsum plasterboards”, *Thin-Walled Structures*, vol. 115, pp. 86–99, 2017.
- [23] V. Jatheeshan and M. Mahendran, “Fire resistance of lsf floors made of hollow flange channels”, *Fire Safety Journal*, vol. 84, pp. 8–24, 2016.
- [24] P. V. Real, *Incêndio em estruturas metálicas: Cálculo estrutural*. Edições Orion, 2003.
- [25] T. L. Bergman and F. P. Incropera, *Fundamentals of heat and mass transfer*. John Wiley & Sons, 2011.
- [26] E. 1991-1-2, *Eurocode 1: Actions on structures - part 1-2: General actions - actions on structures exposed to fire*. Brussels: European Committee for Standardization, 2002.
- [27] J.-M. Franssen and T. Gernay, “Modeling structures in fire with safir®: Theoretical background and capabilities”, *Journal of Structural Fire Engineering*, vol. 8, no. 3, pp. 300–323, 2017.
- [28] E. 1993-1-2, *Eurocode 3: Design of steel structures. part 1-2: General rules - structural fire design*. Brussels: European Committee for Standardization, 2005.

- [29] P. Keerthan and M. Mahendran, “Thermal performance of load bearing cold-formed steel walls under fire conditions using numerical studies”, *Journal of Structural Fire Engineering*, vol. 5, no. 3, pp. 261–290, 2014.
- [30] S. Lundberg, “Material aspects of fire design. talat lectures 2502 (training in aluminium application technologies, leonardo da vinci project tas/wp (pp. 21)”, *EAA - European Aluminium Association*, Queensland University of Technology 1997.
- [31] P. Keerthan and M. Mahendran, “Thermal performance of composite panels under fire conditions using numerical studies: Plasterboards, rockwool, glass fibre and cellulose insulations”, *Fire technology*, vol. 49, no. 2, pp. 329–356, 2013.
- [32] E. 1995-1-2, *Eurocode 5 – design of timber structures. part 1-2: General – structural fire design*. Brussels: European Committee for Standardization, 2004.
- [33] ISO834, *Iso 834-1. fire-resistance tests - elements of building construction – part 1: General requirements*. Switzerland: Technical Committee ISO/TC 92, 1999.
- [34] P. N. Kokarkar, “Structural and thermal performance of cold-formed steel stud wall system under fire conditions”, *PhD thesis*, Queensland University of Technology September 2010.



# Appendix A

## Experimental Results

This appendix brings more informations about the experimental tests, as some photographs and detailed results.

### A.1 Specimen 0

The figure A.1 and A.2 presents the IR thermal images of the specimen 0 and his evolution in the time.

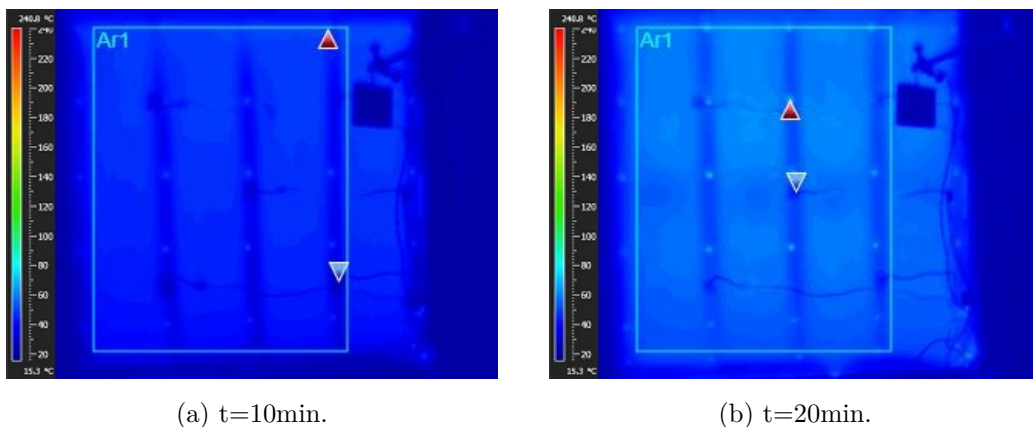


Figure A.1: Test 0 - IR Thermal Camera Results.

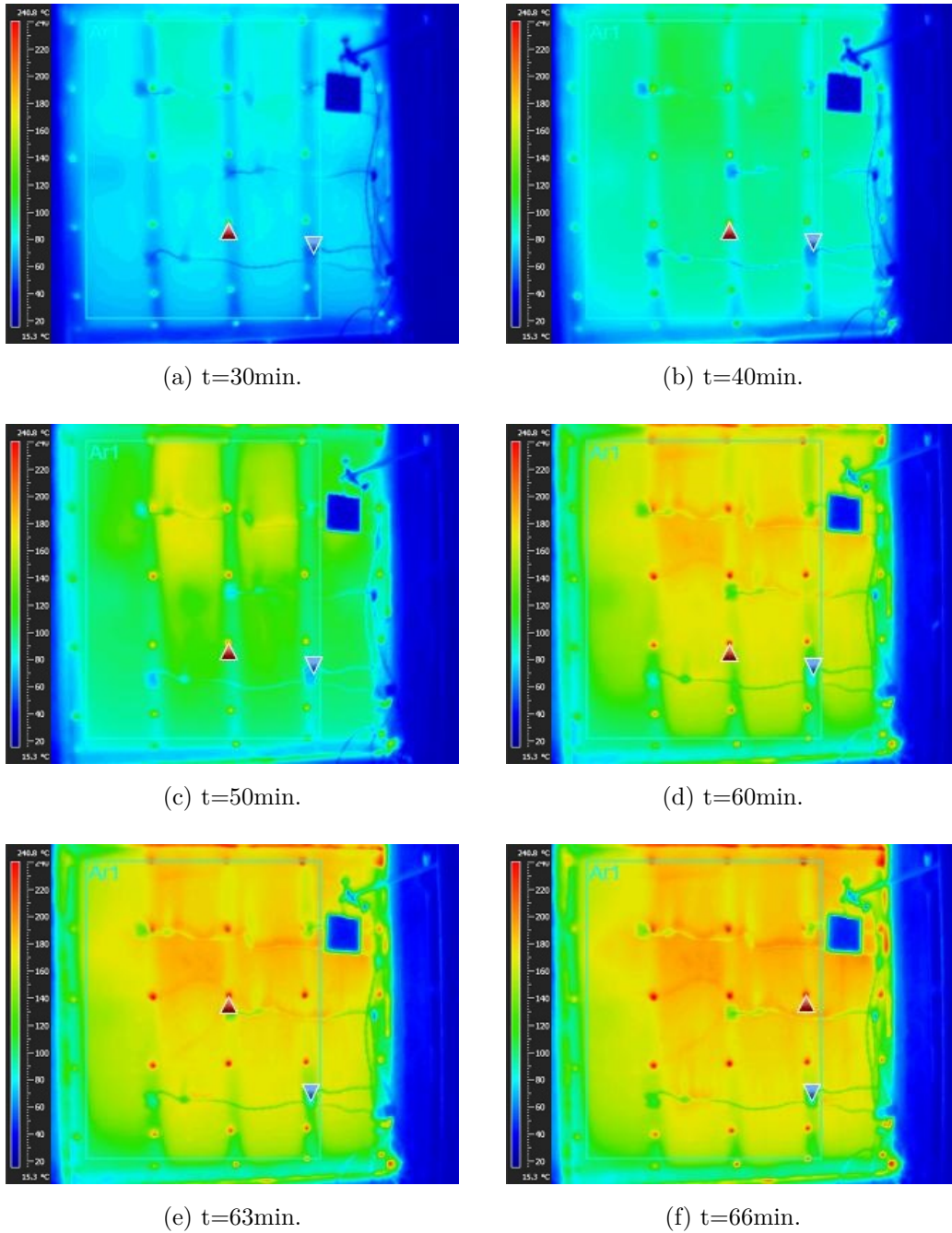
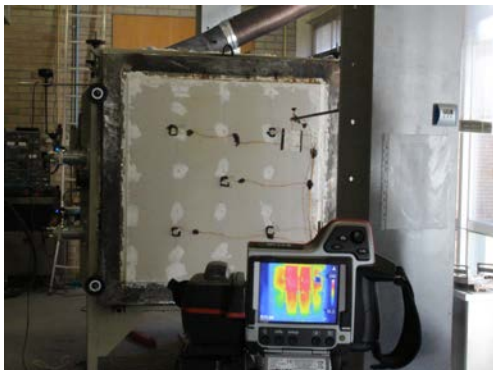


Figure A.2: Test 0 - IR Thermal Camera Results.

The area Ar1 represents the area used for measurement of the maximum temperature ( $T_{max}$ ), minimum temperature ( $T_{min}$ ) and average temperature ( $T_{average}$ ). The small separated cool zone represents the back surface of the plate thermocouple identified as

AMB.

The figure A.3 shows the specimen ready to be tested, and photos before and after the test. In this test is possible to see that the thermal expansion was not so important, and the integrity of the unexposed plate was maintained, without cracks and nothing more that just brown marks of fire in some parts of the paper that coat the gypsum, see fig. A.3b In this specimen, a small local web buckling was verified.



(a) Specimen 0 with IR Camera.



(b) Specimen 0, with emphases for the Disk Thermocouples and the Ambient Thermocouple.



(c) The exposed side after the end of the test.



(d) The cavity after the end of the test.

Figure A.3: Specimen 0 after the end of the test.

## A.2 Specimen 1

The figure A.4 and A.5 presents the temperature field evolution of the specimen 1 in time, captured by the IR Thermal Camera. The area Ar1, that covers approximately all the region of the wall, corresponds the area that provides information for the maximum temperature ( $T_{max}$ ), minimum temperature ( $T_{min}$ ) and average temperature ( $T_{average}$ ) used to estimate the fire resistance. Using the same procedure to previous test, the fire resistance using the thermal images is about 62 minutes.

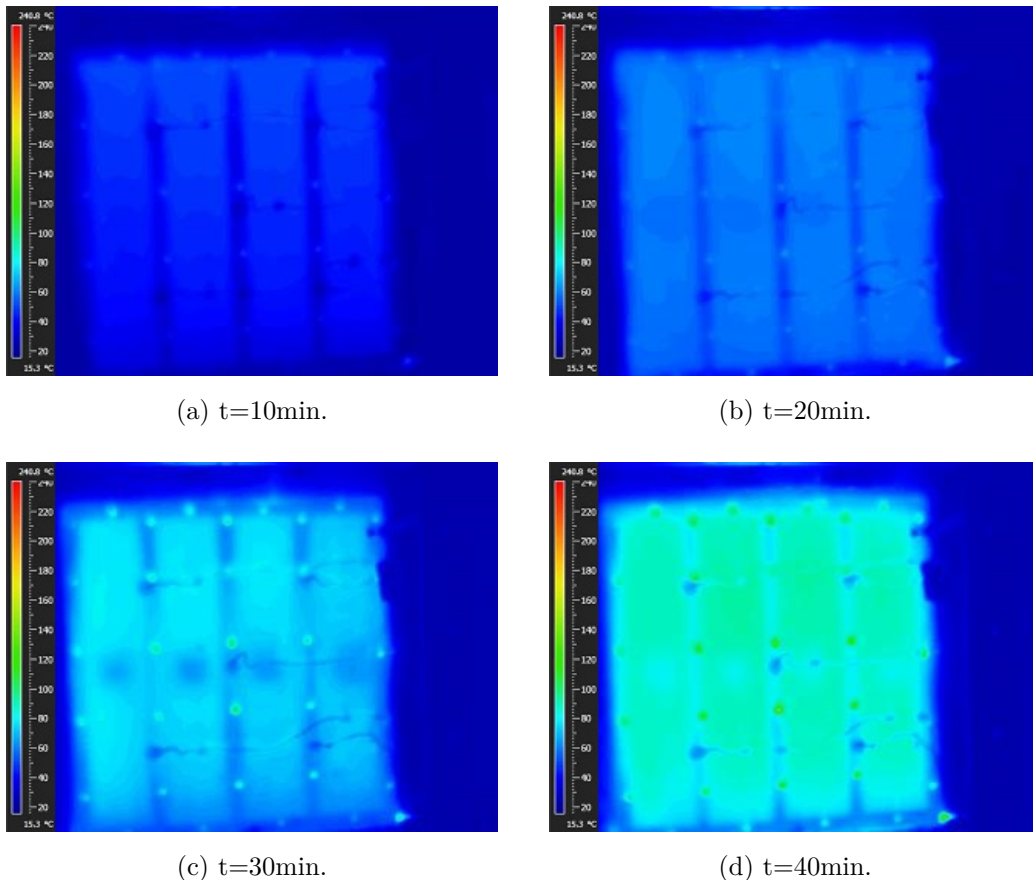


Figure A.4: Test 1 - IR Thermal Camera Results.

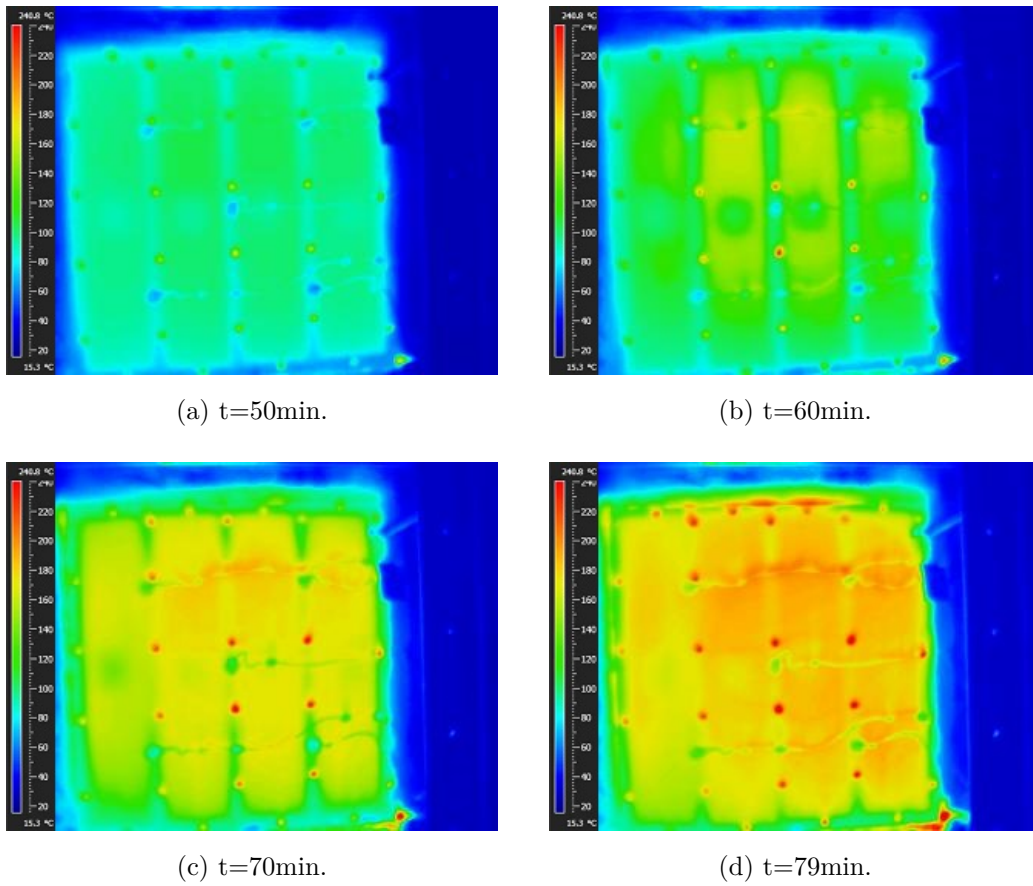
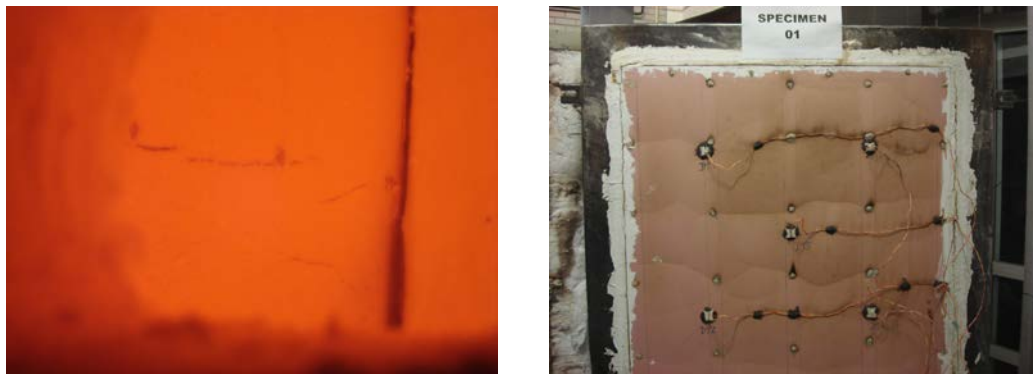


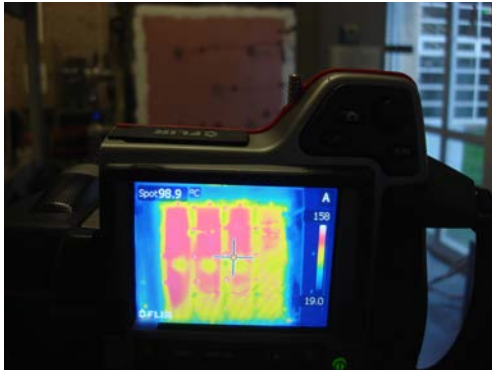
Figure A.5: Test 0 - IR Thermal Camera Results.

The figures A.6 and A.7 shows some images captured during the test.



(a) Specimen 1 by the window in the furnace. (b) The unexposed side after the end of the test.

Figure A.6: Specimen 1 after the end of the test.



(a) Specimen 1 with IR Camera.



(b) The exposed side after the end of the test.

Figure A.7: Specimen 1 after the end of the test.

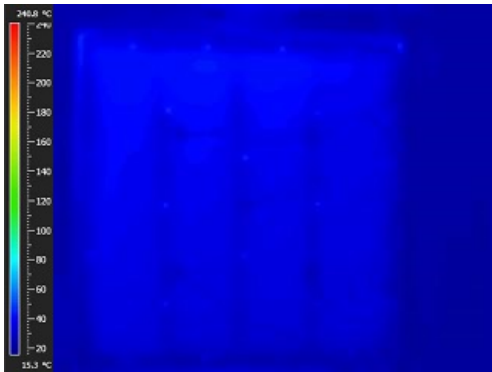
The furnace has a small window that allows that some images of the exposed face can be captured, see fig A.6a. The unexposed plate has an acceptable integrity, see fig A.6b, had an acceptable integrity, but with more brown masks than the specimen 0. The steel structure presents also some local web buckling.

### A.3 Specimen 2

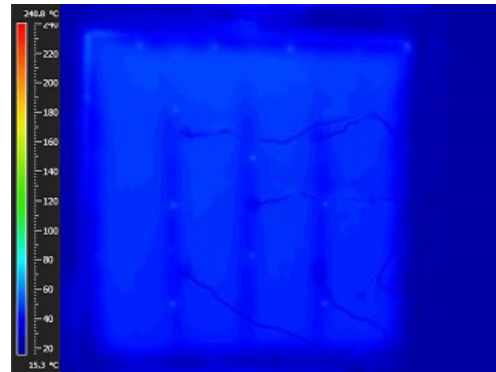
The figures A.8 to A.10 present the temperature evolution of the specimen 2 during time captured by the IR thermal Camera.

(a)  $t=10\text{min}$ .(b)  $t=20\text{min}$ .

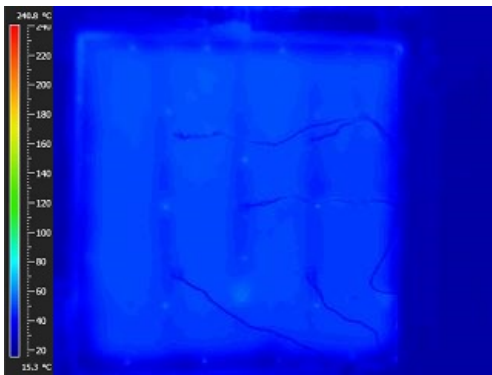
Figure A.8: Test 2 - IR Thermal Camera Results.



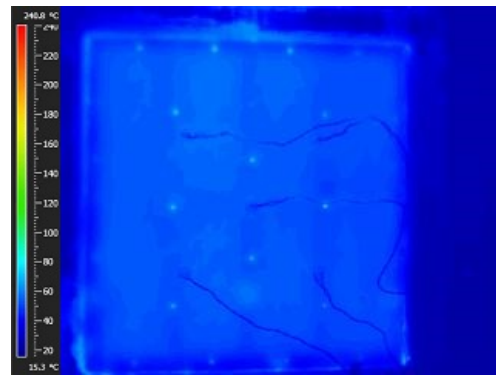
(a) t=30min.



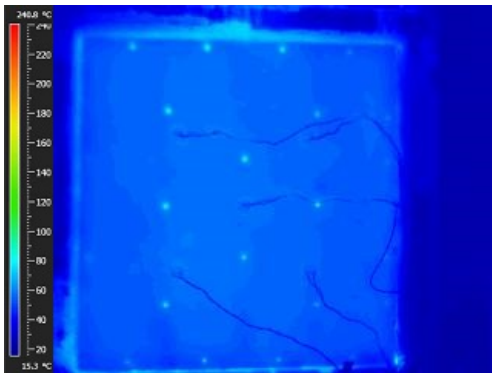
(b) t=40min.



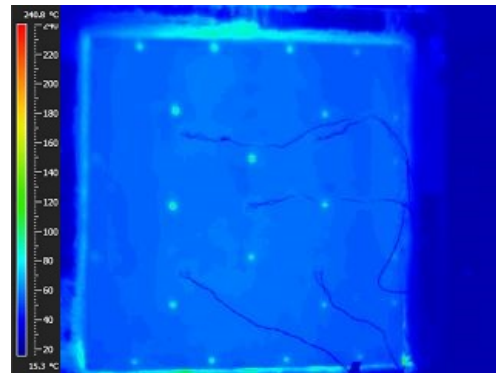
(c) t=50min.



(d) t=60min.



(e) t=70min.



(f) t=80min.

Figure A.9: Test 2 - IR Thermal Camera Results.

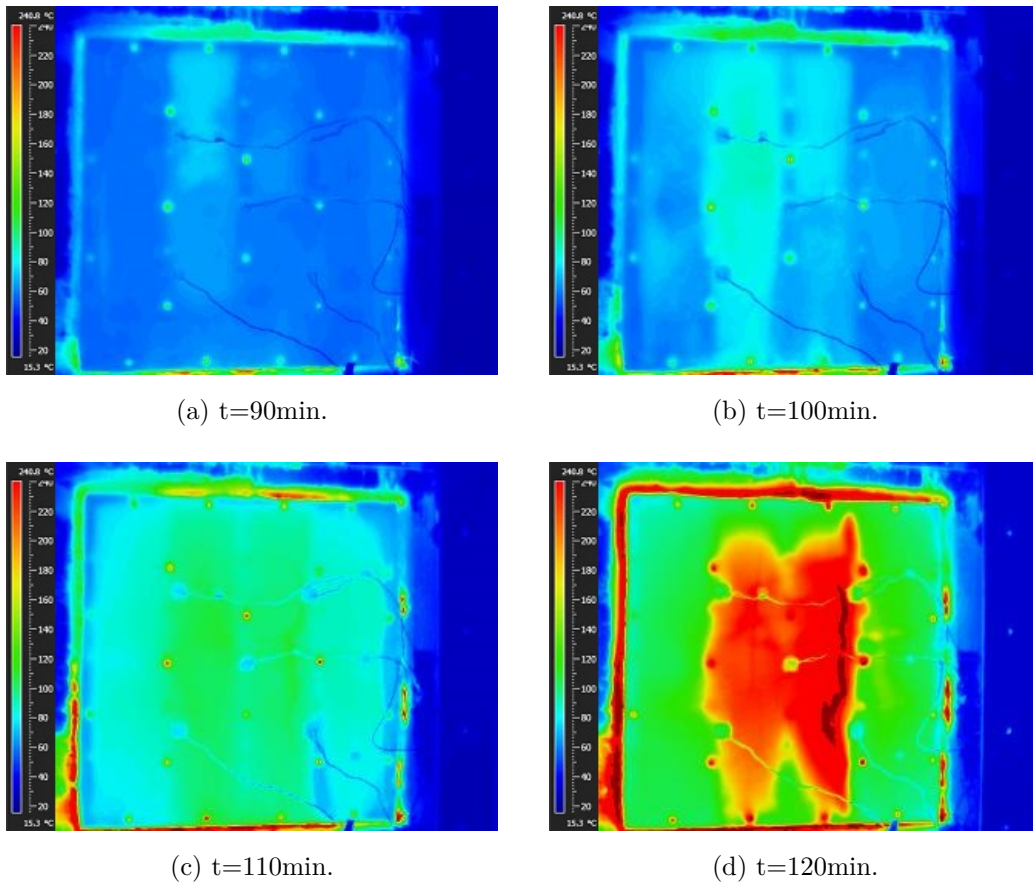


Figure A.10: Test 2 - IR Thermal Camera Results.

The figure A.11 and A.12 shows some images captured during and after the test.

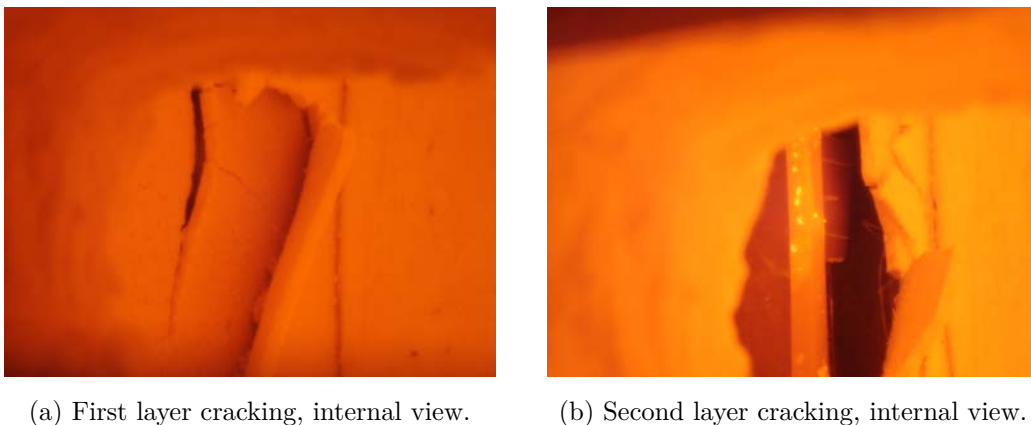
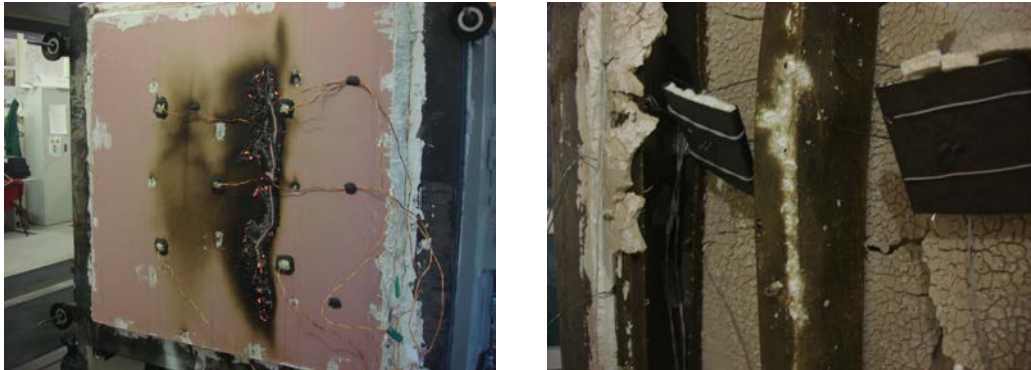


Figure A.11: Specimen 2 during and after the end of the test.





(a) Unexposed side after the end of the test. (b) Exposed side after the end of the test.

Figure A.12: Specimen 2 during and after the end of the test.

The fig A.11a shows the first plasterboard already cracked with the second plasterboard loosing integrity. The fig A.11b shows the cavity and the LSF exposed to fire, with the steel stud presenting some local web instability. The fig A.12a shows the unexposed plasterboard already cracked, after the end of the test. The fig A.12b represents a view from the exposed side. The steel stud presents local web instability and distortional instability modes due to thermal expansion. The fire resistance using the thermal images is about 117 minutes. This result is closer to the value obtained by direct measurement of the disk thermocouples.

## A.4 Specimen 3

The figures A.13 and A.14 show the IR thermal camera results. The fire resistance, using the thermal images, is about 72 minutes. The exposed layer fall down completely at approximately 80 min, and the cracks started at approximately 16 min. This justifies the rapid increase of the temperature in this regions. The thermal image corresponding to 100 min shows the first crack in the unexposed surface.

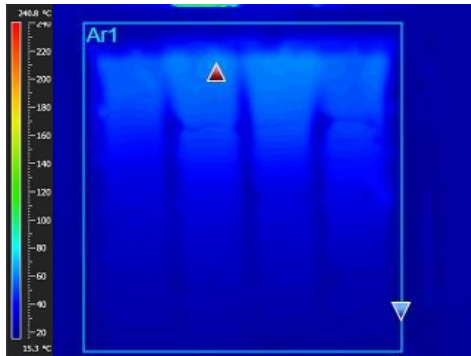
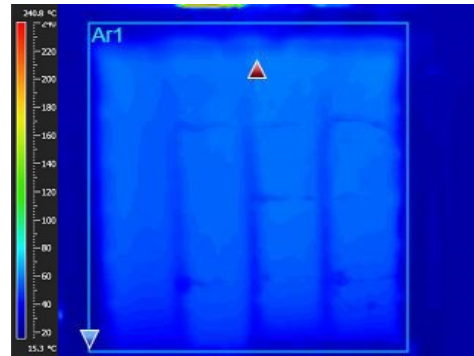
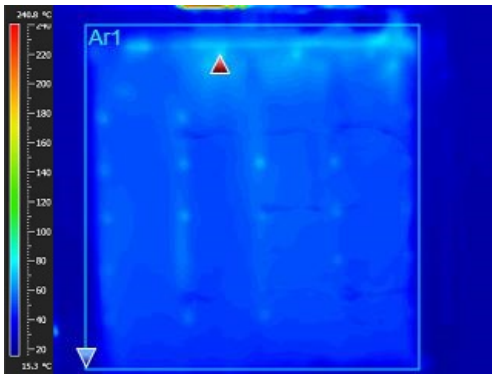
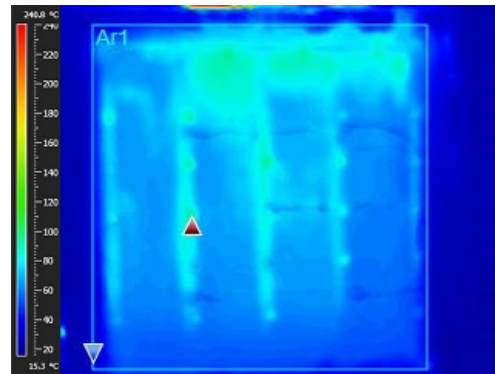
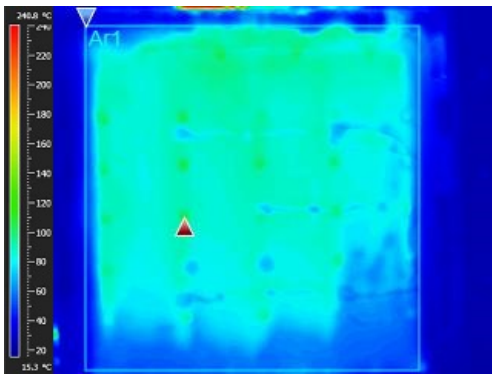
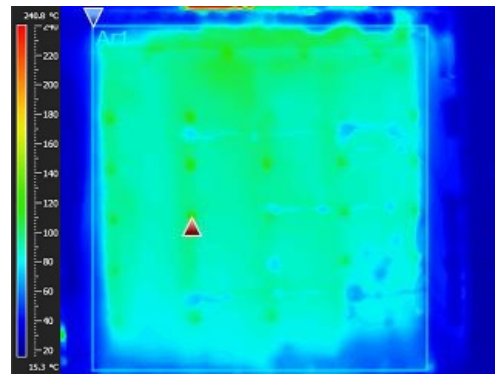
(a)  $t=10\text{min.}$ (b)  $t=20\text{min.}$ (c)  $t=30\text{min.}$ (d)  $t=40\text{min.}$ (e)  $t=50\text{min.}$ (f)  $t=60\text{min.}$ 

Figure A.13: Test 3 - IR Thermal Camera Results.

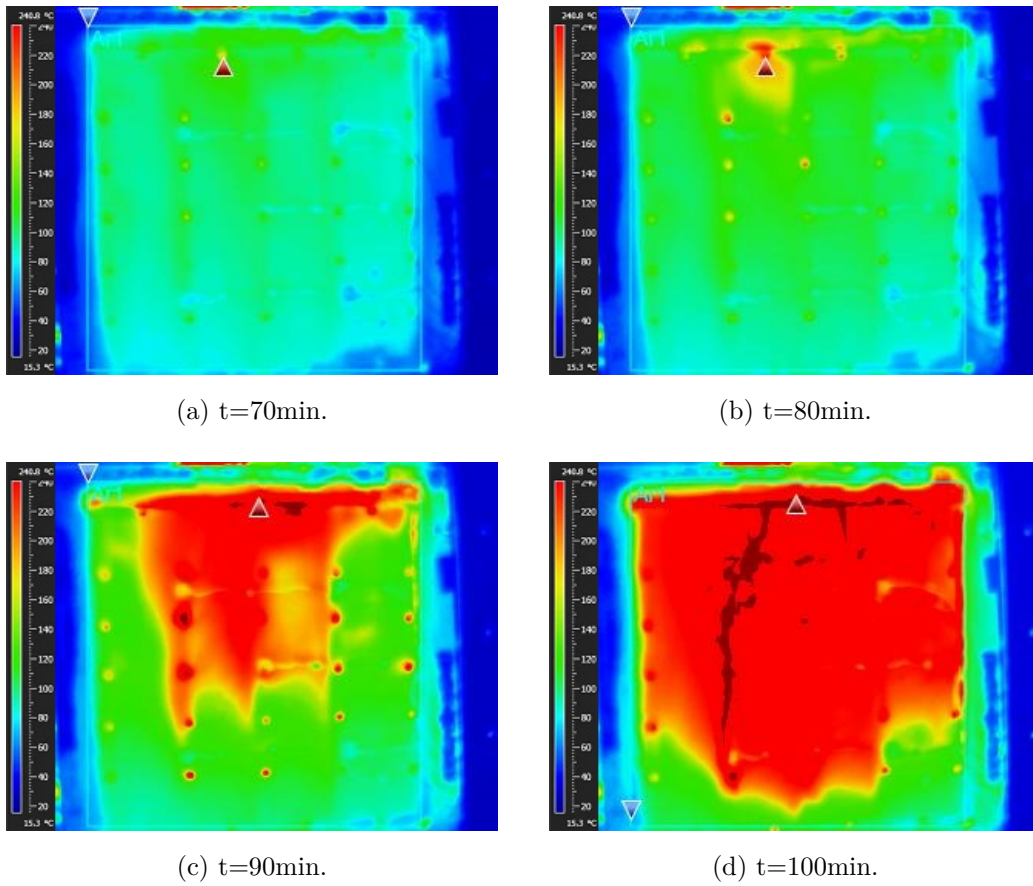


Figure A.14: Test 3 - IR Thermal Camera Results.

The figure A.15 and A.16 present some pictures during and after the test.

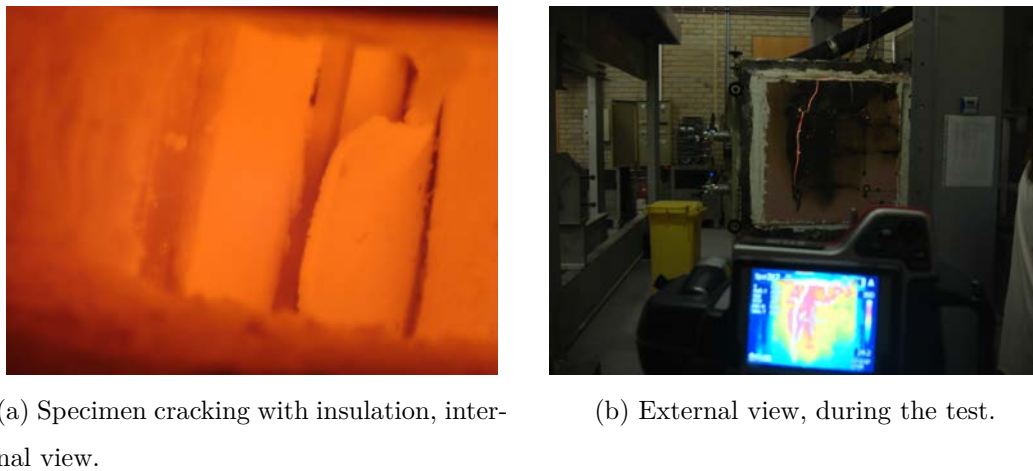


Figure A.15: Specimen 3 during and after the end of the test.



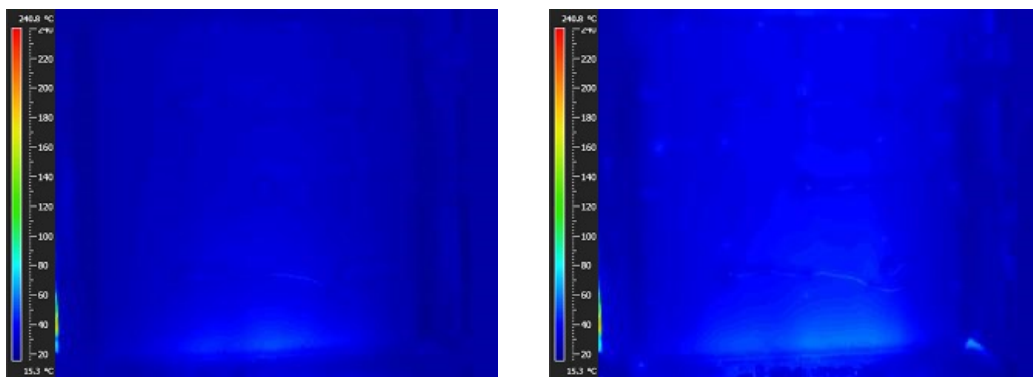
(a) Exposed side after the end of the test. (b) Exposed side after the end of the test.

Figure A.16: Specimen 3 during and after the end of the test.

The insulation did not melt, as expected, see fig A.16a and the deformations of the structure were smaller than in the previous tests. Distortional buckling and global buckling was identified for most of the studs, see fig A.16b. Local web instabilities were also detected. The figure A.16a and A.15b presents the gypsum plasterboard damage during the test.

## A.5 Specimen 4

The figure A.17 and A.18 and shows the IR thermal Camera images of this test.



(a)  $t=10\text{min}$ .

(b)  $t=20\text{min}$ .

Figure A.17: Test 4 - IR Thermal Camera Results.

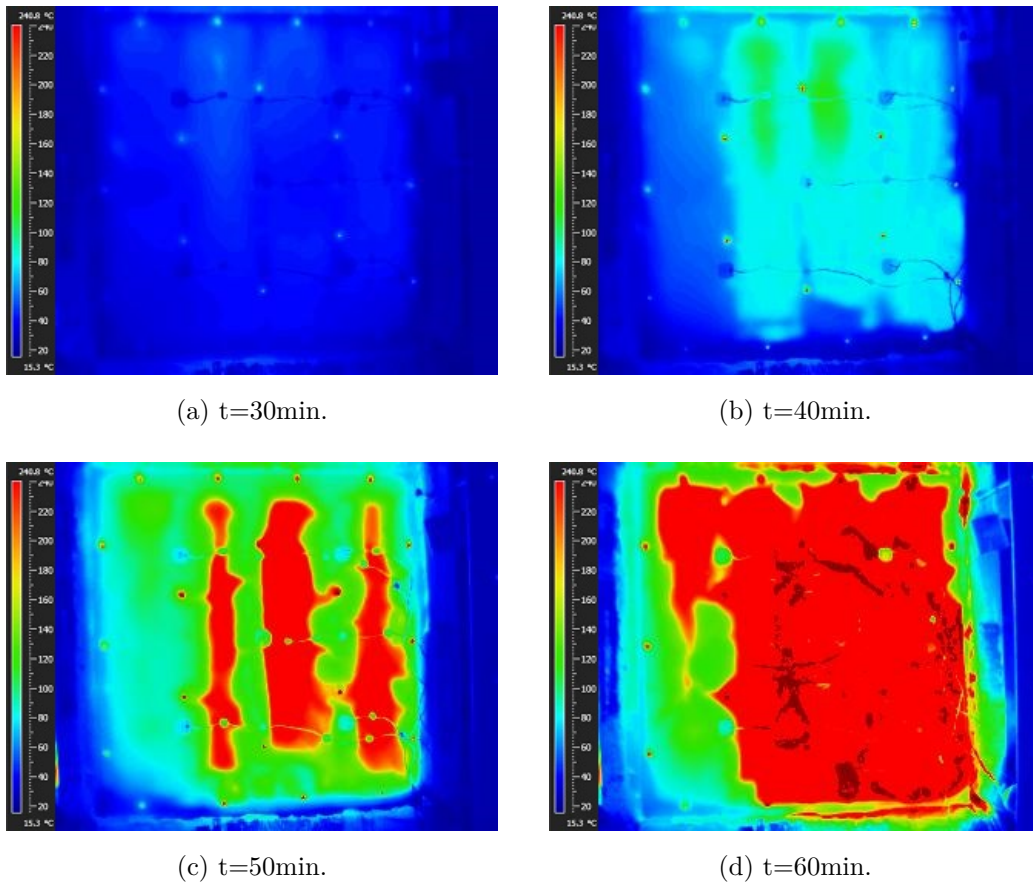


Figure A.18: Test 4 - IR Thermal Camera Results.

The figure A.19 and A.20 presents some images during the test and the final state of the wall.



(a) Cork starting to burn through the crack. (b) Cork burning after the fall of the layer.

Figure A.19: Specimen 4 during and after the end of the test.



(a) The unexposed side after the end of the test. (b) The exposed side after the end of the test.

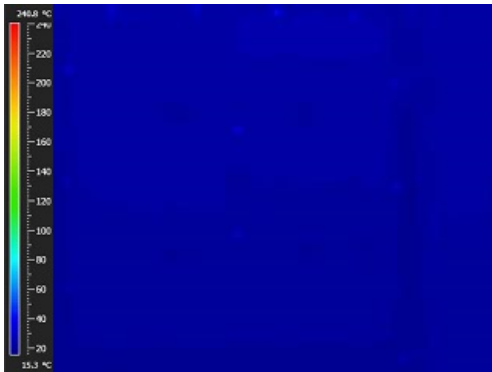
Figure A.20: Specimen 4 during and after the end of the test.

This test was stopped when a big crack appears in the wall, at 67 minutes, that was already visible in 60 min thermal image. The fire resistance using the thermal images is about 60 minutes. Is possible to observe when the cork starts to burn, with the fire entering trough the crack of the plasterboard, and to observe the broken plasterboard with some big flames causing by the cork combustion. The fig A.20a presents the unexposed surface for a time near the end of the test. The fig A.20b presents some pieces of cork still burning.

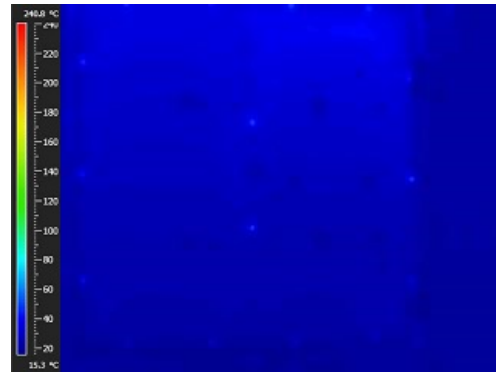
## A.6 Specimen 5

The figure A.21 and A.22 shows the IR thermal images of this test. The fire resistance estimated by the thermal images was 67 minutes, close of the fire resistance obtained by the average temperature criterion.

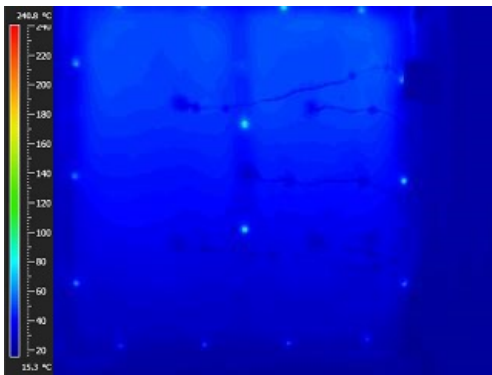
The figure A.23 presents some images of the test. In this test, the furnace window were not included, so internal images was not presented. The second cavity heated faster than the first one, as is possible to see in the pictures. The LSF structure presents global buckling for the central studs, and web and distortional buckling in all the studs.



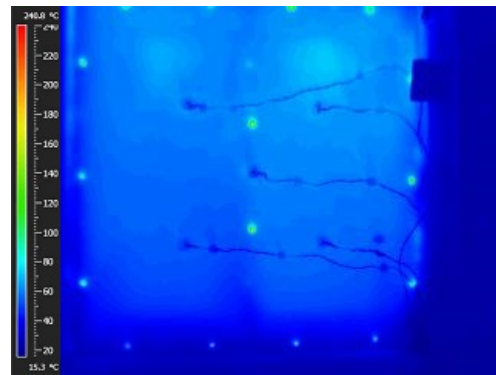
(a) t=10min.



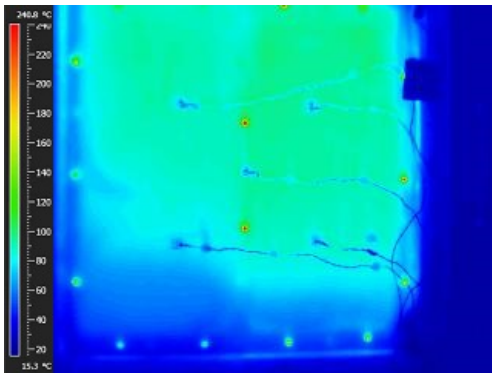
(b) t=20min.



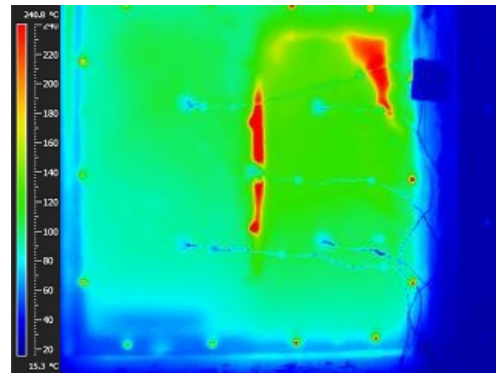
(c) t=30min.



(d) t=40min.



(e) t=50min.



(f) t=60min.

Figure A.21: Test 5 - IR Thermal Camera Results.

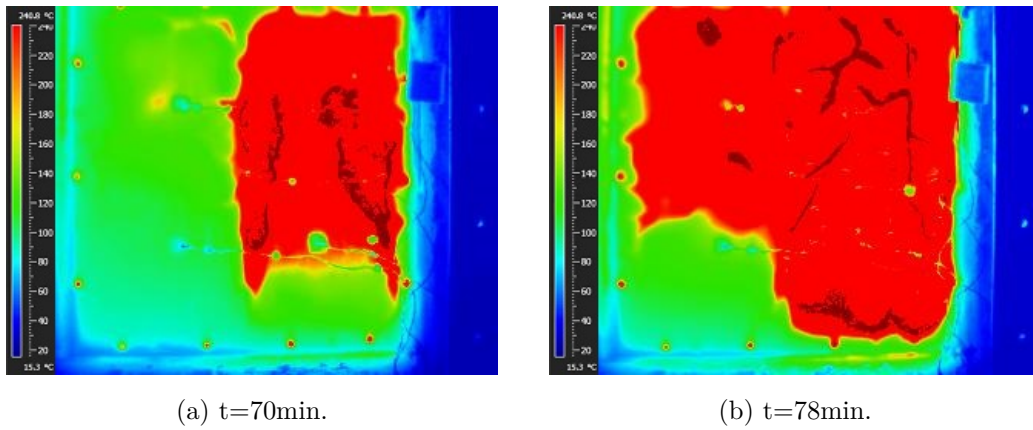


Figure A.22: Test 5 - IR Thermal Camera Results.

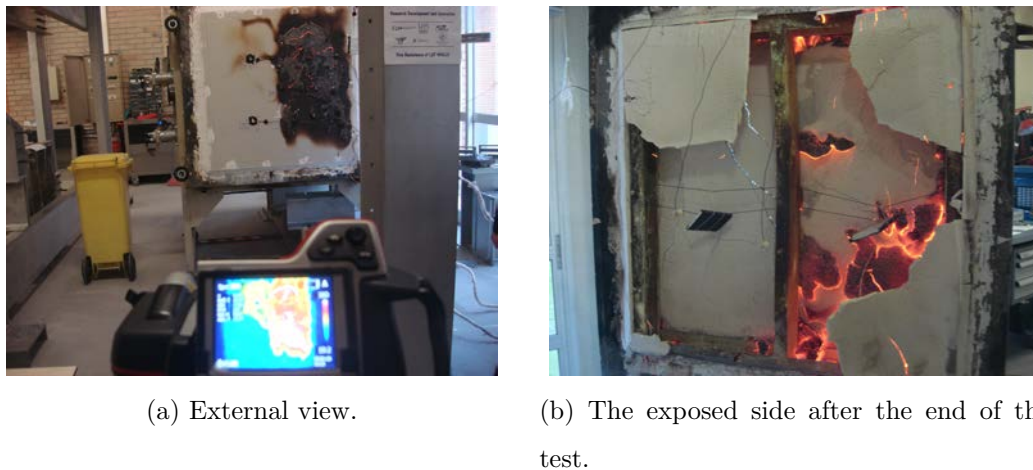


Figure A.23: Specimen 5 during and after the end of the test.

## A.7 Specimen 6

The figure A.24 and A.25 shows the IR Thermal images of this test. The fire resistance estimated by the thermal images was 72 minutes. The four cavities can be distinguished in the thermal images, and the last image corresponds to the failure of the wall.



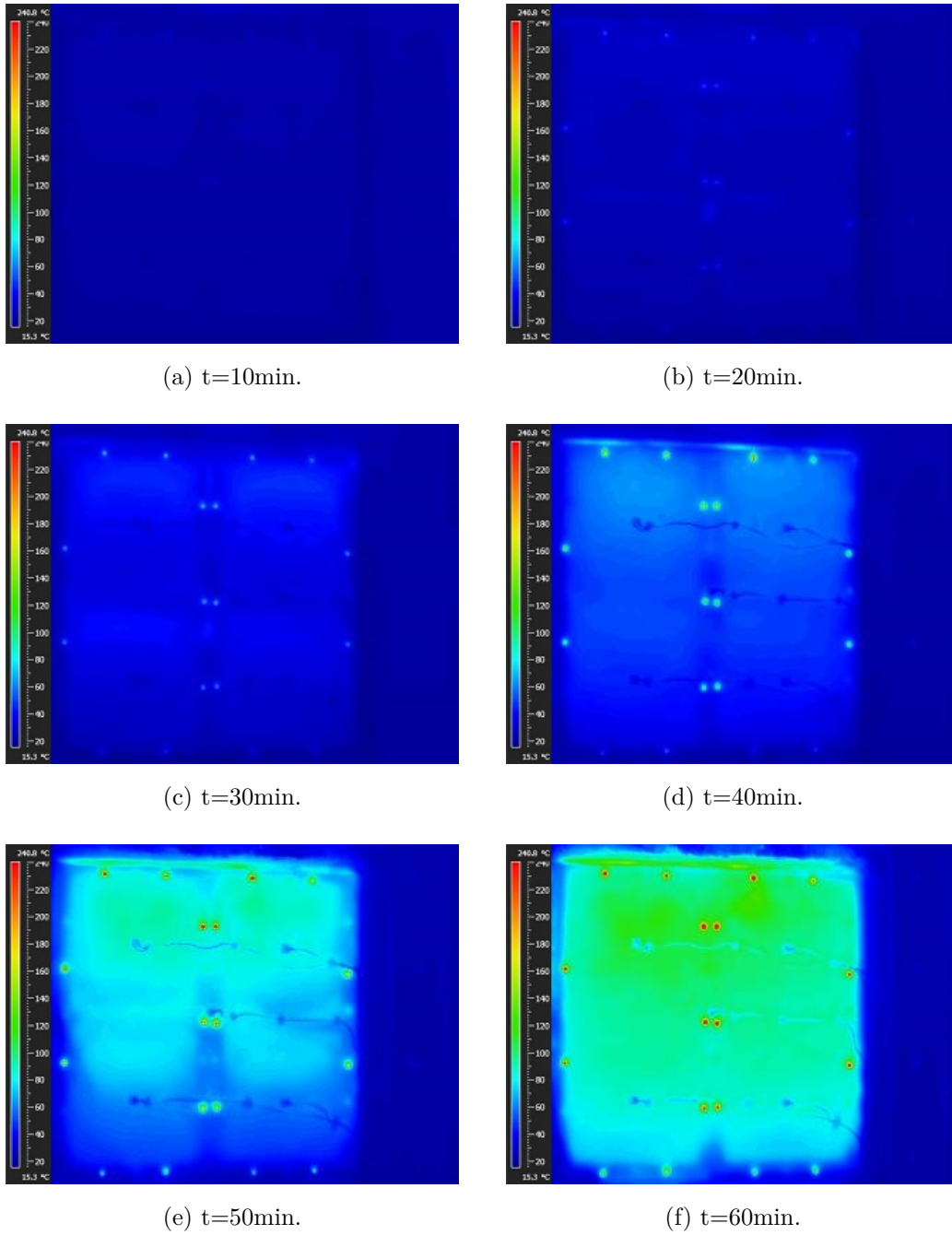


Figure A.24: Test 6 - IR Thermal Camera Results.

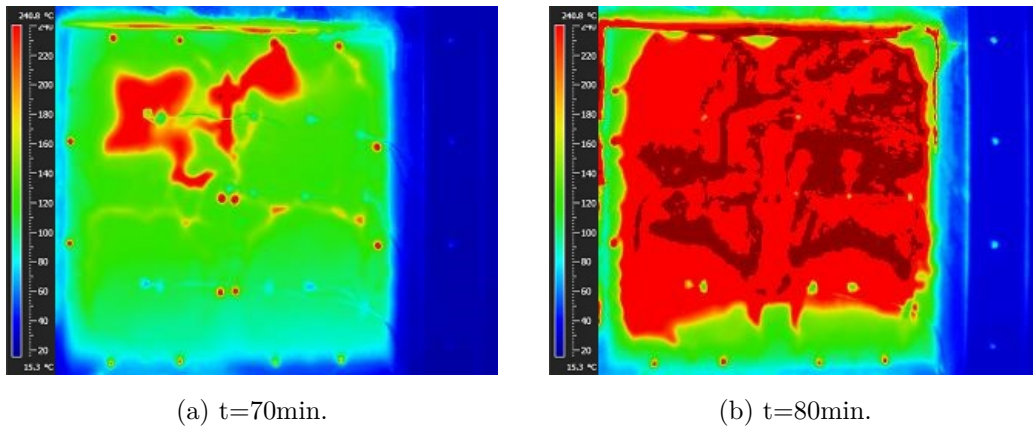
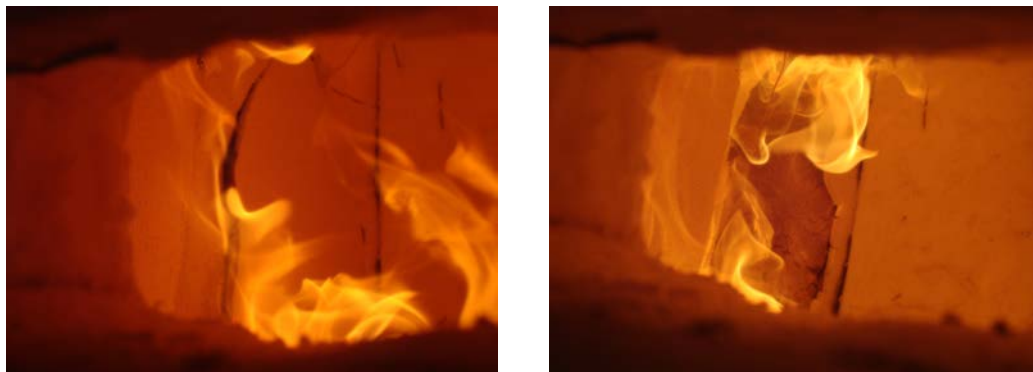


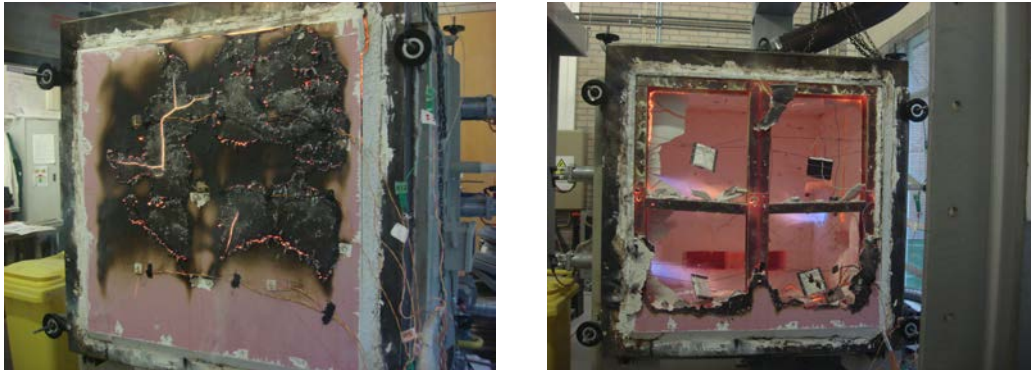
Figure A.25: Test 6 - IR Thermal Camera Results.

The figure A.26 and A.27 presents some internal images during the test and the final state of the wall. Some cracks in the horizontal direction were observed in the region of the reinforcement, as expected, once that the steel is a heat concentrator. This structure had less global buckling due the reinforcement and presented some local web and distortional buckling.



(a) Cracks in the exposed plasterboard, internal view. (b) Cork of the exposed plate submitted directly to the fire state, internal view.

Figure A.26: Specimen 6 during and after the end of the test.



(a) External view in the end of test.

(b) External view, four burners active.

Figure A.27: Specimen 6 during and after the end of the test.

## A.8 Specimen 7

The figure A.28 to A.30 shows the evolution of the global temperature measured by the IR Thermal Camera. The IR thermal images are depicted until 95 minutes because after 80 minutes the furnace has been switched off. The wall still burns just using the wood as combustible. At 95 minutes, the IR thermal camera and the fire was extinguish with water jets.

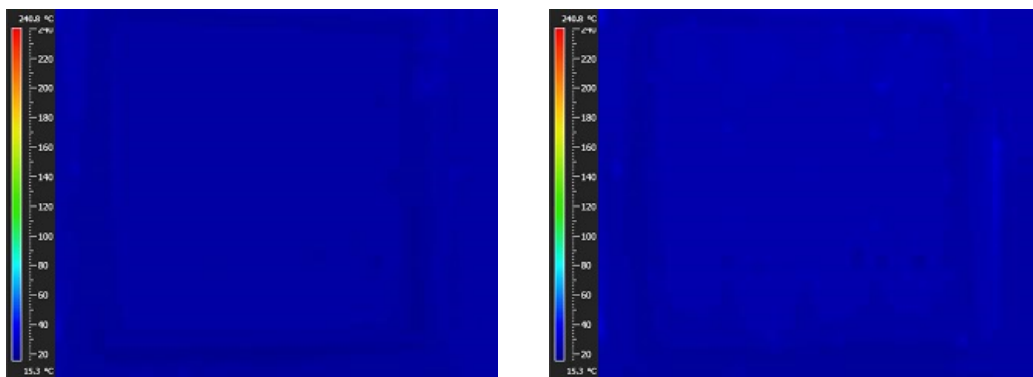
(a)  $t=10\text{min}$ .(b)  $t=20\text{min}$ .

Figure A.28: Test 7 - IR Thermal Camera Results.

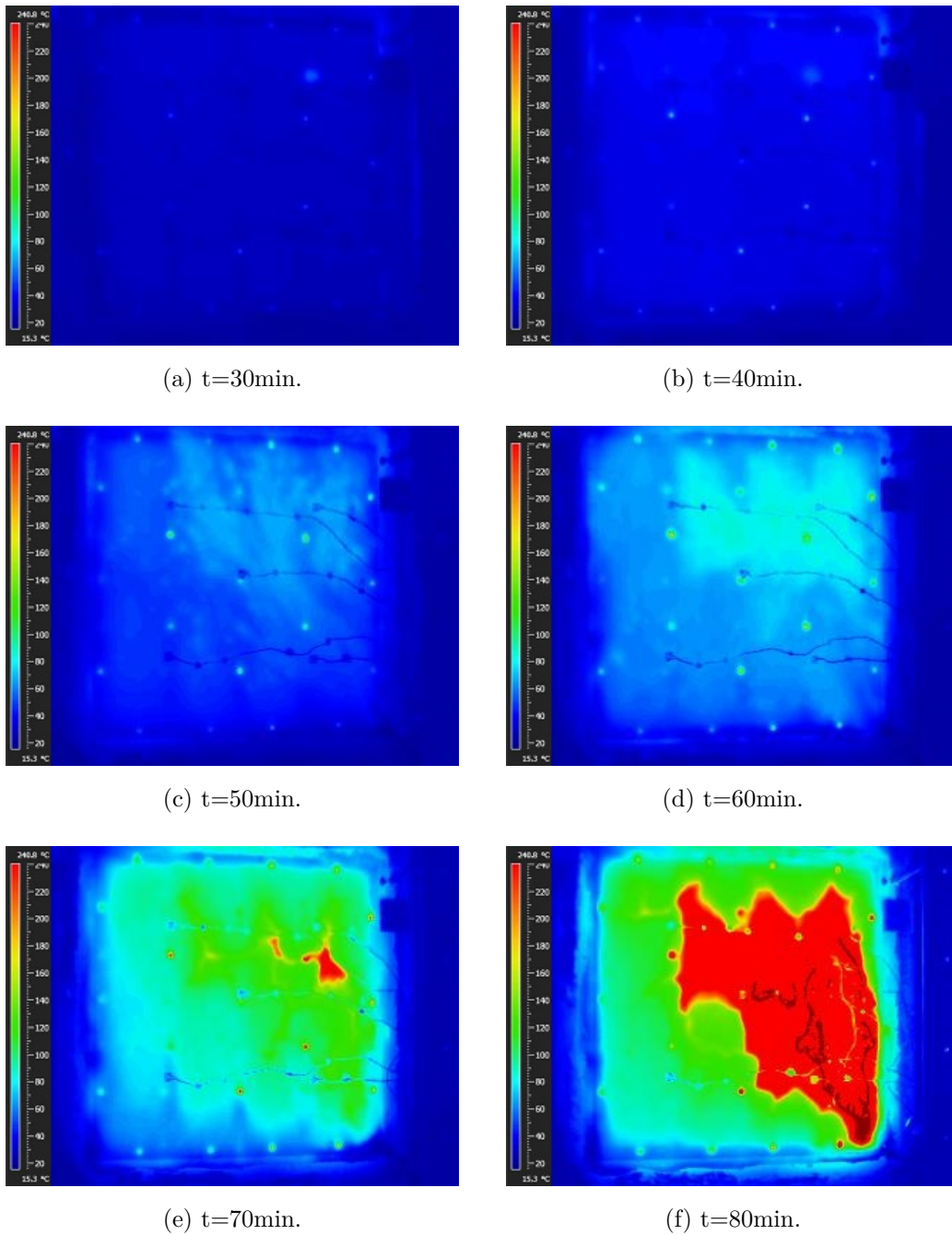


Figure A.29: Test 7 - IR Thermal Camera Results.

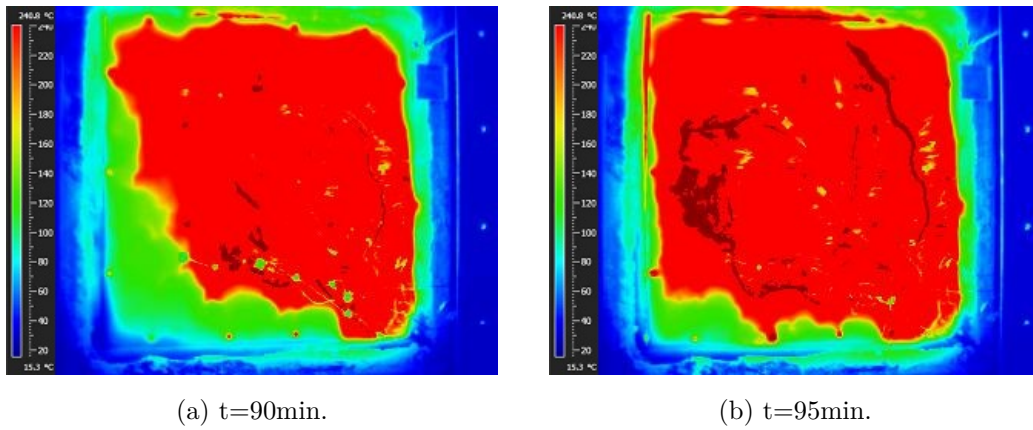


Figure A.30: Test 7 - IR Thermal Camera Results.

The figure A.31 brings some images of the test.

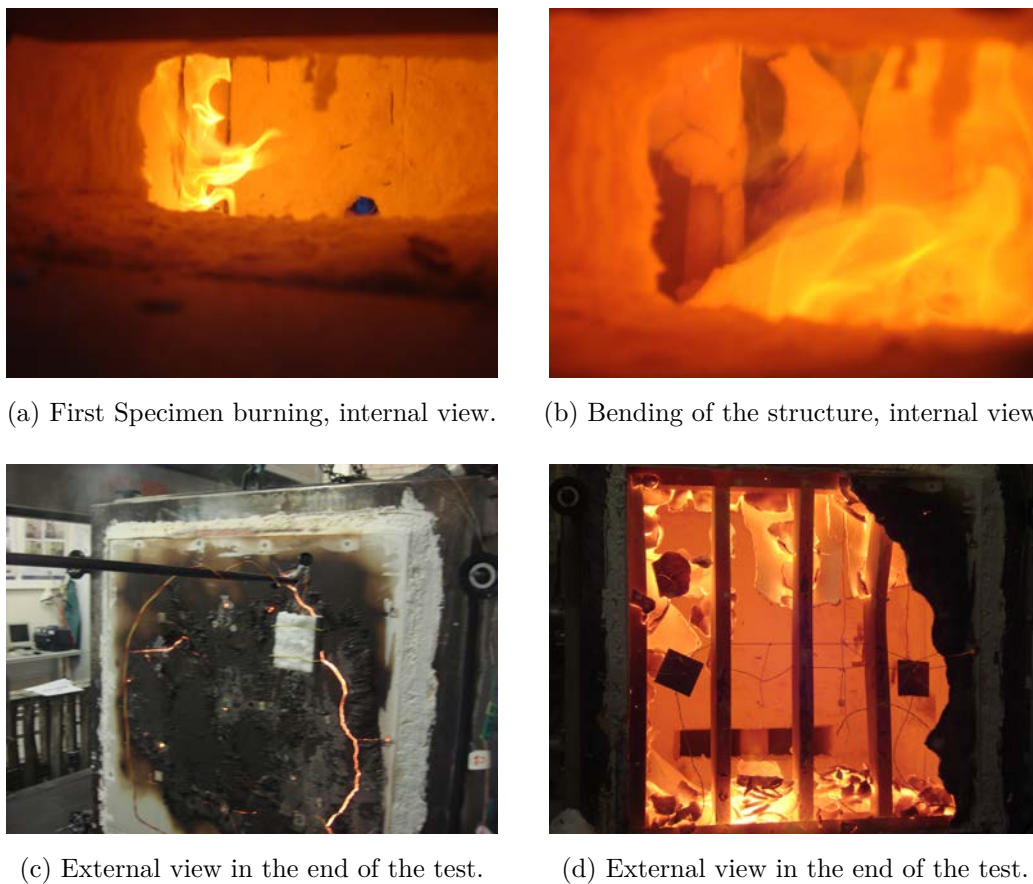


Figure A.31: Specimen 7 during and after the end of the test.

The photographs inside the furnace presents the two time instants discussed in the beginning of this section, at 20 and at 52 minutes. The fig A.31c shows the external unexposed surface in the moment that the furnace was switched off and the fig A.31d shows the final state of the wall. The buckling instability of studs is well demonstrated, by the three modes.

# Appendix B

## Material Properties

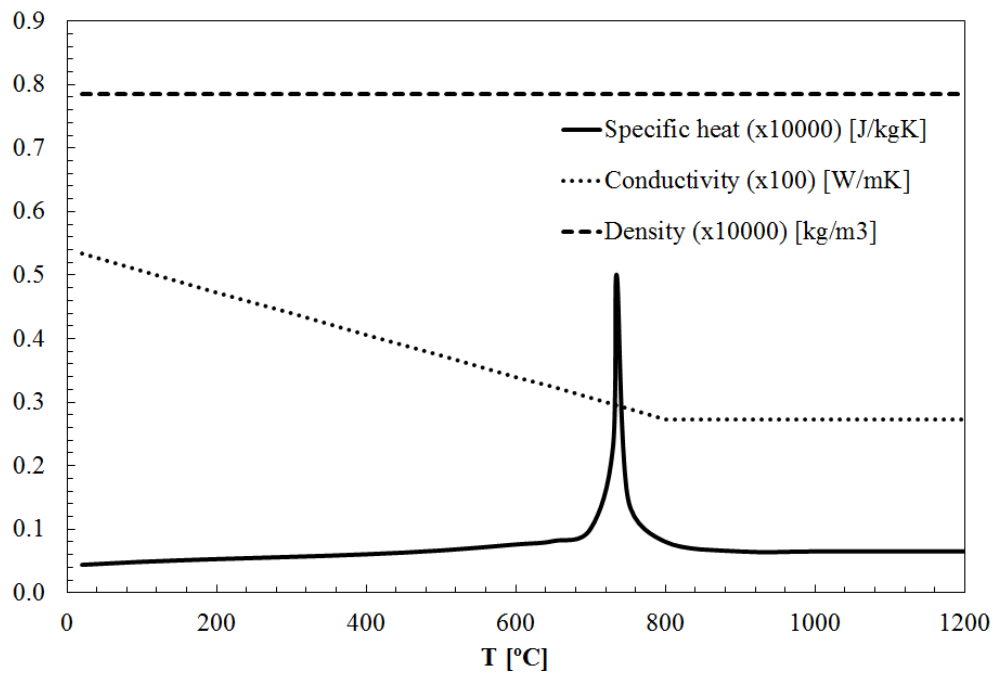


Figure B.1: Thermal properties of steel.

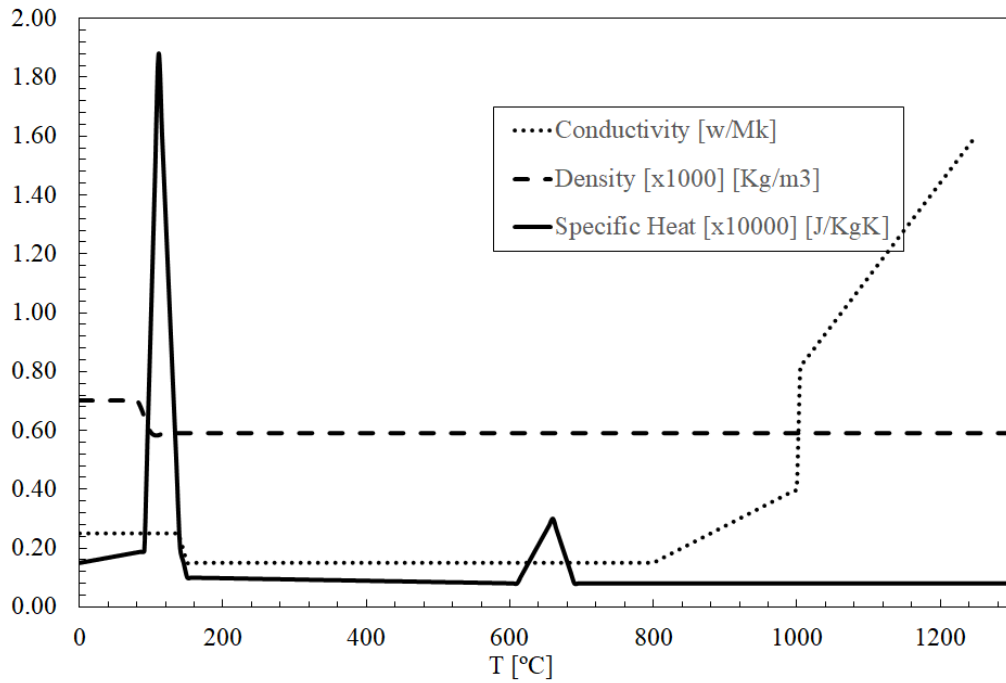


Figure B.2: Thermal properties of gypsum.

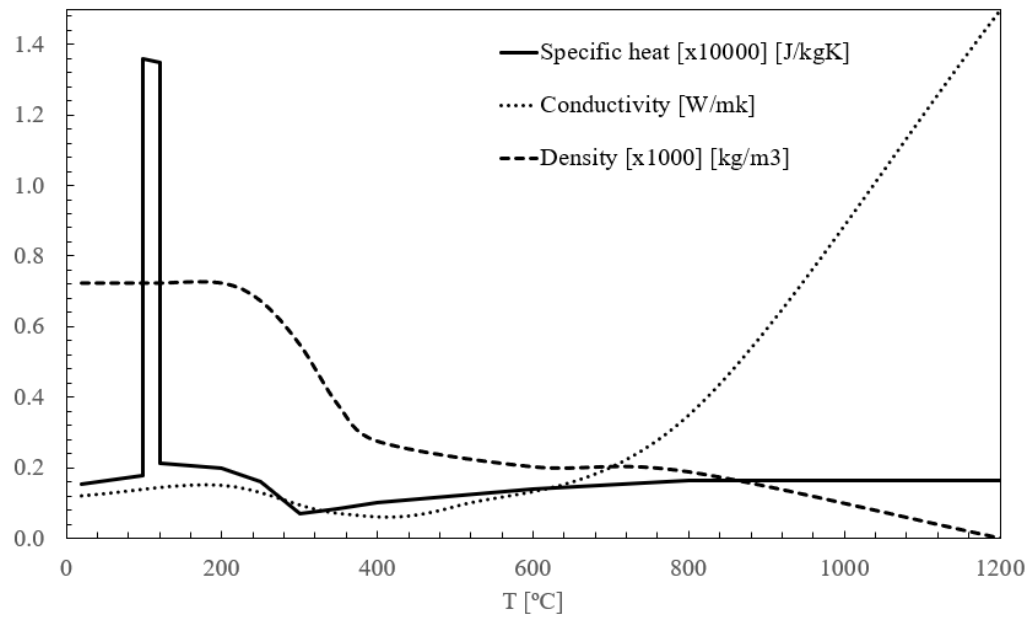


Figure B.3: Thermal properties of wood.



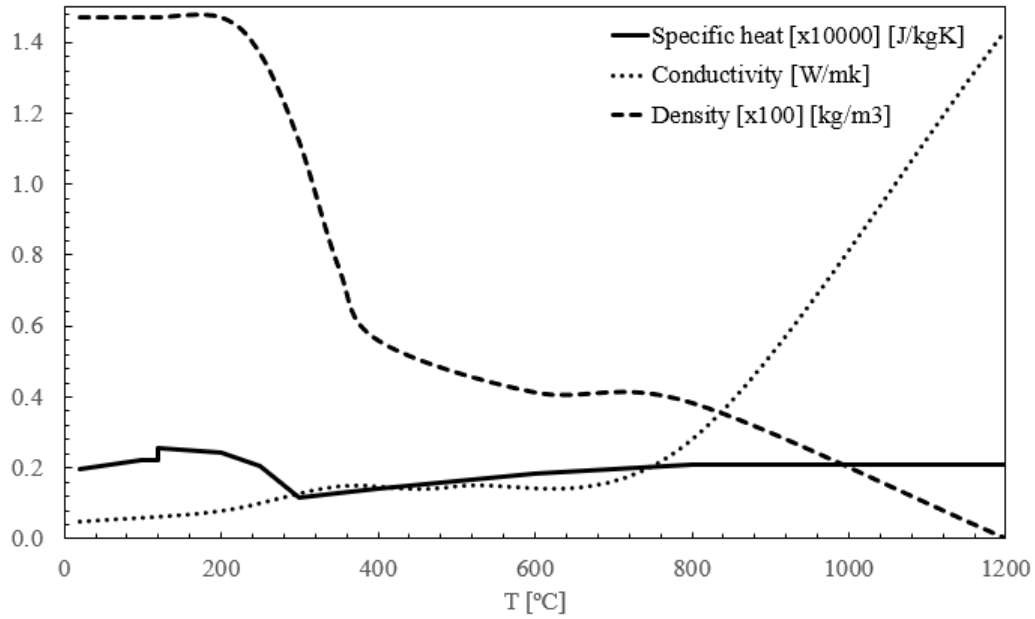


Figure B.4: Thermal properties of cork.

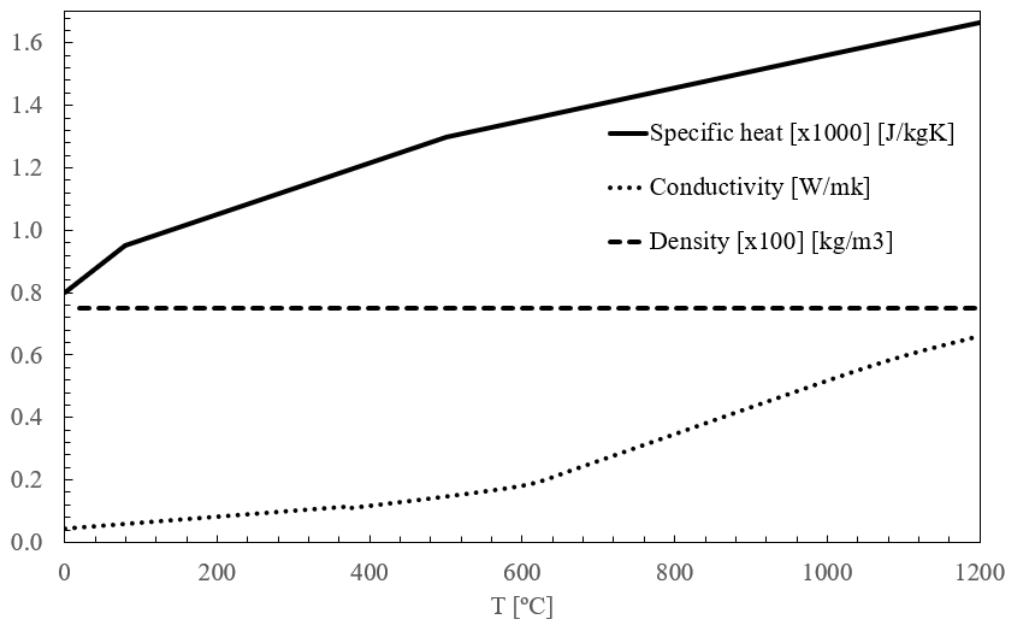
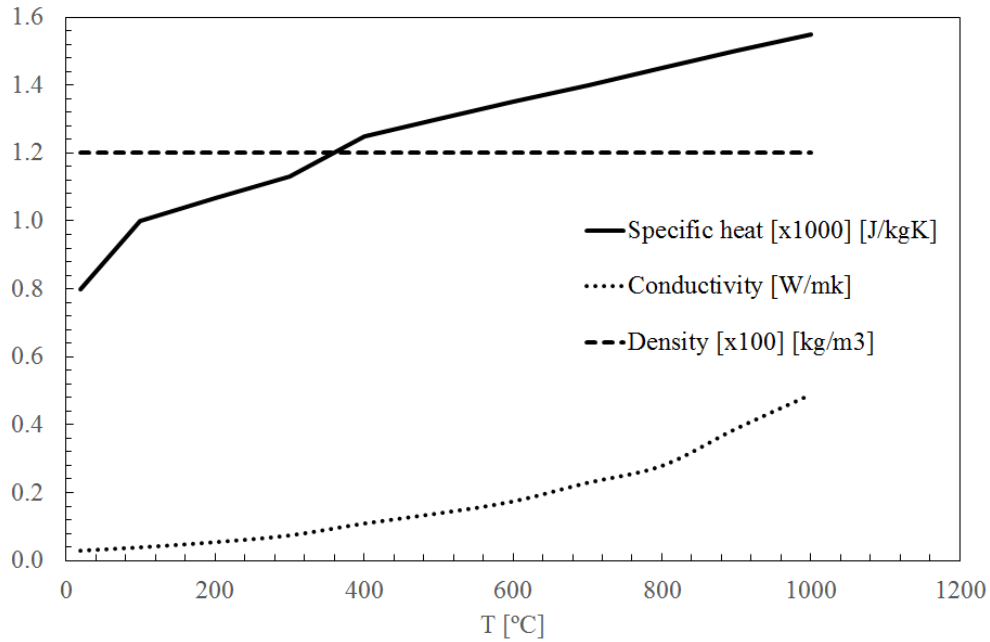
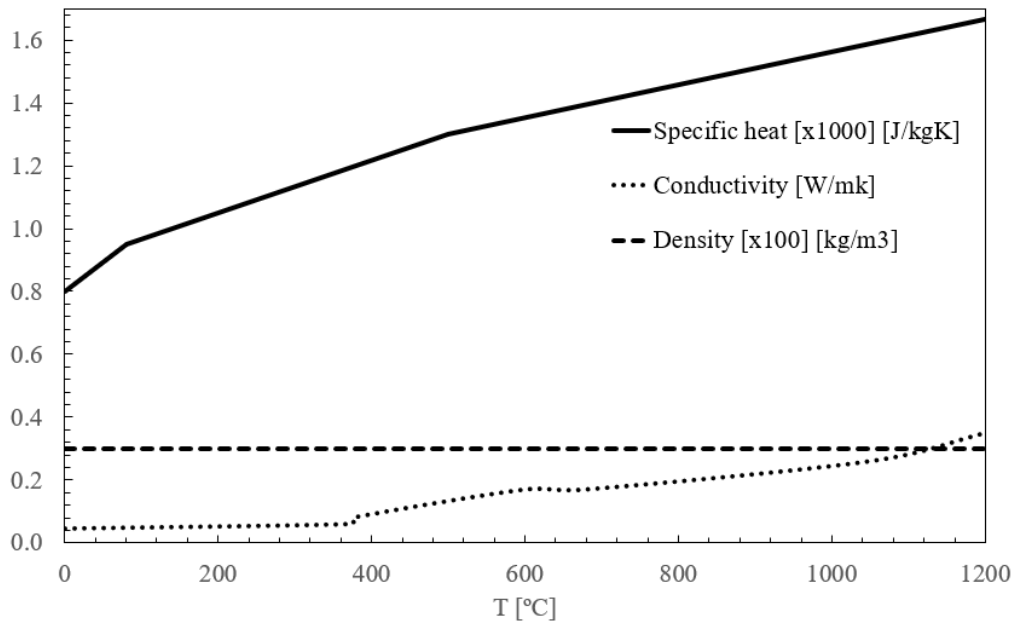


Figure B.5: Thermal properties of rockwool, density 75kg/m3.

Figure B.6: Thermal properties of rockwool, density 120kg/m<sup>3</sup>.Figure B.7: Thermal properties of rockwool, density 300kg/m<sup>3</sup>.

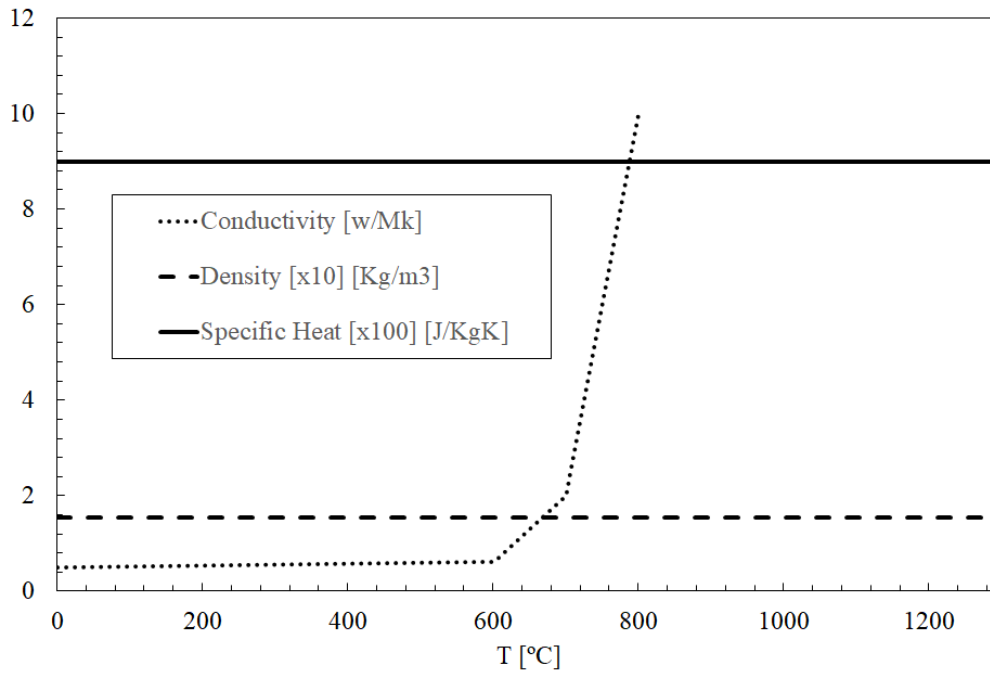


Figure B.8: Thermal properties of glass fiber.

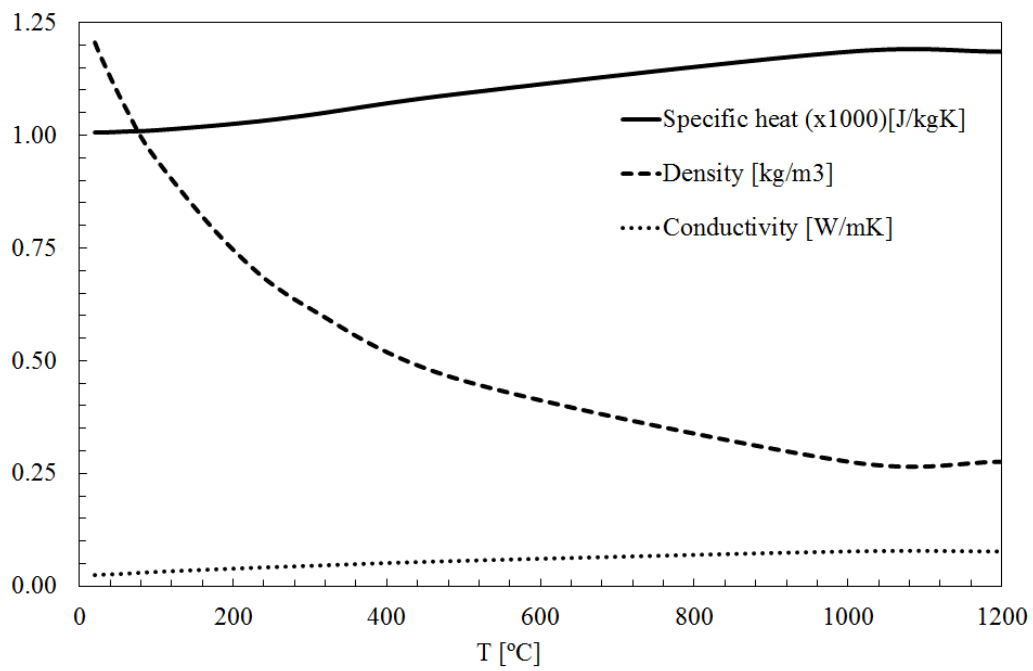


Figure B.9: Thermal properties of air.

# Appendix C

## Numerical Validation

This appendix presents the graphs and some images of the simulations that was generated to the numerical validation chapter.

### C.1 Specimens Geometry A

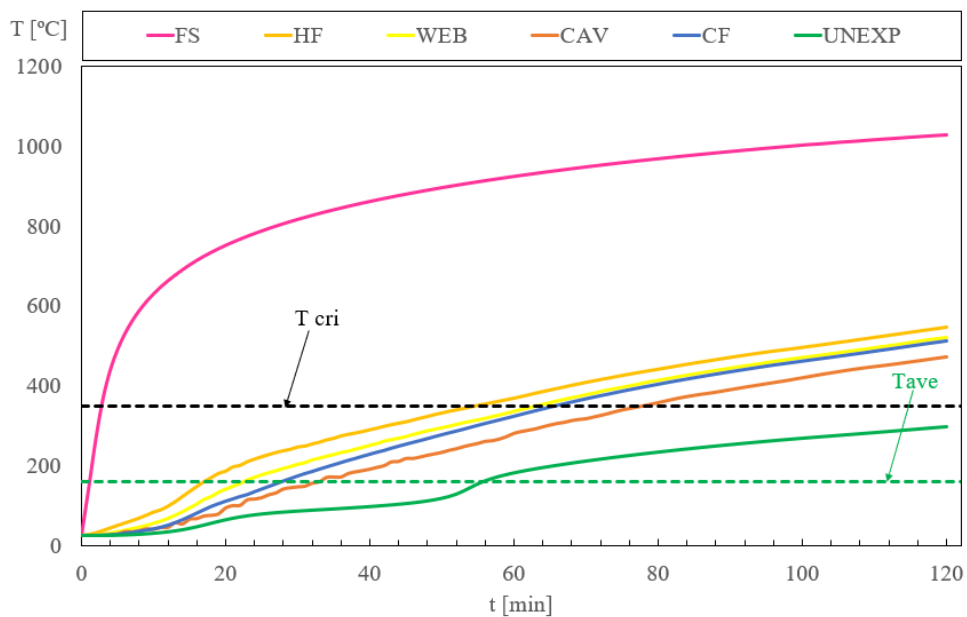


Figure C.1: Specimen 01 – Numerical results.

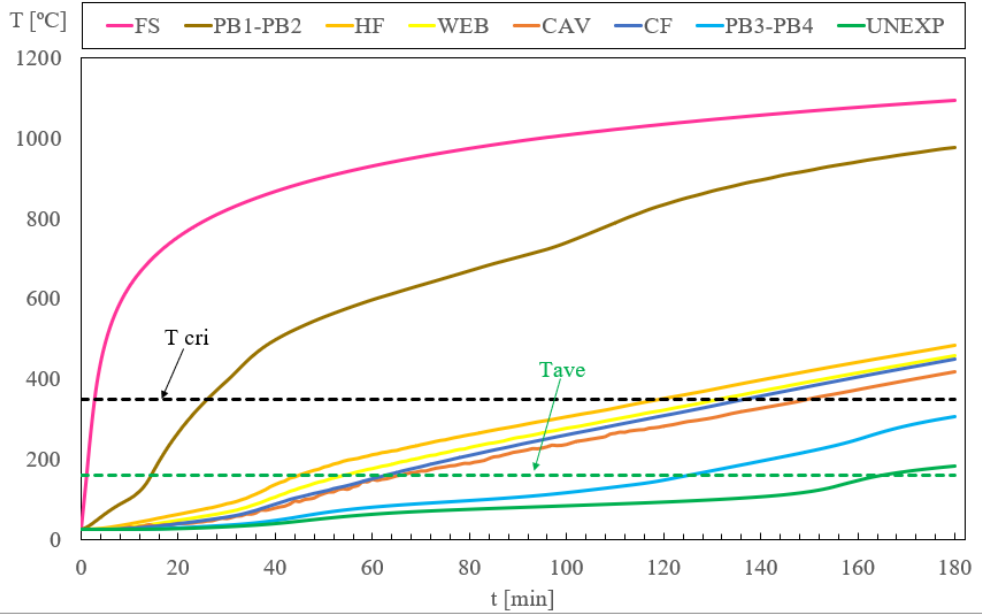


Figure C.2: Specimen 02 – Numerical results.

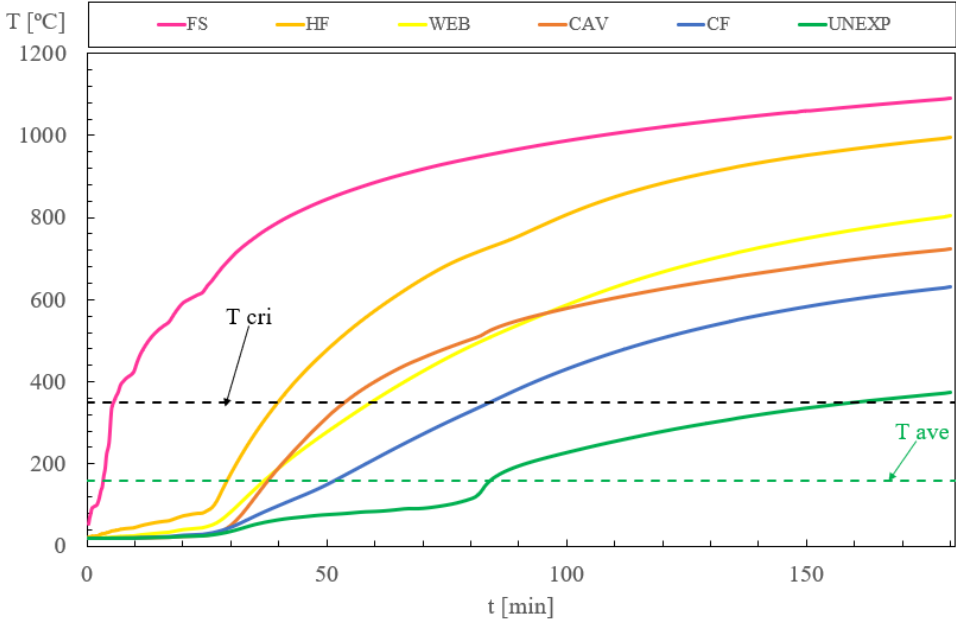


Figure C.3: Specimen 03 – Numerical results.

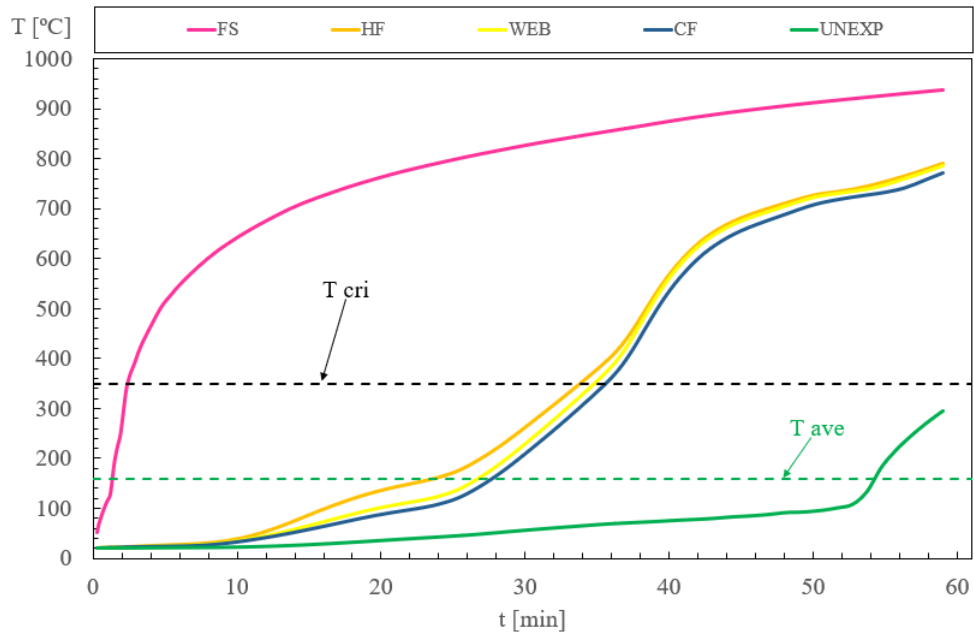


Figure C.4: Specimen 04 – Numerical results.

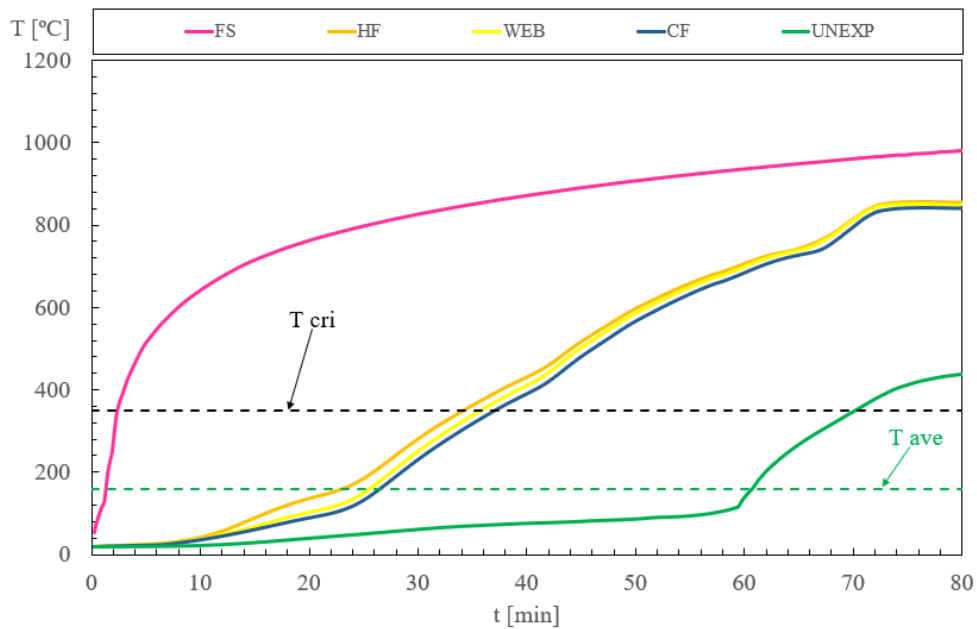


Figure C.5: Specimen 05 – Numerical results.

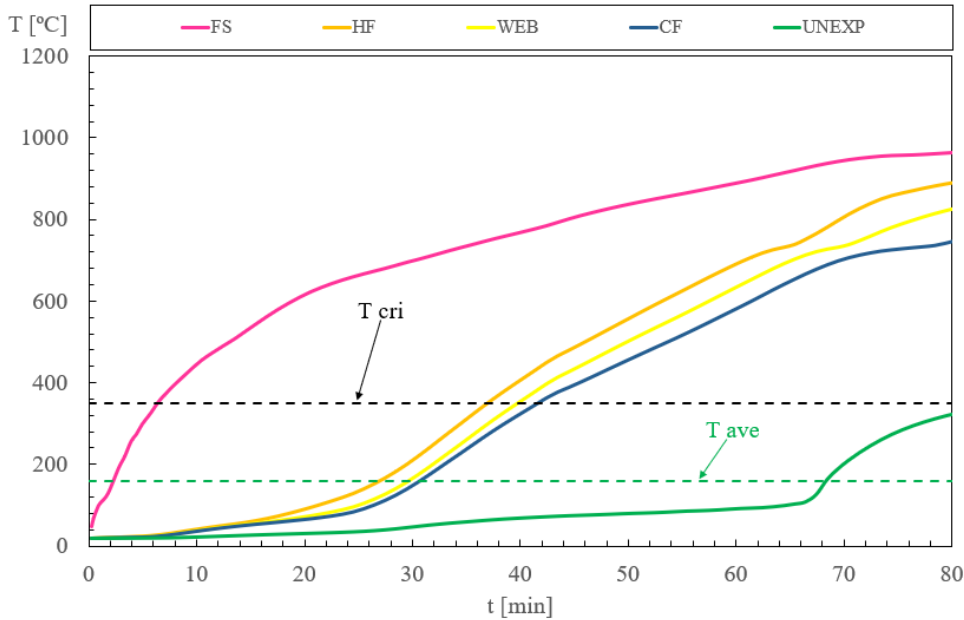


Figure C.6: Specimen 06 – Numerical results.

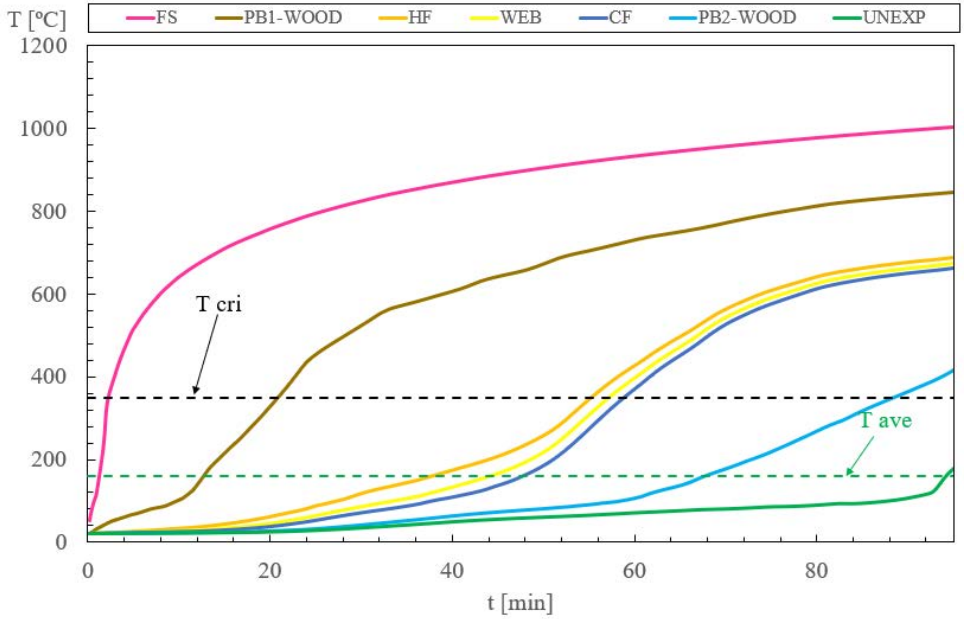


Figure C.7: Specimen 07 – Numerical results.

## C.2 Specimens Geometry B

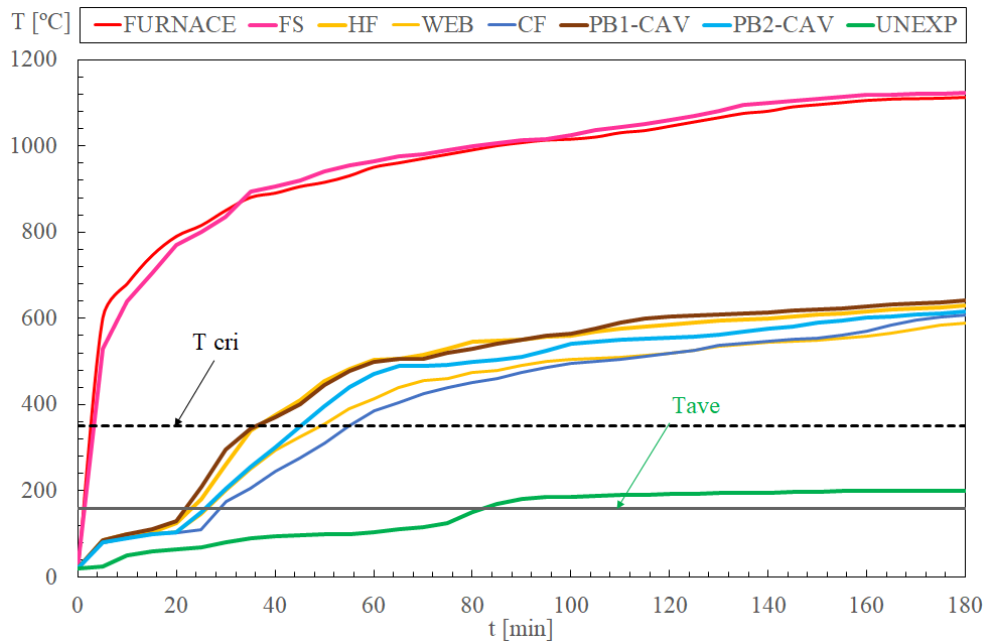


Figure C.8: Case 01 – Experimental results [34].

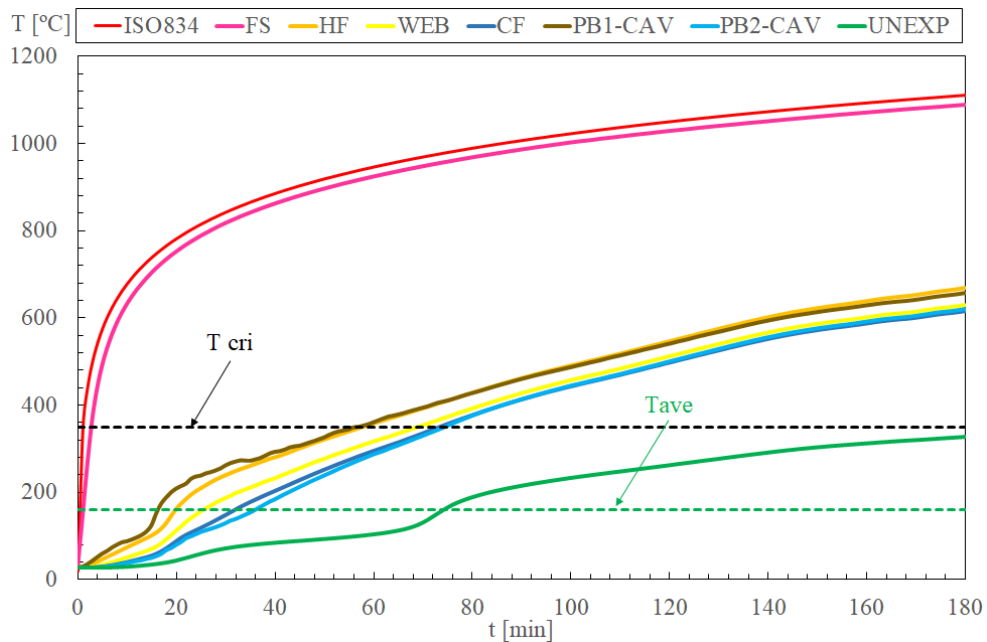


Figure C.9: Case 01 – Numerical results.



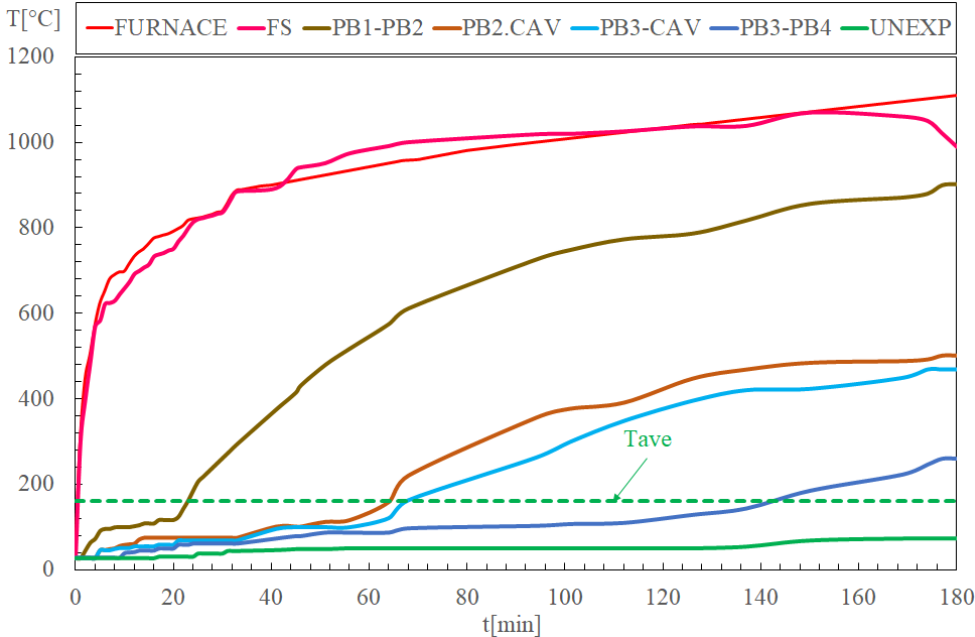


Figure C.10: Case 02 – Experimental results [34].

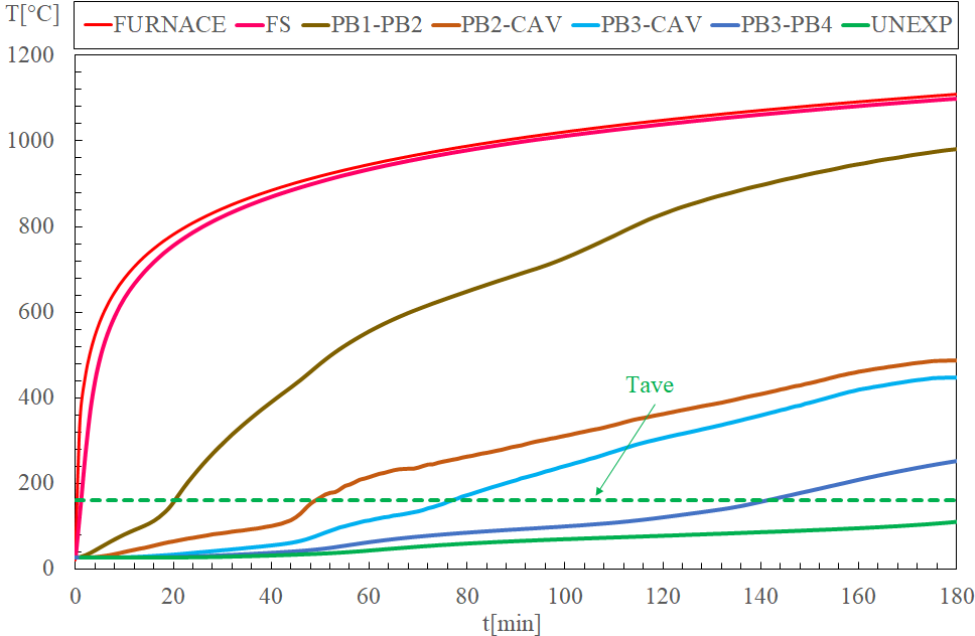


Figure C.11: Case 02 – Numerical results.

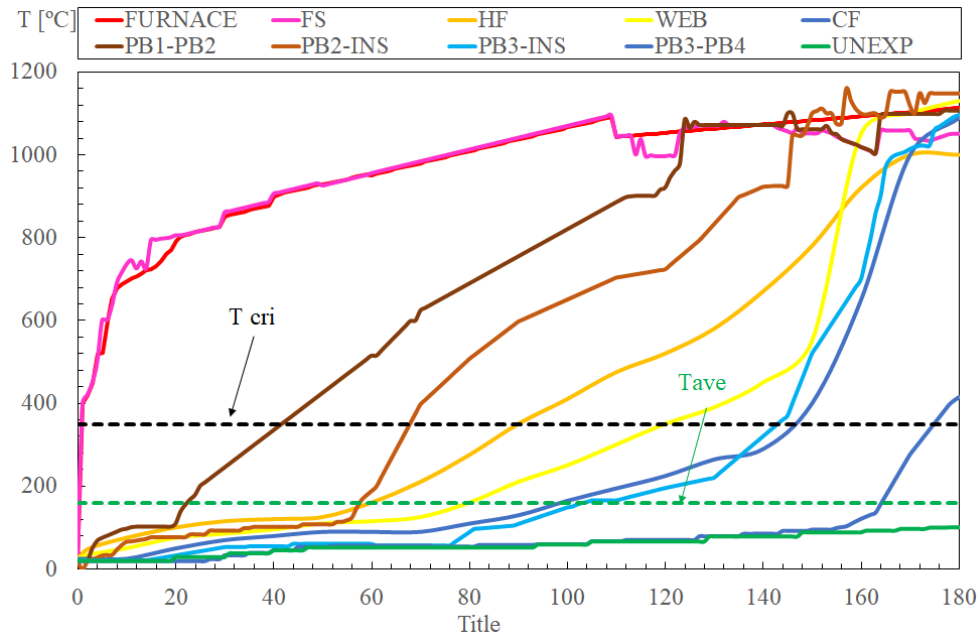


Figure C.12: Case 03 – Experimental results [34].

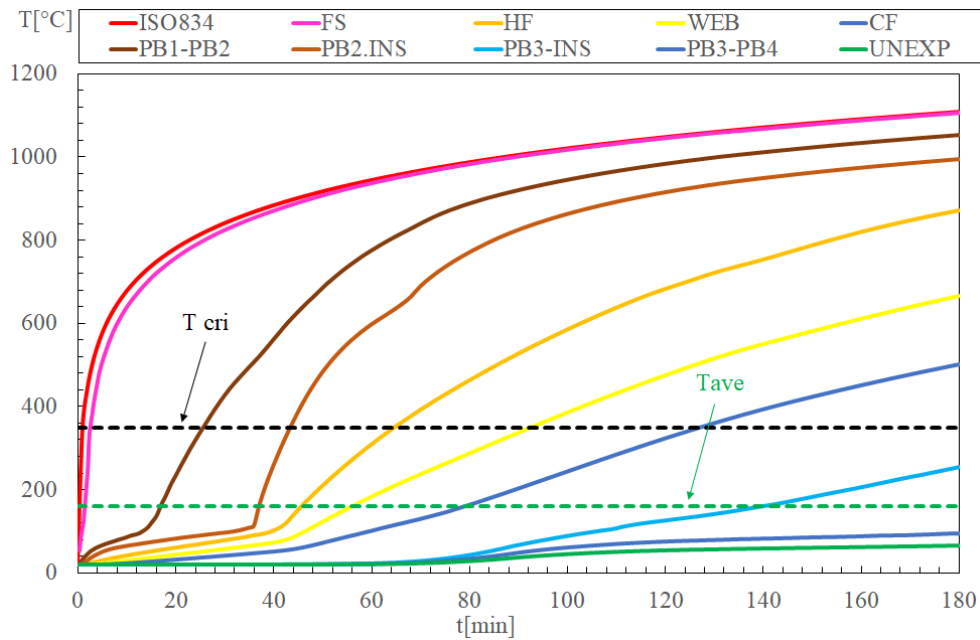


Figure C.13: Case 03 – Numerical results.

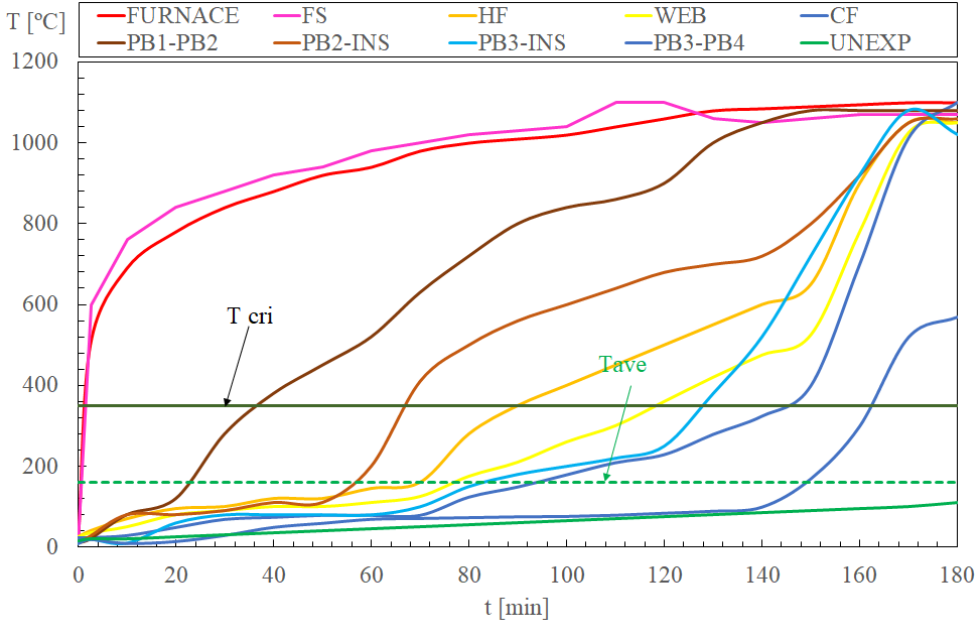


Figure C.14: Case 04 – Experimental results [34].

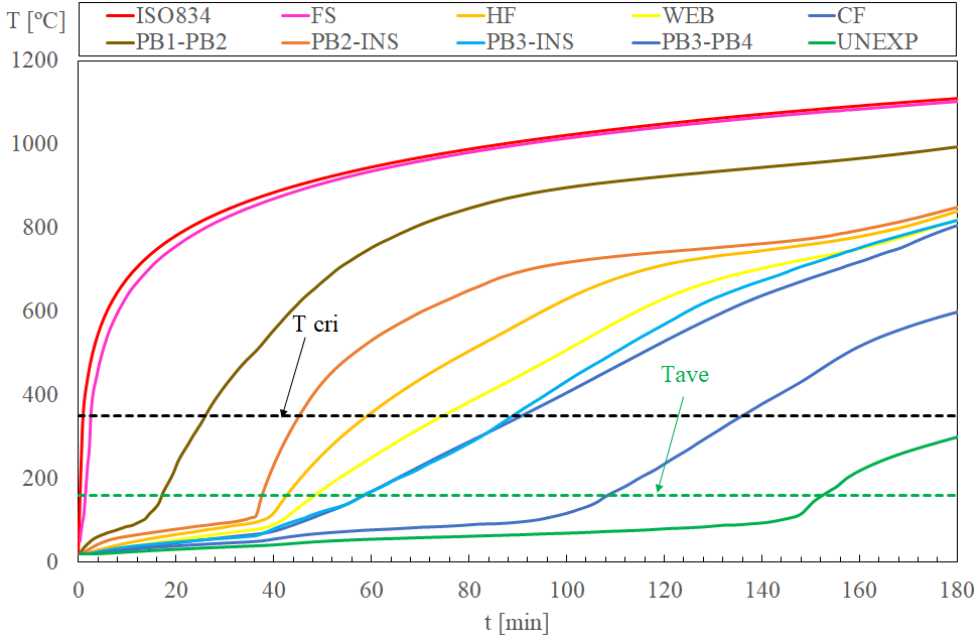
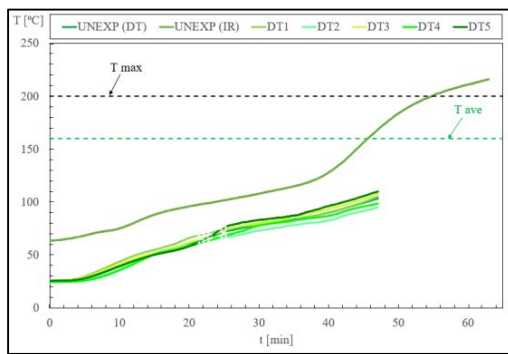
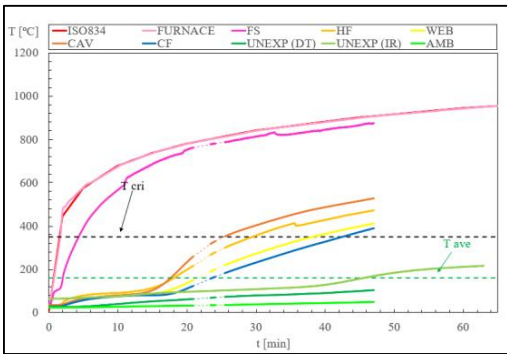
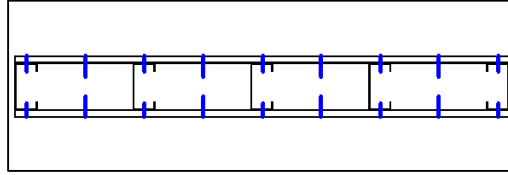
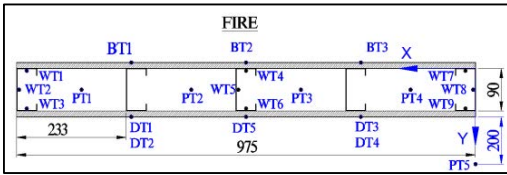
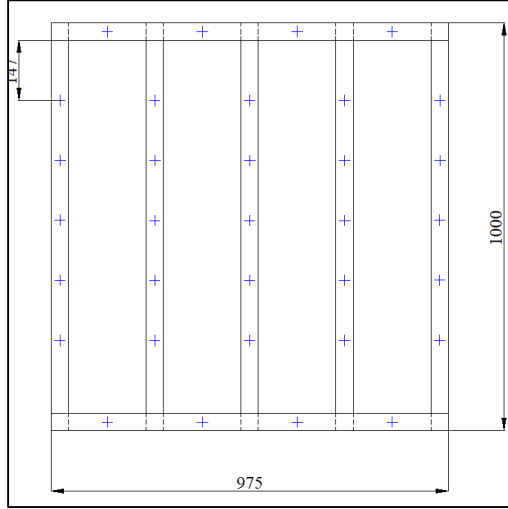
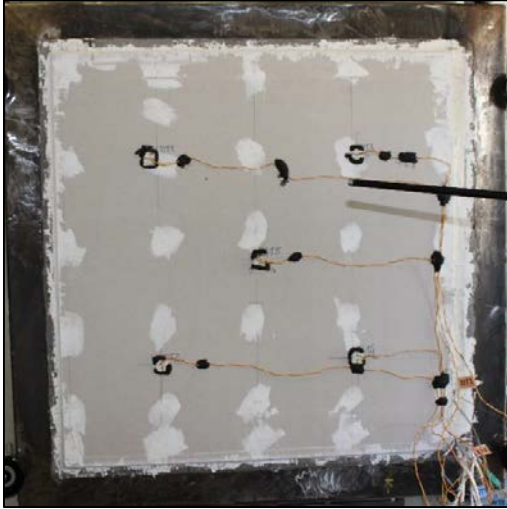


Figure C.15: Case 04 – Numerical results.

# Appendix D

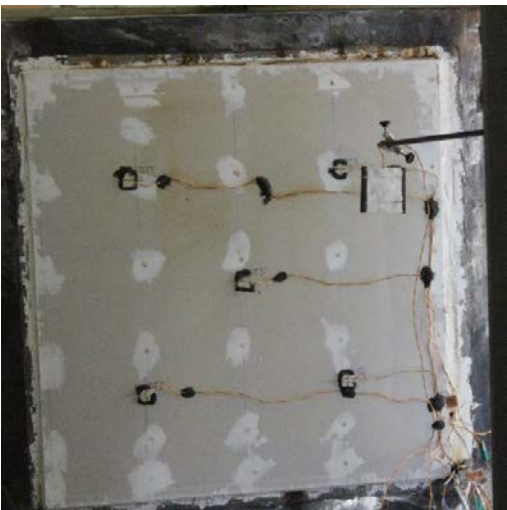
## Specimens DataSheet

Specimen 0 (Test)  
 Test Date: 2017-09-14

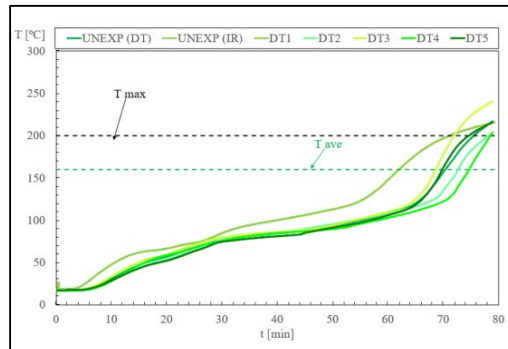
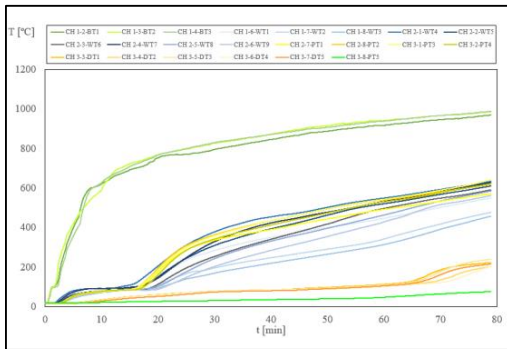
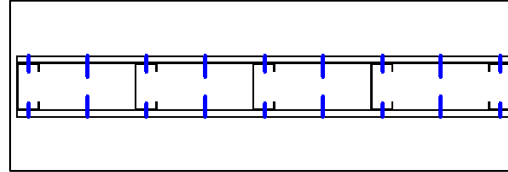
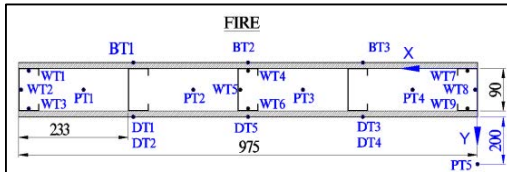
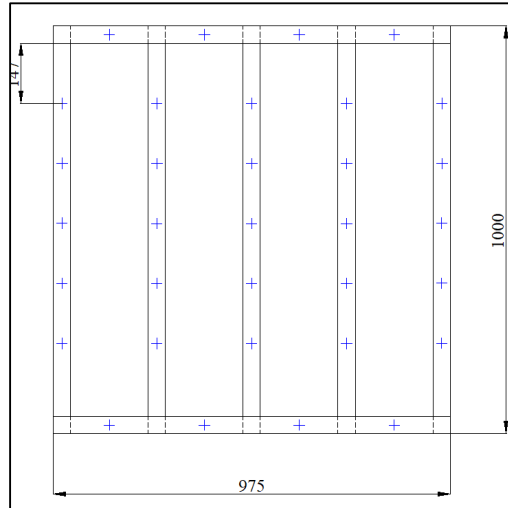
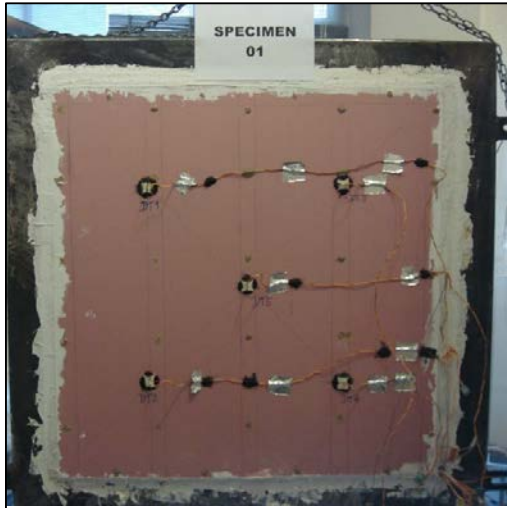


Fire Resistance = 45 minutes (IR estimative)  
 Fire Rating = I45

$FR_{IR\ Thermal} = 45\ minutes$   
 $FR_{Criterion} = X$

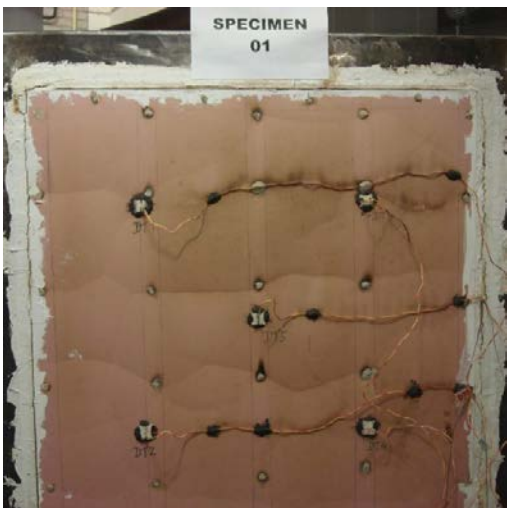


Specimen 1  
 Test Date: 2017-11-07

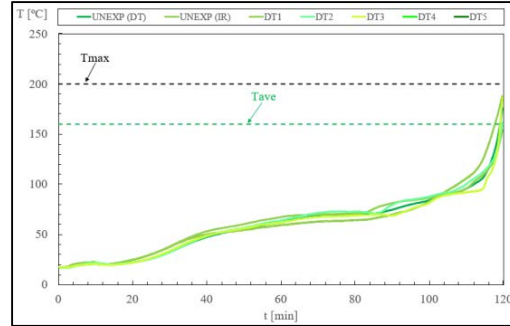
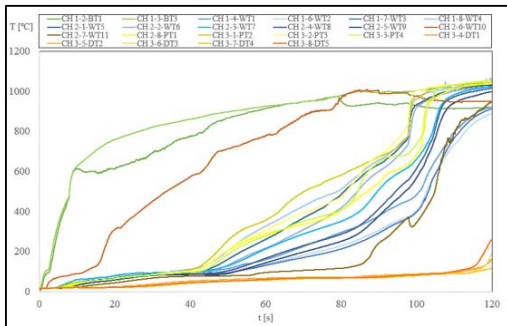
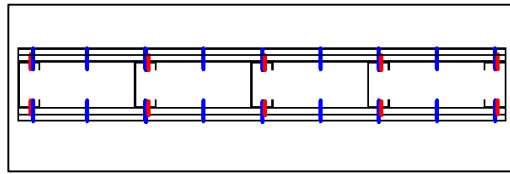
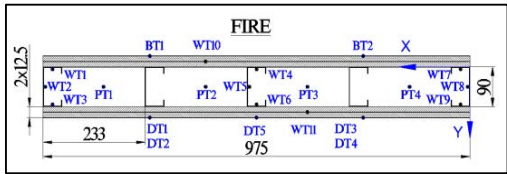
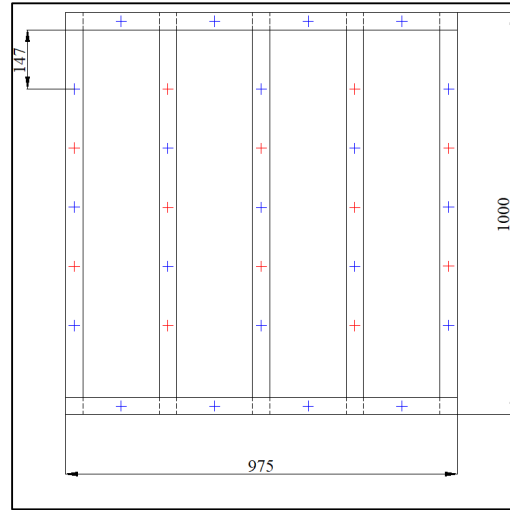
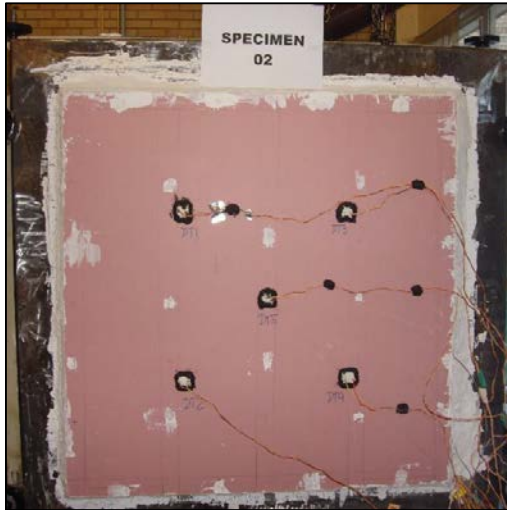


Fire Resistance = 70 minutes  
 Fire Rating = I60

FR<sub>IR Thermal</sub> = 62 minutes  
 FR<sub>Criterion</sub> = Unexposed Average Temperature



Specimen 2  
 Test Date: 2017-11-15

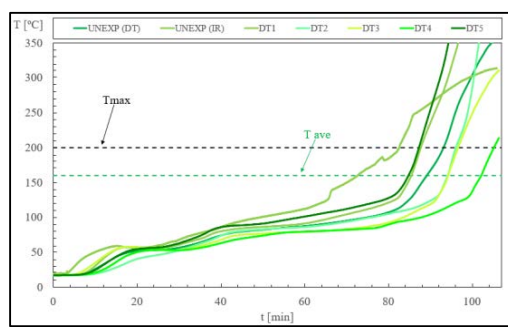
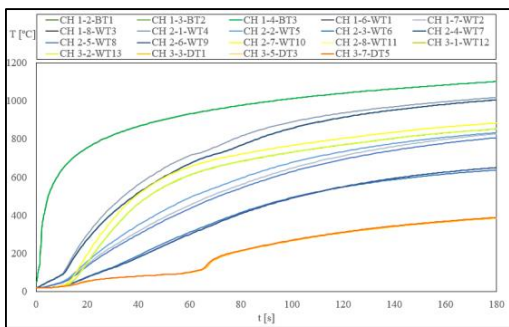
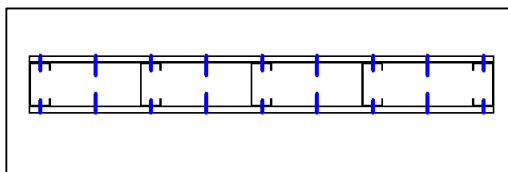
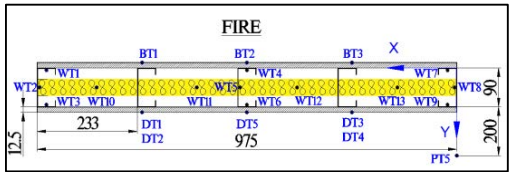
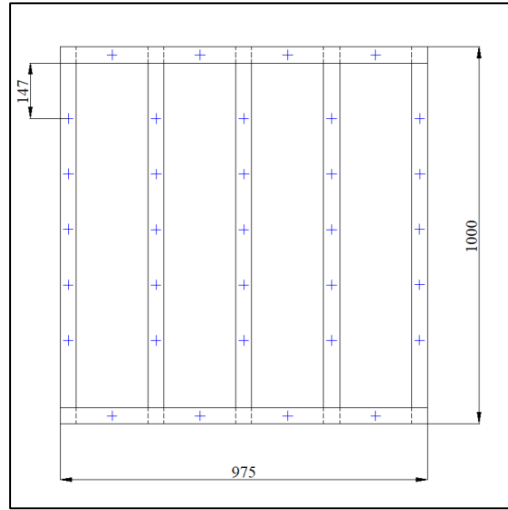
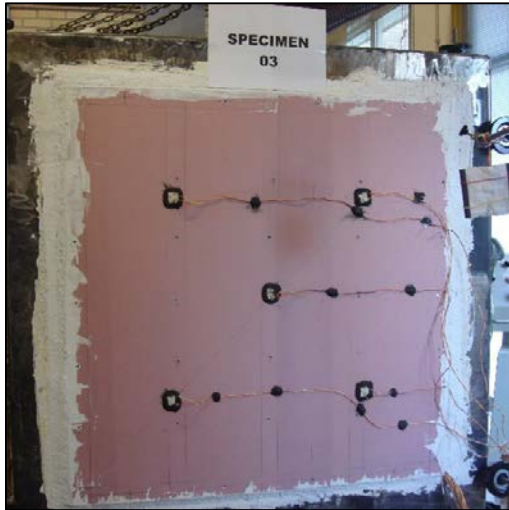


Fire Resistance = 118 minutes  
 Fire Rating = I90

FR<sub>IR Thermal</sub> = 117 minutes  
 FR<sub>Criterion</sub> = Maximum Temperature (DT5)

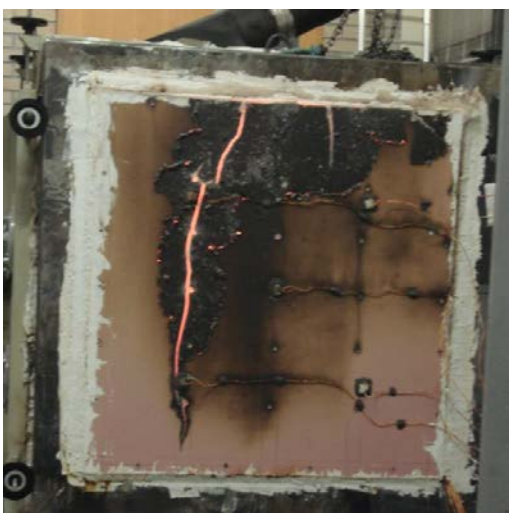


Specimen 3  
 Test Date: 2017-12-11



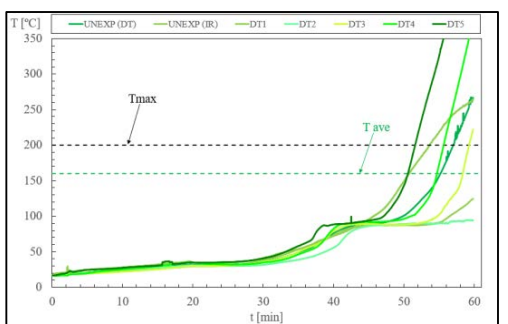
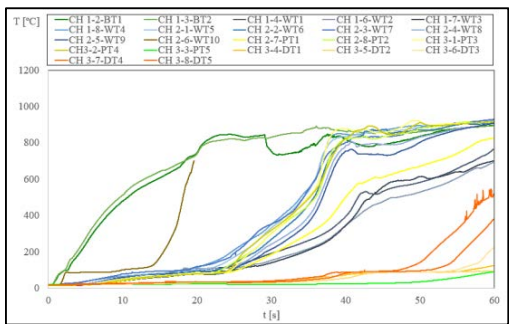
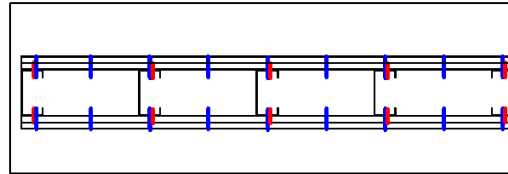
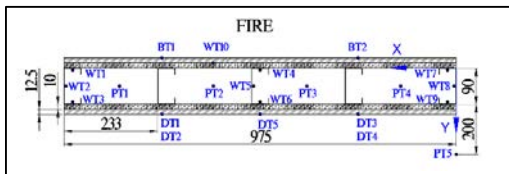
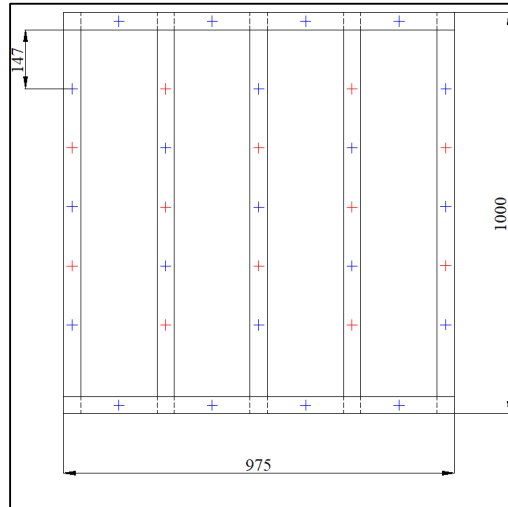
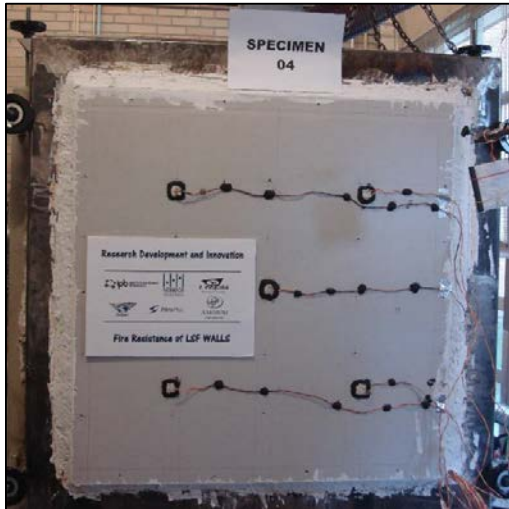
Fire Resistance = 87 minutes  
 Fire Rating = I60

FR<sub>IR Thermal</sub> = 72 minutes  
 FR<sub>Criterion</sub> = Maximum Temperature (DT5)



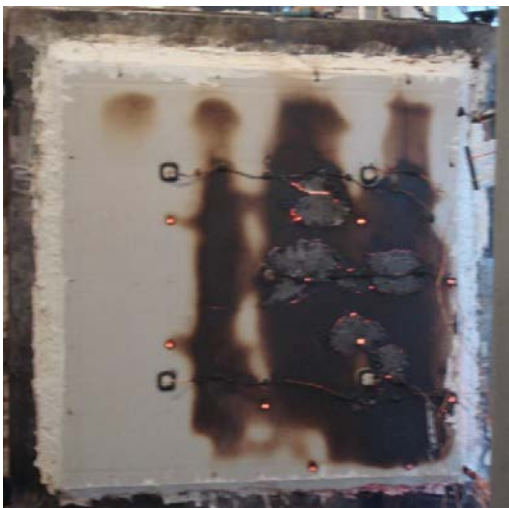


Specimen 4  
 Test Date: 2017-11-27

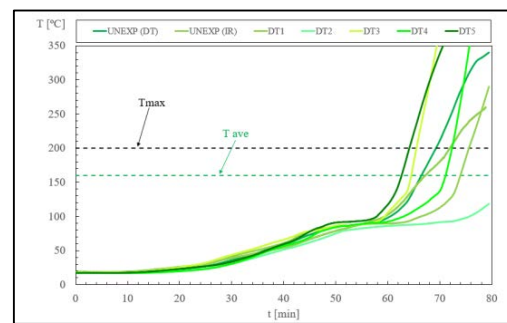
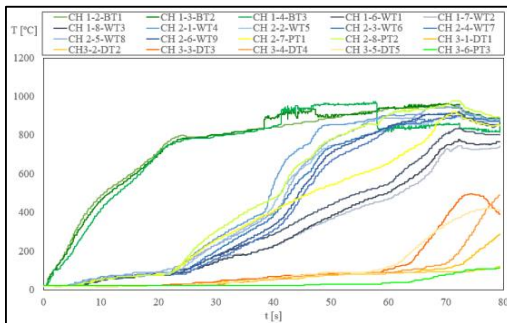
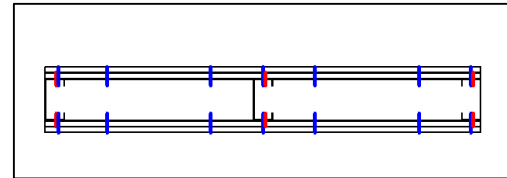
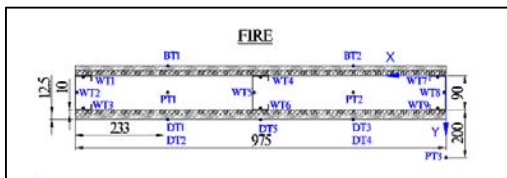
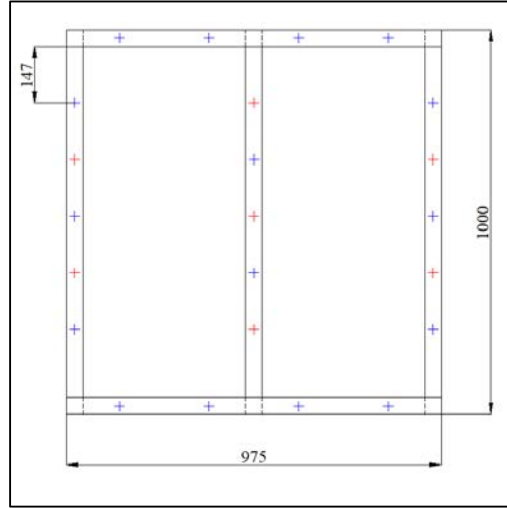
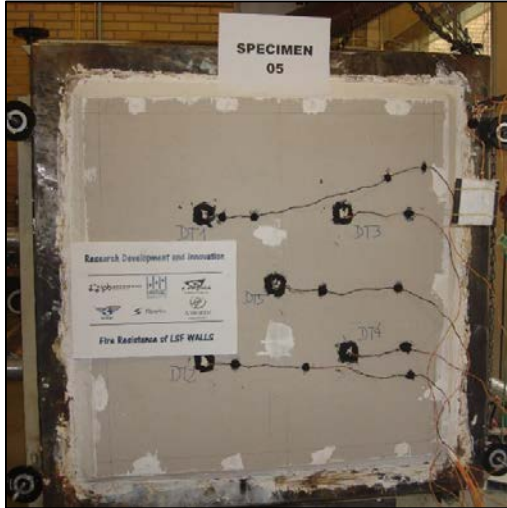


Fire Resistance = 51 minutes  
 Fire Rating = I45

FR<sub>IR Thermal</sub> = 50 minutes  
 FR<sub>Criterion</sub> = Maximum Temperature (DT5)



Specimen 5  
 Test Date: 2018-01-16

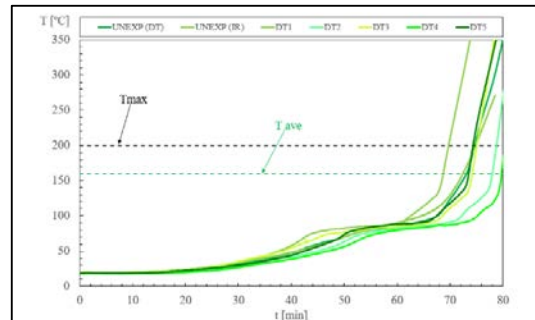
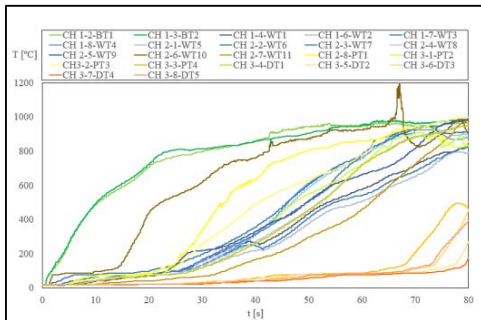
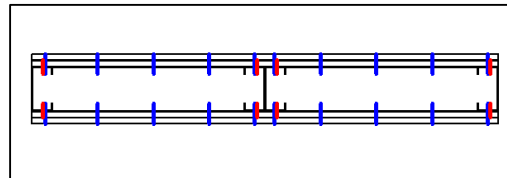
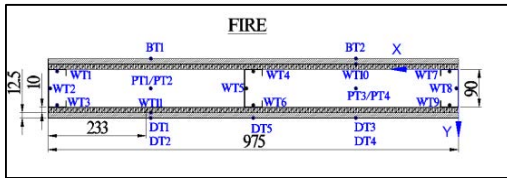
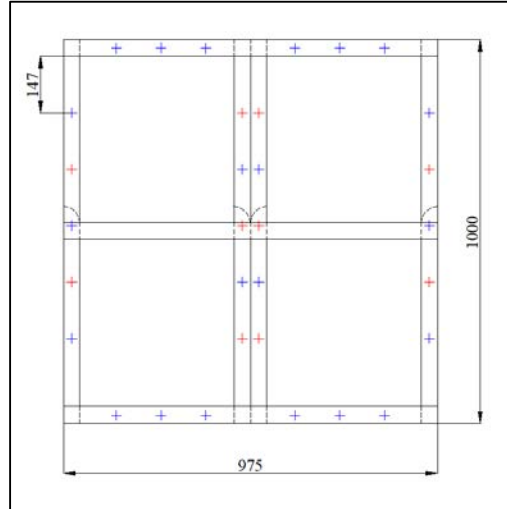
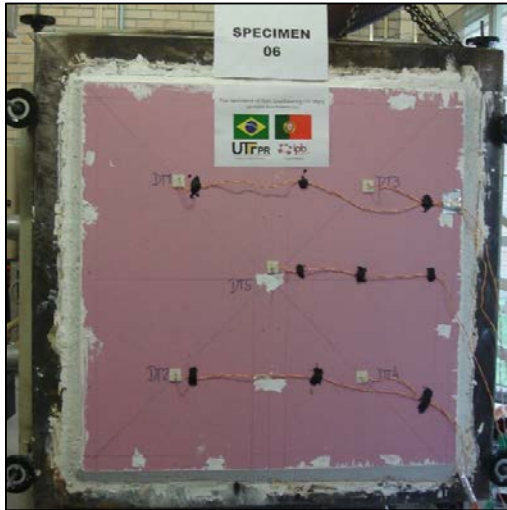


Fire Resistance = 64 minutes  
 Fire Rating = I60

FR<sub>IR Thermal</sub> = 67 minutes  
 FR<sub>Criterion</sub> = Maximum Temperature (DT5)

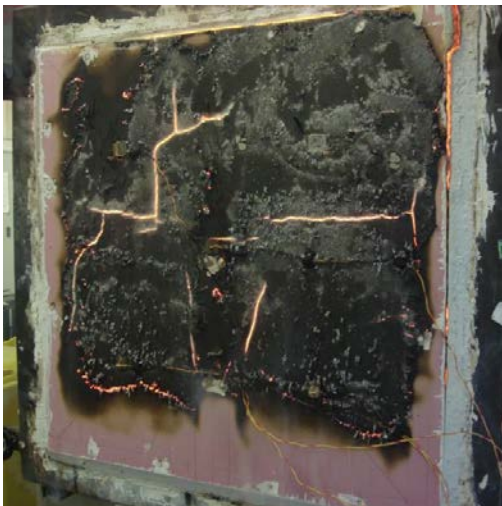


Specimen 6  
 Test Date: 2018-01-23

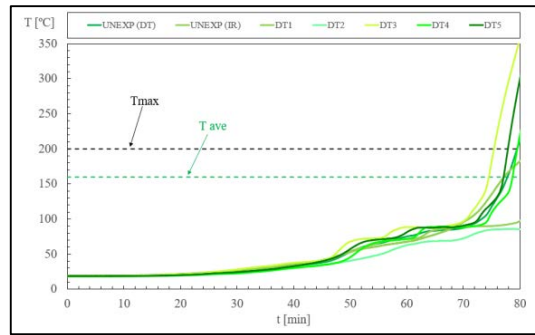
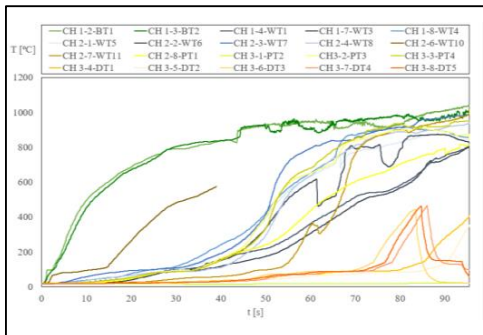
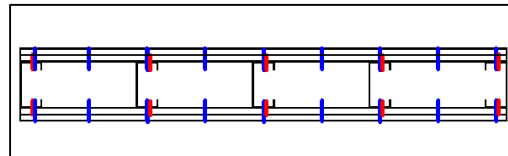
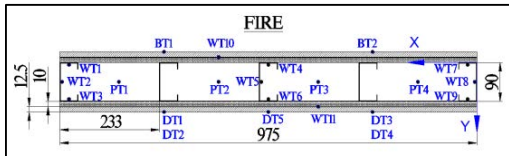
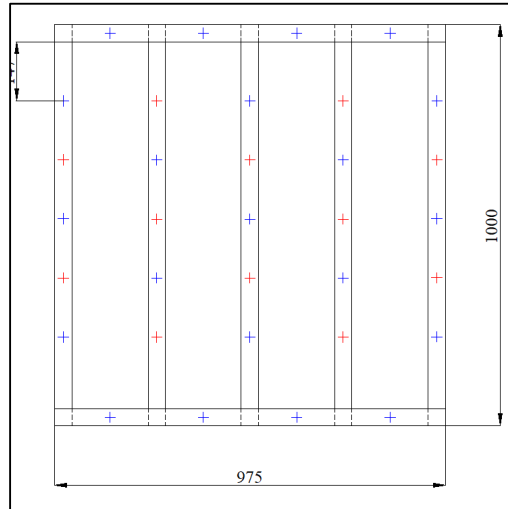
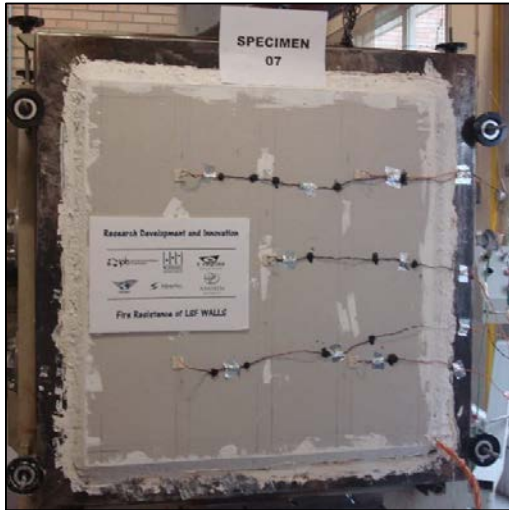


Fire Resistance = 69 minutes  
 Fire Rating = I60

FR<sub>IR Thermal</sub> = 72 minutes  
 FR<sub>Criterion</sub> = Maximum Temperature (DT1)



Specimen 7  
 Test Date: 2017-12-13



Fire Resistance = 75 minutes  
 Fire Rating = I60

FR<sub>IR Thermal</sub> = 77 minutes  
 FR<sub>Criterion</sub> = Maximum Temperature (DT3)

